Power performance verification in complex terrain using nacelle lidars: the Hill of Towie (HoT) campaign

Borraccino, Antoine; Wagner, Rozenn; Vignaroli, Andrea; Meyer Forsting, Alexander Raul

Publication date:
2017

Document Version
Publisher's PDF, also known as Version of record

UniTTe

Innovation Fund Denmark
RESEARCH, TECHNOLOGY & GROWTH

DTU

Power performance verification in complex terrain using nacelle lidars: the Hill of Towie (HoT) campaign

DTU Wind Energy E-Report-0158

A. Borraccino, R. Wagner,
A. Vignaroli, A. R.M. Forsting

DTU Wind Energy E-0158

December 2017

DTU Wind Energy
Department of Wind Energy

Author(s): A. Borraccino, R. Wagner, A. Vignaroli, A. R.M. Forsting

Title: Power performance verification in complex terrain using nacelle lidars: the Hill of Towie (HoT) campaign

Department: DTU Wind Energy

Abstract:
Nacelle lidars are an attractive alternative to meteorological masts for power performance testing in complex terrain, because of the ease of deployment. This report presents the comparison of wind speed and power curve measurements using two commercial nacelle lidar system – one *Avent* 4-beam Wind Iris and one *ZephIR* Dual Mode – and a ground-based profiling lidar (ZP300), in a complex site. The model-fitting wind field reconstruction technique using measurements between 0.5D and 1D upstream, which has previously been demonstrated in flat terrain (Nørrekær Enge campaign), is here tested in complex terrain.

The two nacelle lidars have been deployed on a Siemens 2.3MW turbine at the Hill of Towie wind farm in Scotland between July and October 2017. The data analysis has been performed with three different wind speed estimates applied to the exact same dataset:

1) the ZP300 wind speed measurements at hub height, located 2.7D (220m) from the turbine.
2) the nacelle lidar wind speed estimate using the wind model fitting to the measurement at 2.5D upstream.
3) the nacelle lidar wind speed estimate using the wind-induction model fitting to the measurements between 0.5D and 1D upstream.

With the wind model, the wind speed estimate is within 2% from the ZP300 measurements, corresponding to an error in AEP in the order of 4%. With the wind-induction model, the free stream wind speed estimate is within 1% from the ZP300 corresponding to an AEP error of approximately 2%. In the second case, the reference wind speed is the ZP300 wind speed measurements corrected using the site calibration.

The power curve measured using the three measurement systems were compared to the turbine manufacturer warranted power curve as reference. The reduction in the statistical power uncertainty (type A) usually clearly observed in flat terrain when using nacelle lidars was demonstrated to be of a lesser extent. Here, the wind-induction model performed slightly better than the wind model.

In this study, measurements from nacelle lidars close to the turbine rotor were used to estimate the free stream wind speed. The resulting measured power curve was at least as accurate as the one obtained using the ground-based profiler measurements corrected with the site calibration. Thus, it was demonstrated that it is possible to measure a turbine's power curve at a (moderately) complex site without the need for a site calibration.

DTU Wind Energy E-0158

December 2017

ISBN: 978-87-93549-26-5

Contract no.: InnovationsFondens 1305-00024B

Project: UniTTe
http://www.unitte.dk/

Funding:
Innovation Fund Denmark

Pages: 99
Tables: 10
Figures: 47
References: 15

Technical University of Denmark
DTU Wind Energy
Risø Campus
Frederiksborgvej 399
DK-4000 Roskilde
Denmark

www.vindenergi.dtu.dk

Table of contents

Figures and tables

Preface

This document reports the results of the data analysis of a measurement campaign conducted in 2017 at Hill of Towie (Scotland), which investigated the use of nacelle-mounted lidars for power performance verification in complex terrain.

Additionally, this campaign allowed, during a short period of time, testing nacelles lidars for conducting a site calibration, and the report contains these results as well (Annex E).

The campaign was run by *Renewable Energy Systems Ltd* (RES) in close collaboration with *DTU Wind Energy*. The studies were performed by *DTU Wind Energy* as part of work package 4 of the Unified Turbine Testing project (UniTTe, http://www.unitte.dk/) funded by *Innovation Fund Denmark*.

The report is the deliverable D4.7 of the UniTTe project.

Acknowledgements

The authors would like to thank all the RES personnel involved in the long-time planning and operation of this campaign, in particular Lee Cameron, Simon Feeney (former employee of RES) and David Gleave.

Three lidar systems were used in the HoT campaign. They were all kindly provided by several parties and we would like to thank them for their contribution, namely:

- *RES* for the ground-based Zephir300 profiler.
- *Avent Lidar Technology* for the 4-beam Wind Iris – thanks to Paul Mazoyer.
- *Siemens Gamesa Renewable Energy* for the Zephir Dual Mode – thanks to Ioannis Antoniou and Gabriele Salcuni.

The authors also acknowledge the funding support to UniTTe by *Innovation Fund Denmark*.

Finally, I, Antoine Borraccino would like to sincerely thank you, Rozenn Wagner, for all the time you have spent working with me in UniTTe over the last four years. This report is without any doubt my very last UniTTe contribution, and I kind of will miss those. Thanks also to Andrea Vignaroli for leading work package 3 and your persistence that truly was needed to make this campaign – which will be remembered as a very challenging and unlucky one in terms of operational planning – in the end happen. Thanks also for handling and reporting on the site calibration part of this 2017 campaign in Hill of Towie.

Chapter 1

1 Introduction

Nacelle-mounted lidars are able to replace mast-mounted anemometers to measure the wind speed for wind turbine power performance verification in flat terrain, as demonstrated in [1], [2]. For modern turbines, it is much easier and faster to install a lidar on the nacelle of a turbine than erecting a hub height met mast. As the erection of meteorological masts in complex terrain is particularly challenging and costly, nacelle lidars represent a very attractive alternative for power performance verification in such sites. The UniTTe project aims at testing this approach and proposing adequate solutions.

Power performance verification relates the power output of a wind turbine to the energy present in the wind, through the proxy of the wind speed. Ideally, this wind speed should be the wind speed at the turbine location if there was no turbine, commonly called “free wind speed”. In flat terrain or offshore, it is fair to assume that the wind speed measured upstream of the turbine rotor is identical to the wind speed at the turbine location if there was no turbine, as long as the measurements are taken far enough from the rotor not to feel the induction effect. In that respect, the IEC standard 61400-12-1 recommends to measure at 2.5D upstream [3].

However this assumption is failing quickly when the terrain becomes complex enough that it is affecting the homogeneity of the flow within 200 to 500m of the turbine, e.g. in hilly or forested areas. In such sites, it is then necessary to establish the relation between the wind speeds at the mast location and at the turbine location before the turbine is erected. This is done through a site calibration process usually providing the ratio of the wind speed measured by cup anemometers on the two masts (see Annex C in [3]).

A similar approach could be adopted with nacelle-mounted lidars. The lidar could be used to measure the wind speed at 2.5D upstream of the turbine rotor. This however still requires performing a site calibration beforehand. An alternative method has been proposed by Borraccino et al and tested in flat terrain [4]. In this method, the nacelle-mounted lidar measures at several ranges between 0.5 and 1D upstream of the turbine rotor. The wind speed measured at such short distance from the turbine is expected to be more similar to the wind speed at the turbine location (if there was no turbine) than at 2.5D. However, this area is within the induction zone where the wind speed is slowed down by the operating rotor. Borraccino’s method uses the multiple-range measurements to fit a simple induction model and thus retrieves the free wind speed from the lidar measurements.

In the UniTTe project, this method has been tested on two datasets from two measurement campaigns using nacelle-mounted lidars in two different moderately complex sites. This report is presenting the results for one of the site: Hill of Towie, in Scotland.

Two advantages of the Hill of Towie site for this analysis were:

1) that the turbine to be tested for power performance is similar to the turbine used in the UniTTe baseline campaign (Nørrekær Enge) where the short-range nacelle lidar measurements technique was developed and demonstrated. The turbine has indeed the same Siemens 2.3MW platform, although it features a lower hub height and smaller rotor diameter. And, the Hill of Towie turbine controller is certainly configured in different manners too.

2) that a proper site calibration, as per IEC 61400-12-1 Ed.1 ([5]), has been performed in 2011 prior to the commissioning of the wind farm.

All the data was collected and relevant information (including the site calibration report) was kindly provided to DTU by *Renewable Energy Systems Ltd*.

This report focuses on the measurement campaign performed with two nacelle-mounted lidars between July and October 2017. The report describes the site and the instrumentation, the lidar performance and data, the data processing, the data analysis in terms of wind characteristics comparison between the lidar and the reference wind measurement system – here a ground-based profiling lidar – and the resulting measured power curves.

Chapter 2

2 Measurement campaign

2.1 Site description

The Hill of Towie wind farm is located near Drummuir in Moray, Scotland. It is located approximately 7km south-west of Keith and spans the high ground of Hill of Towie. The wind farm is at an altitude of about 250-400m above sea level. The vicinity of the test turbine is characterized by complex terrain, i.e. terrain with hills and slopes. The area is forested which adds elements of complexity to the wind flow. However, due to the presence of this mature forestry – tree heights estimated to be up to 10-15m – the forest was clear felled to a minimum of approximately seven rotor diameters (D_{rot}) of the test turbine.

The wind farm consists of 21 wind turbines of the same type SWT-2.3MW with a hub height of 58.5m and a rotor diameter of 82m. Obstacles as per the definition of IEC 61400-12-1 [5] are not present at the site [6].

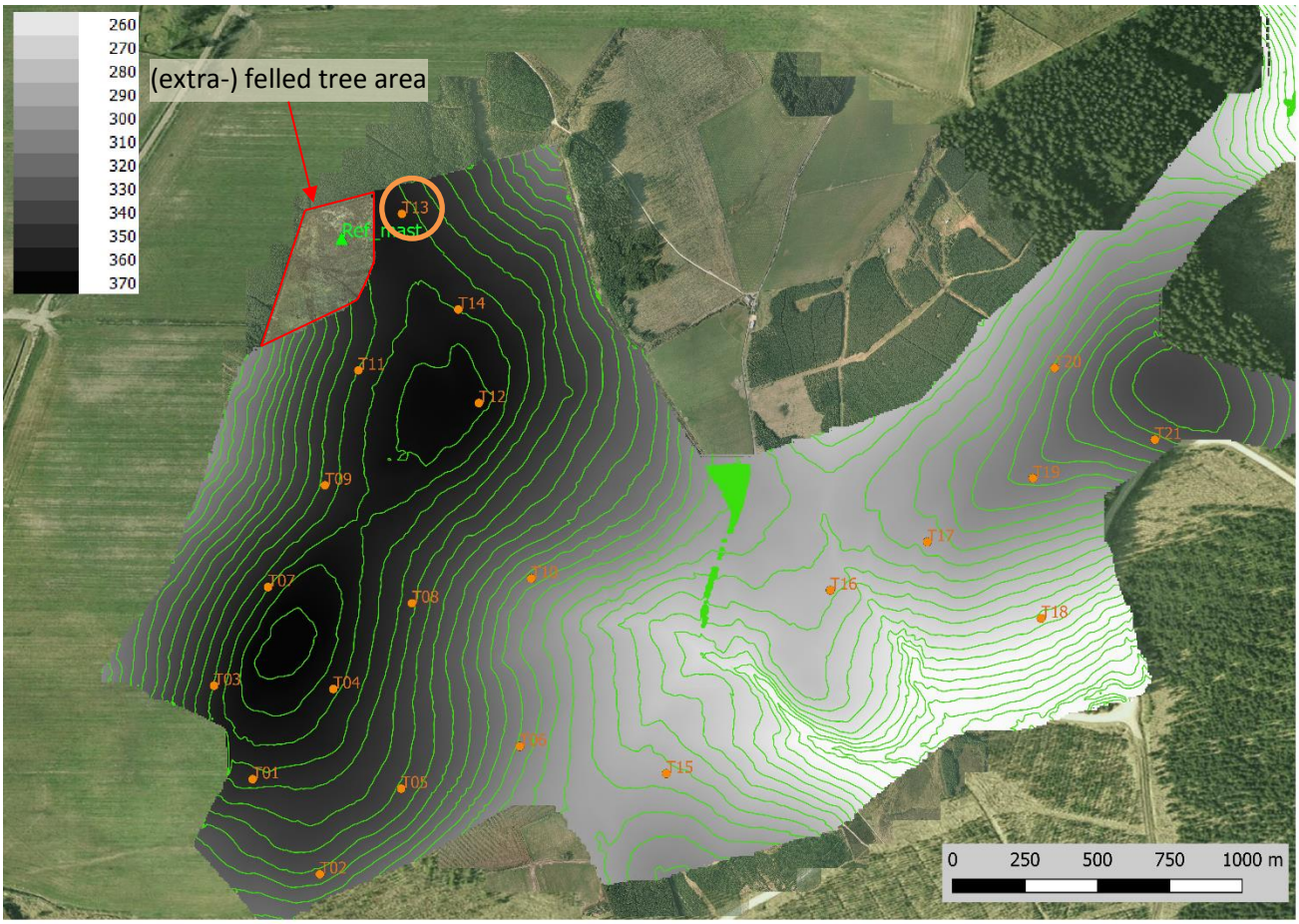

Figure 1. High resolution elevation map of the terrain around the Hill Of Towie Wind farm (satellite image: Google Earth), North oriented. Contour lines are shown every 5m (max = 360m).

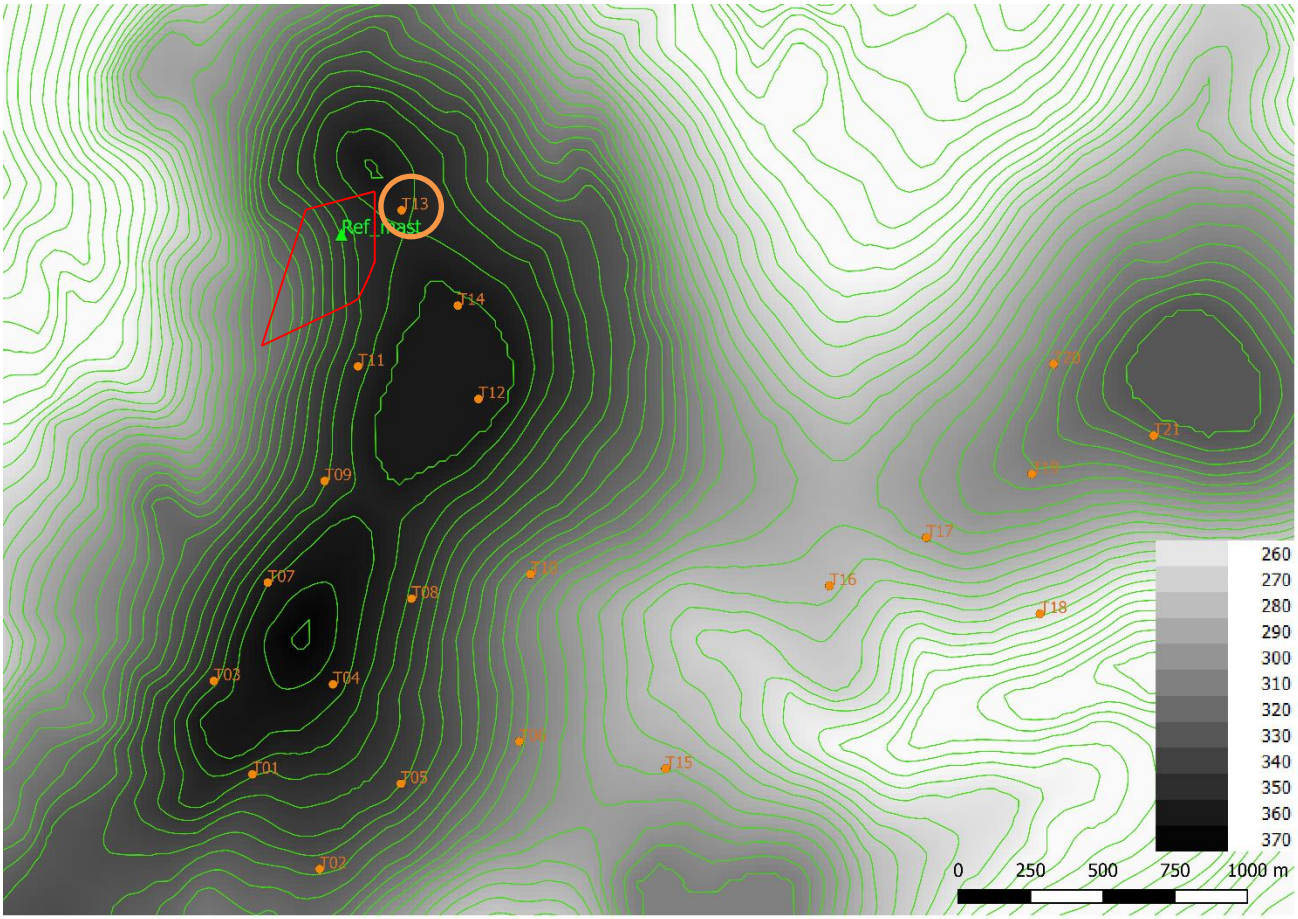

Figure 2. Elevation map (SRTM) of the terrain around the Hill Of Towie Wind farm (Google Earth), North oriented. Contour lines are shown every 5m (max = 360m).

The power performance test is conducted on turbine number 13 ("T13"), see orange circle in the northernmost part of Figure 1. Elevation maps are shown:

- in Figure 1, based on high-resolution digital data (5m XYZ resolution): unfortunately, no data was available in the sector of interest, most likely due to the presence of forestry prior to the site calibration. The felling of this forestry was completed on 4th July 2011.
- in Figure 2, based on SRTM data (Shutter Radar Topography Mission, NASA). This data is used to extract elevation profiles needs for the terrain correction in the wind field reconstruction (Figure 26).

The test site requirements for a power performance measurement, according to IEC 61400-12-1, Annex B [3], about topographical variations are not fulfilled for the present site. Therefore, a site calibration measurement was performed by *RES* between the dates of 04-07-2011 and 23-09-2011 (see analysis in [7]), in compliance with the IEC standard.

Table 1. Site calibration results in Hill Of Towie, as obtained by *Renewable Energy Systems* in [7].

Wind direction [°]	min	230	240	250	260	270
	max	240	250	260	270	280
Wind speed ratio $V_{turbine}/V_{ref}$ [-]		1,065	1,048	1,033	1,022	1,036

2.2 Measurement setup and instrumentation

The instrumentation of the campaign is composed of four different measurement systems:

- SCADA (Supervisory Control And Data Acquisition) of turbine T13.
- One ground-based profiling lidar of type ZephIR 300 (ZP300), commercially available lidar product by *Zephir Lidar*.
- Two nacelle-mounted lidars
    - One ZephIR Dual Mode (ZDM), commercially available lidar product by *Zephir Lidar*.
    - One four-beam Wind Iris (4BWI), commercially available lidar product by *Avent Lidar Technology*.

The coordinates of the ZP300 and test turbine are given in Table 2. The ZP300 used as reference in this analysis is at the exact same position as the reference meteorological mast from the site calibration ([7]). The ZP300 complies with the IEC 61400-12-1 Ed. 2 for power performance measurement in flat terrain.

Table 2. Test turbine and ZP300 coordinates.

	Unit	East	North
Turbine T13	Decimal degrees	57.516721	-3.078109
	UTM (30V)	495321.0	6374910.0
ZP300	Decimal degrees	57.51598	-3.08153
	UTM (30V)	495115.97	6374828.49

2.2.1 SCADA

The SCADA of the test turbine contains 10-minute statistics of: mean turbine power, mean turbine yaw, shutdown duration (status signal), mean and standard deviation of wind speed from nacelle anemometer.

2.2.2 Ground-based profiling lidar

A ground-based profiling lidar was deployed by *RES* (see details in [8]) on 1st June 2017 in order to act as a replacement of the formerly present reference meteorological mast during the power performance measurement campaign.

The profiling lidar is a ZephIR 300 (unit 534). The ZP300 is a continuous wave lidar system having a conical scanning pattern. The unit employed in Hill of Towie features a cone angle of 30° – angle from the vertical to the lidar beam propagation path. The ZP300 has the capability of measuring at up to ten ranges. This is done by interrogating successively different ranges: the lidar beam is refocused between each range. With one wedge revolution at each range, one complete 10-range cycle takes about 11 seconds.

Based on the coordinates in Table 2, the ZP300 in Hill of Towie was located 220.5m (2.7 rotor diameters) from the turbine, in the 248.3° direction. The 10-minute data extracted from the ZP300 ("WIND10.zph files) are listed in Table 4.

The ZP300 was configured to measure at ten ranges covering the entire span of the turbine rotor. The range configuration is listed in Table 3. The ZP300 lens height is approximately 1m, which must be added to the configured range to obtain the effective measurement height above ground level (agl.).

Table 3. Measurement range configuration of the ground-based ZP300 profiling lidar. One meter must be added to the range to arrive at the height agl.

Number	Configured range [m]	Comment
1	17	Low blade tip height
2	27	-
x	38	Default height for fog detection
3	48	-
4	52	-
5	58	Hub height
6	68	-
7	79	-
8	89	-
9	99	-
10	119	Max blade tip height

Table 4. List of 10-minute data available from the ground-based ZP300 lidar.

Type	Data name	Unit	Statistic
Status	Status flags	-	-
	GPS position	°	mean
	Battery voltage	V	mean
	Generator voltage	V	mean
	Pod humidity	%	mean
	Bearing	°	mean
	Tilt inclination	°	mean
MET station	Air temperature	°C	mean
	Air pressure	mbar	mean
	Relative humidity	%	mean
	Packets with rain	-	-
Wind data (at each range)	Wind speed	ms^{-1}	mean min max stdv
	Wind direction	°	mean
	Turbulence intensity	-	-
	Packets in average	-	-

2.2.3 Nacelle lidar: 4-beam Wind Iris

An *Avent 4-beam Wind Iris* (4BWI) nacelle lidar was installed by RES on the nacelle of T13 on the 5th of July 2017 ([9]).

The 4BWI is a pulsed lidar system. The beams – also called lines-of-sight (LOS) – are numbered from 0 to 3 as described in Table 5. LOS 0 and 2 (resp. 1 and 3) are separated by a vertical opening angle of 10° (in the plane defined by those two beams). LOS 0 and 1 (resp. 2 and 3) are separated by a horizontal opening angle of 30° (in the plane defined by those two beams, total opening angle).

Table 5. Beam position of Avent 4-beam Wind Iris relative to each other – seen from behind the lidar optical head.

	Left	Right
Top	0	1
Bottom	2	3

The 4BWI lidar was installed on its tripod (see pictures in Figure 3) on a platform attached to the turbine safety light brackets and fixed on the roof of the nacelle via strength pull magnets to obviate the need for drilling the nacelle's steel roof. The lidar (lens) was measured to be 2.64m above hub height ([9]) and estimated to be 3.5m behind the rotor plane (horizontal distance). The lidar was closely aligned with the nacelle centreline using its visible laser – lidar centreline slightly offset by approximately 0.15m (parallel to nacelle centreline).

Figure 3. Photo of the two nacelle lidars installed on the nacelle of T13. The 4-beam Wind Iris (orange optical head) is sitting under the ZephIR Dual Mode.

The 4BWI lidar was configured to measure at ten ranges as detailed in Table 6 below.

Table 6. Range configuration of the 4-beam Wind Iris lidar in Hill of Towie.

Range	#	1	2	3	4	5	6	7	8	9	10
	[m]	48	64	85	107	126	146	167	187	208	249
Upstream dist.	[D_{rot}]	0.55	0.75	1.01	1.27	1.51	1.75	2.01	2.25	2.51	3.01

The 208m range corresponds to an upstream distance of $2.5D_{rot}$, the distance recommended by the IEC61400-12-1 standard [3].

The beam trajectory of the 4BWI as configured in the Hill of Towie campaign can be visualised in Figure 4. The curve representing the ground corresponds to the elevation profile when the turbine points in the direction of the ground-based ZP300 lidar.

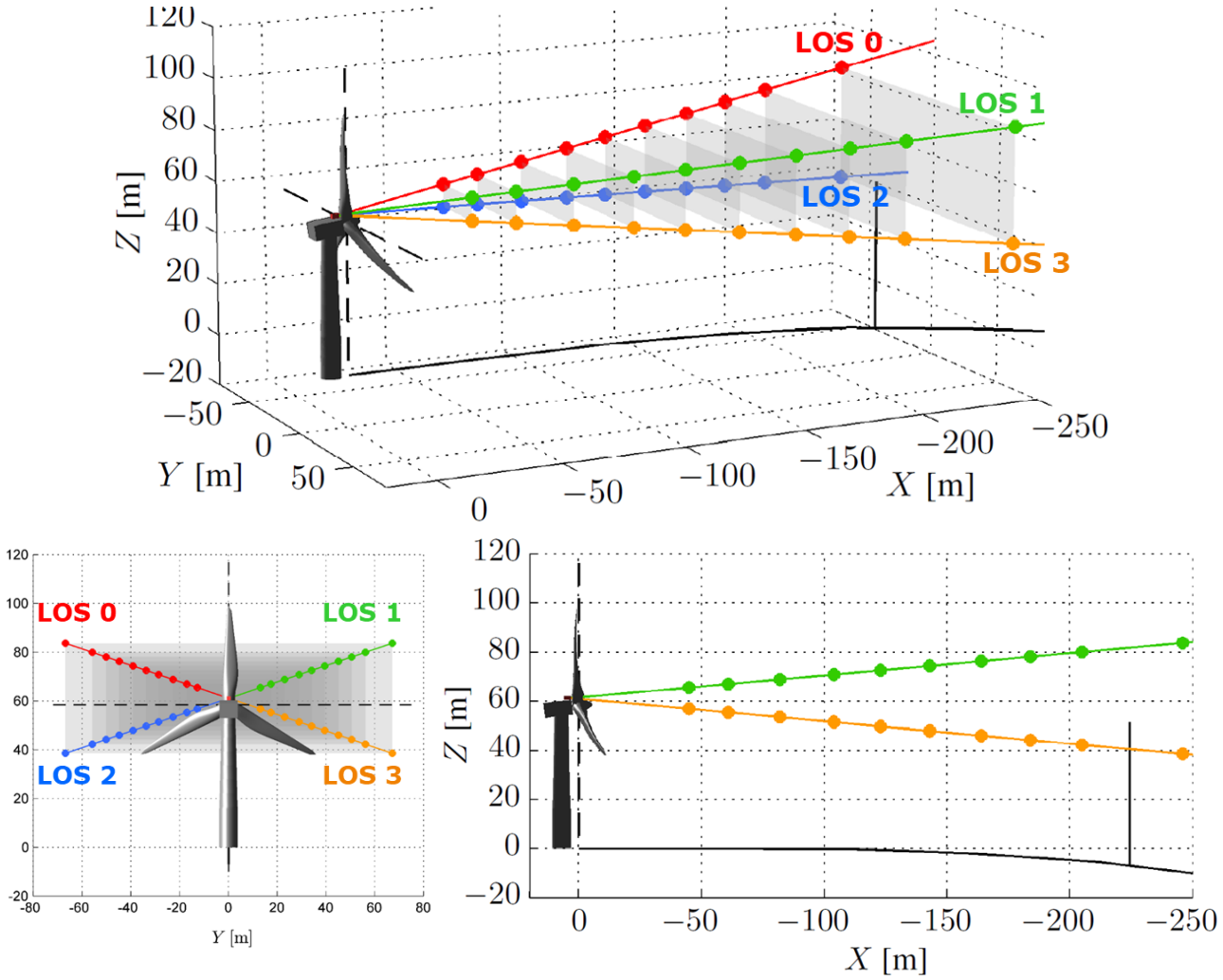

Figure 4. Measurement trajectory of the 4-beam Wind Iris lidar. Top: 3D view. Bottom left: view from the back. Bottom right: side view. The black vertical line represents the hub height at the ZP300 distance.

2.2.4 Nacelle lidar: ZephIR Dual Mode

A *ZephIR Dual Mode* (ZDM) nacelle lidar has been installed by RES on the nacelle of T13 on the 5th of July 2017 ([9]). The unit is number 622 and was provided (lent) by *Siemens Gamesa Renewable Energy*.

The ZDM is a continuous wave lidar system. The ZDM conically scans the wind with an angle of 15 degrees – cone angle from the optical centerline – and can interrogate up to 10 ranges similarly to ZP300 (see Section 2.2.2).

The ZDM 622 pod was installed on its three legs and on the same platform as the 4BWI (see pictures in Figure 3). The lidar was measured to be 3.03m above hub height ([9]) and estimated to be 3.1m behind the rotor plane (horizontal distance). The lidar was closely aligned with the nacelle centreline using its visible laser system.

The ZDM lidar was configured to measure at six different ranges as detailed in Table 7Table 6 below, performing five revolutions per range – i.e. a complete cycle takes approximately 30 to 35 seconds.

Table 7. Range configuration of the ZephIR Dual Mode (unit 622) lidar in Hill of Towie.

Range	#	1	2	3	4	5	6
	[m]	10	48	64	85	126	208
Upstream dist.	[D_{rot}]	0.09	0.55	0.75	1.01	1.51	2.51

The 208m range corresponds to an upstream distance of $2.5D_{rot}$, the distance recommended by the IEC61400-12-1 standard [3]. Due to the blockage from the nacelle and blades' roots, the 10m range is hardly usable for wind measurement but practically used by the lidar manufacturer's algorithms to detect the presence of fog via the backscatter signals (and its variation at different ranges).

The beam trajectory of the ZDM as configured in the Hill of Towie campaign can be visualised in Figure 5. The curve representing the ground corresponds to the elevation profile when the turbine points in the direction of the ground-based ZP300 lidar.

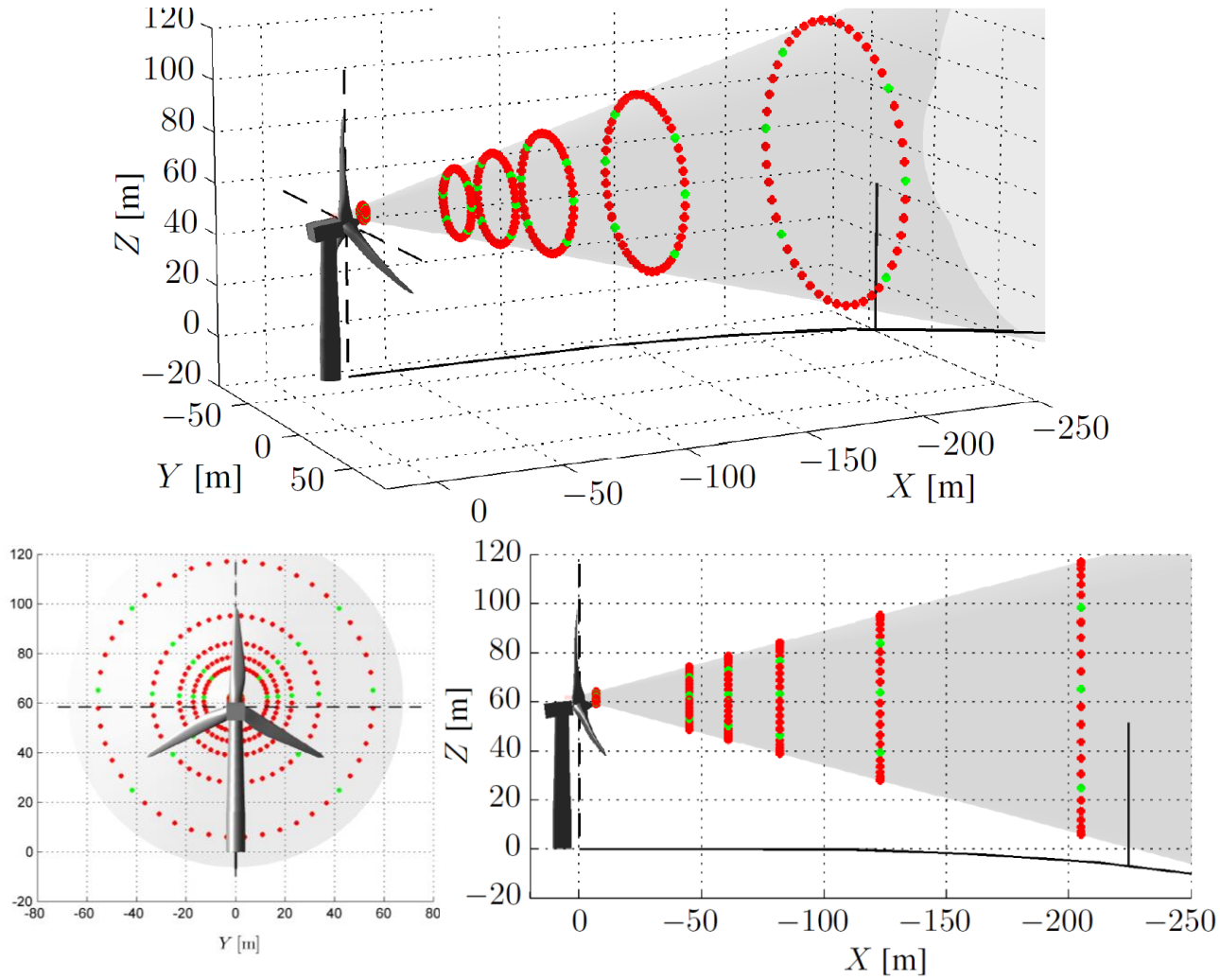

Figure 5. Measurement trajectory of the ZDM lidar. Top: 3D view. Bottom left: view from the back. Bottom right: side view. The black vertical line represents the hub height at the ZP300 distance. The green dots correspond to the "six beam" used to provide LOS velocity inputs to the wind field reconstruction algorithms.

2.3 Timeline

Due to powering issues (voltage of British electricity grid), the 4BWI lidar was not operational until the issue was solved on 30th July 2017 by plugging the lidar to an intermediate electrical transformer.

On 2nd October 2017, around 10am, the turbine was voluntarily stopped (brakes on) in the 251° yaw direction in order to perform a site calibration test using the nacelle lidars (see Annex E). The turbine was re-started on 5th October at 10:10. Note: the asset owner has been financially compensated for lost revenue duringthis stop.

All three lidars – 4BWI, ZDM622 and ZP300 (unit 534) – were decommissioned by *RES* on 6th October 2017 and thus the campaign ended.

Consequently, the measurement campaign can be split in two datasets:

- For power performance verification, between 30th July and 2nd October 2017 (> 2 months).
- For site calibration measurement with nacelle lidars, between 2nd and 5th October 2017 (3 full days).

All three measurement systems ran continuously over these two periods.

2.4 Synchronisation of data

The time configuration of the different data acquisition systems is detailed in Table 8. Due to the time stamping convention of the different systems, and due to different automatized MySQL database processes (employed by DTU Wind Energy), the synchronisation was checked on a 10-minute time basis with reference to the SCADA (see Figure 6, Figure 7 and Figure 8) using primarily the wind speed signals.

Table 8. Time configuration of the different data acquisition systems.

Measurement system	Clock config.	Time stamping .. of 10-minute period
SCADA	UTC+1 (local time)	at the end
ZP300 (unit 534)	UTC+1	at the beginning
4-beam Wind Iris	UTC+1	at the end
ZephIR Dual Mode (unit 622)	UTC+1	at the beginning

The 4BWI was configured to be synchronised with the same time server as the turbine SCADA (NTP server IP 10.171.88.71/24, see [9]). The ZP300 and ZDM lidars were synchronised using their internal GPS clocks.

All data were loaded into a MySQL database. The 10 minute statistics data from the 4BWI and ZDM lidar were derived from the real time data (see Chapter 5) and time-shifted ("Name_sync") forward in order to match the SCADA data time. In the MySQL database, data are therefore stamped at the end of the 10-minute periods.

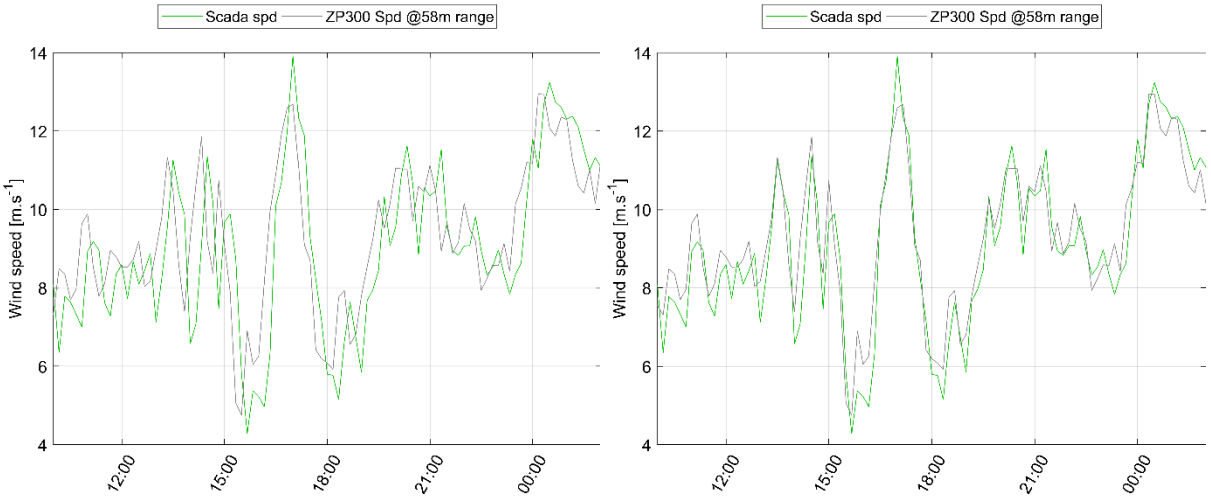

Figure 6. Synchronisation between ZP300 and SCADA data: timeseries of wind speed (8th July 2017). Left: before synchronization. Right: after synchronization.

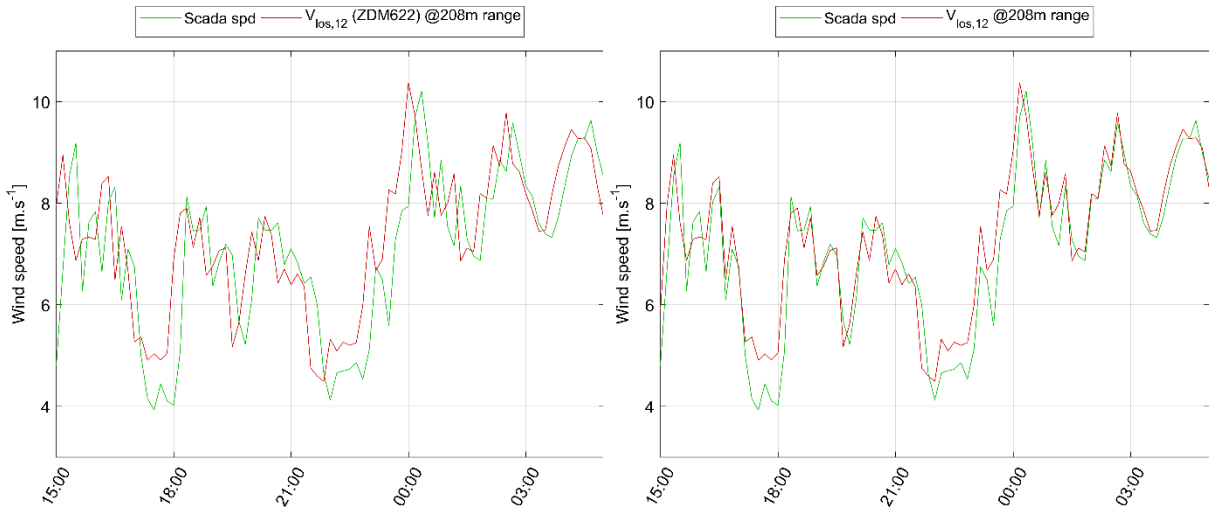

Figure 7. Synchronisation between ZDM622 and SCADA data: timeseries of wind speed (6th August 2017). Left: before synchronization. Right: after synchronization. Seen from the back, $V_{los,12}$ is the LOS velocity for the azimuthal sector at the "right" side of the circular scan of ZDM622 and closest to hub height.

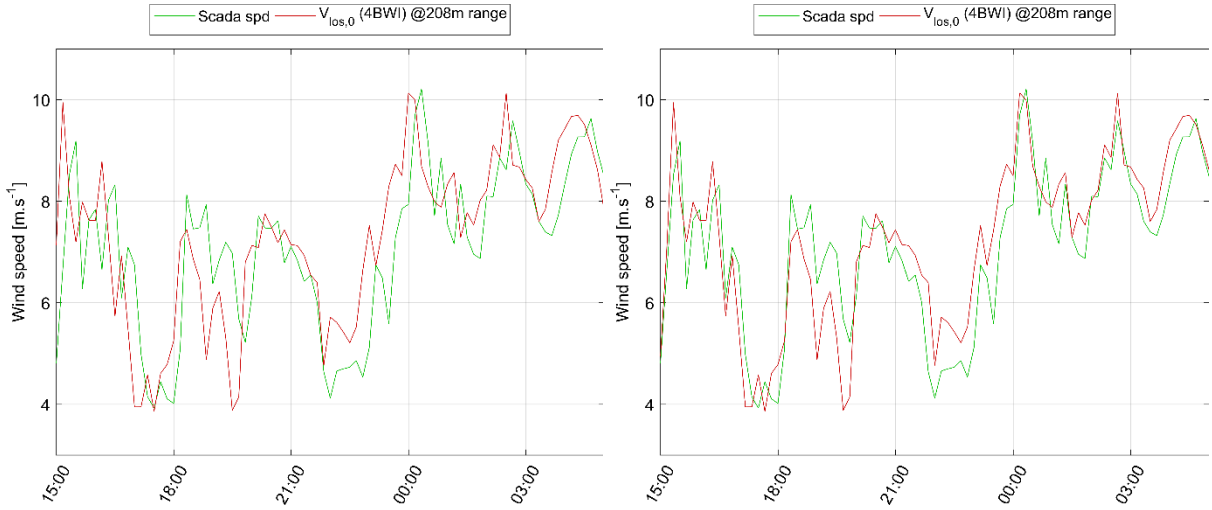

Figure 8. Synchronisation between 4BWI and SCADA data: timeseries of wind speed (6th August 2017). Left: before synchronization. Right: after synchronization. Seen from the back, $V_{los,0}$ is the LOS velocity for the beam at the top left of the 4BWI beam trajectory.

Although the synchronization based on 10-minute statistics is satisfactory, issues were identified in the real-time synchronization between on one hand the two ZephIR systems (ZP300 and ZDM622) and the other hand the SCADA and 4BWI. As the two ZephIR lidar systems were running on their internal GPS clocks, the synchronization may be somewhat variable compared to the time server of the SCADA. An investigation of the real-time synchronization was conducted using raw measurement data from the two nacelle lidars, by comparing LOS velocities for four time periods of approximately one hour each. The statistical analysis revealed plausible clock synchronization issues with offsets estimated to be between 30 seconds and one minute. In the future, such an issue could be avoided by feeding the lidar data directly into the SCADA system or by synchronizing the lidar clock to the same time server as the one used for the SCADA.

Chapter 3

3 Wind conditions

This section provides information and graphs describing the atmospheric wind conditions observed during the power performance test. All graphs are based on 10-minute data.

3.1 Wind rose

The wind rose in Figure 9 below is based on the wind speed and direction measured by the ZP300 lidar at hub height, i.e. using the 58m configured range. The main wind direction is West-South West. The IEC wind sector – sector for which both reference mast (or remote sensor) and the turbine are free of wake of surrounding obstacles according to requirements from IEC 61400-12-1, Ed. 2, Annex A (see [3]) – within which the site calibration is valid is between 230 and 280 degrees (see details in [6] and [7]).

One third of the data corresponds to periods with wind directions comprised in the valid measurement sector.

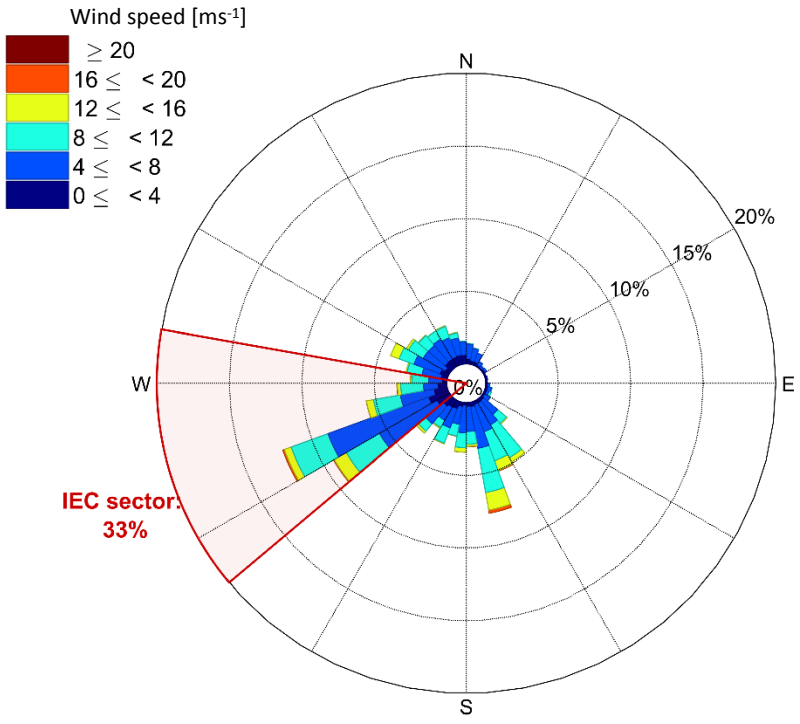

Figure 9. Wind rose for the period from 30th July to 2nd October 2017-10-02 (UTC). Based on measurements at @58.5m agl. (hub height) by the ZP300 lidar.

3.2 Wind direction

Figure 10 shows the variations of wind direction with time and Figure 11 shows the distribution of the wind direction measured by the ZP300 lidar at 58.5m agl., for the period from 2017-07-30 to 2017-10-02 (UTC).

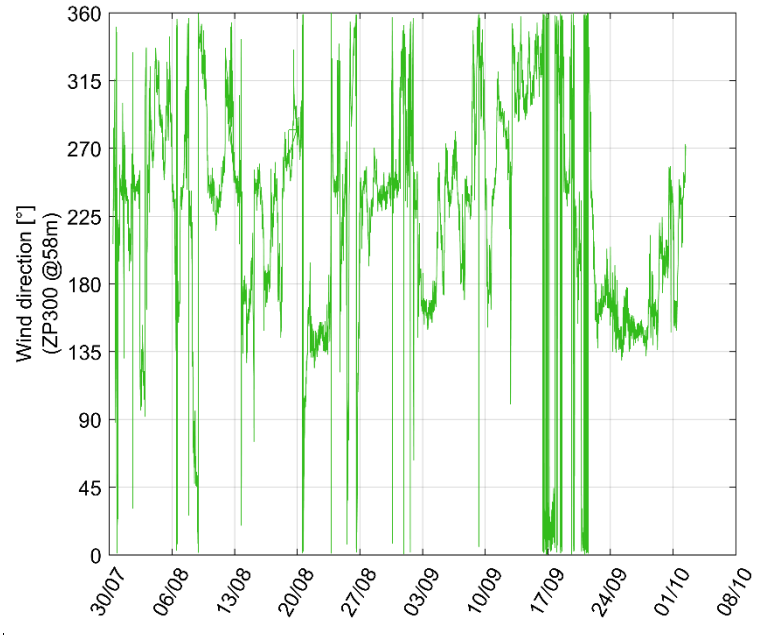

Figure 10. Time series of wind direction @58.5m agl. (hub height) measured by the ZP300 lidar.

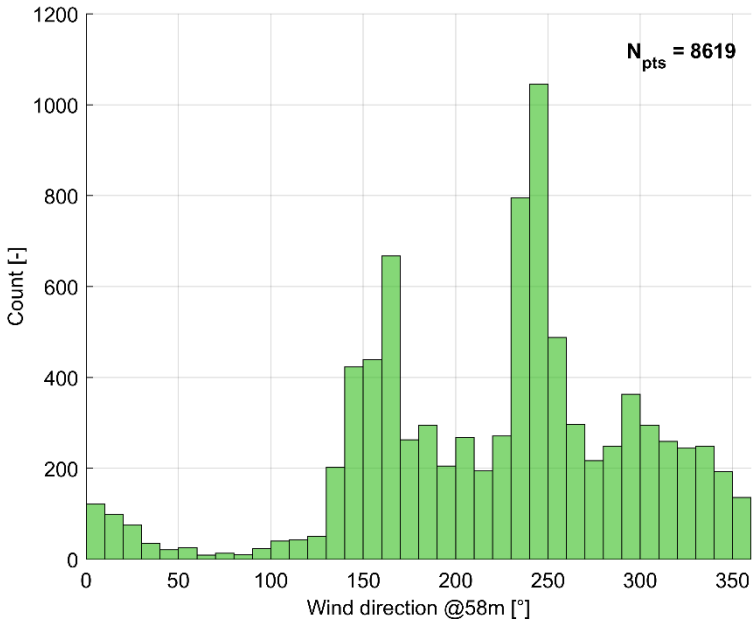

Figure 11. Histogram of wind direction @58.5m agl. (hub height) measured by the ZP300 lidar.

3.3 Wind speed

Figure 12 shows the variations of wind speed with time, with green bars indicating wind direction in the IEC sector. Figure 13Figure 11 shows the distribution of wind speed measured by the ZP300 lidar at 58.5m agl., for the period from 2017-07-25 to 2017-10-02 (UTC). Figure 14 shows the histogram of the wind speed for wind directions within the site calibration sector (230°-280°).

The mean wind speed during the measurement campaign was approximately 7.5 ms^{-1}.

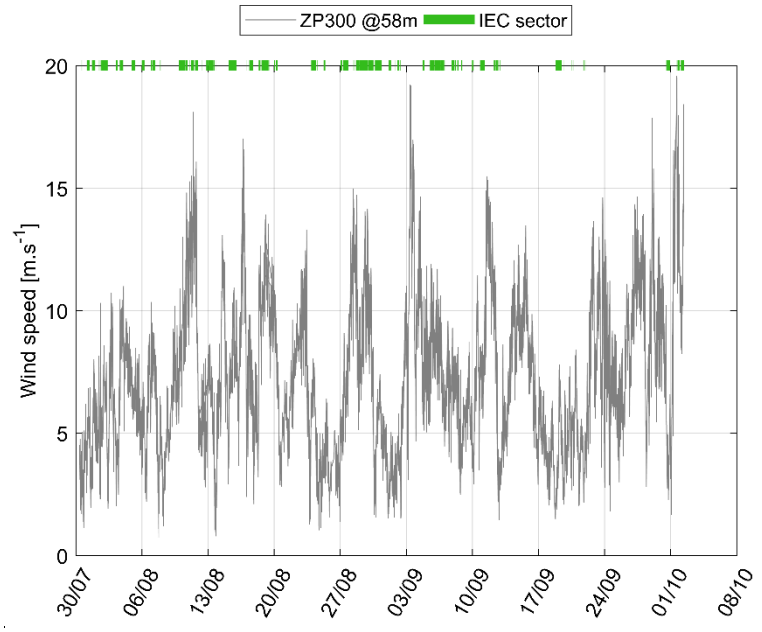

Figure 12. Time series of wind speed @58.5m agl. (hub height) measured by the ZP300 lidar.

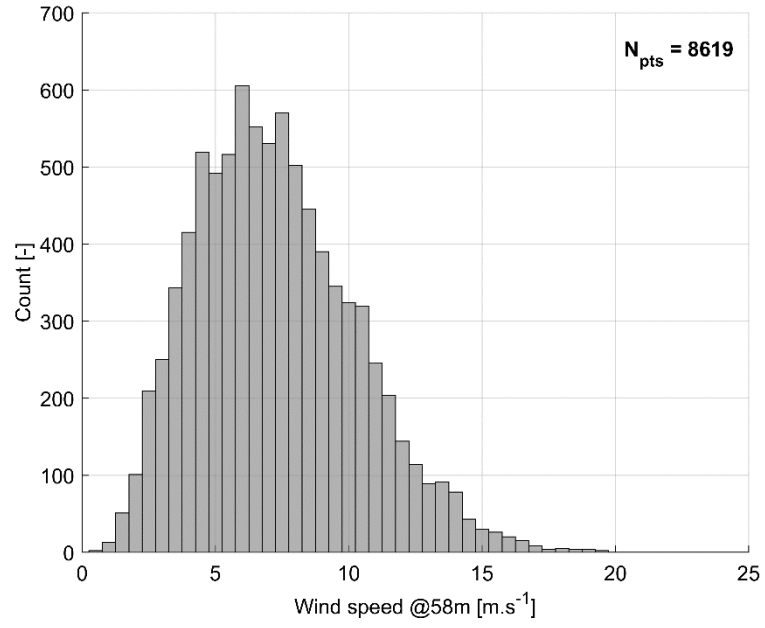

Figure 13. Histogram of wind speed @58.5m agl. (hub height) measured by the ZP300 lidar.

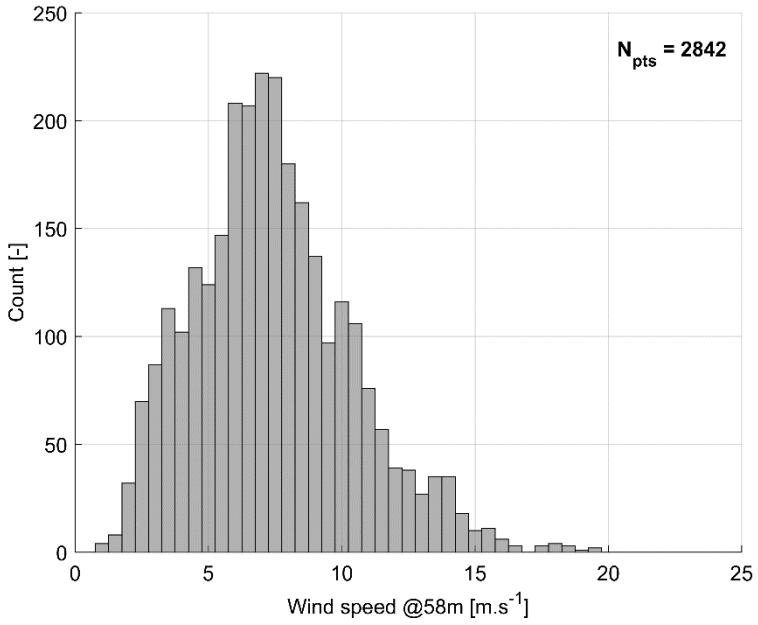

Figure 14. Histogram of wind speed @58.5m agl. (hub height) measured by the ZP300 lidar, for wind directions within the site calibration sector (230-280 deg).

3.4 Shear exponent and turbulence intensity

Figure 15 displays the distribution of the shear exponent within the site calibration sector (230-280 deg). The shear exponent was derived from a least square fit through the ZP300 measurements at all measured heights (11 in total). The shear exponent is the vast majority of the time within the [0, 0.4] range, with an averaged value of approximately 0.2. For completeness of information, Figure 16 shows the goodness of fit of the shear exponent in the form of a scatter plot. 80% of the data shows coefficient of determination values than 0.8.

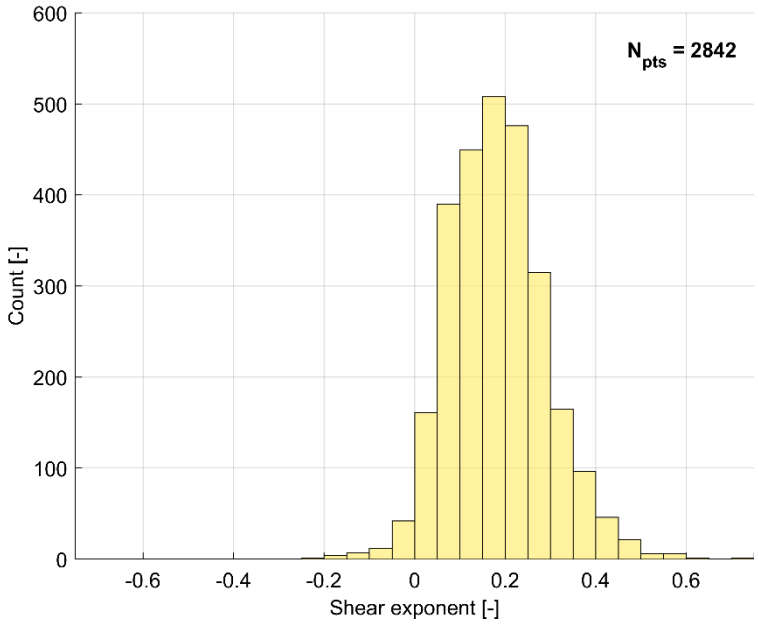

Figure 15. Histogram of shear exponent estimated from the ZP300 lidar measurements, for wind directions within the site calibration sector (230-280 deg).

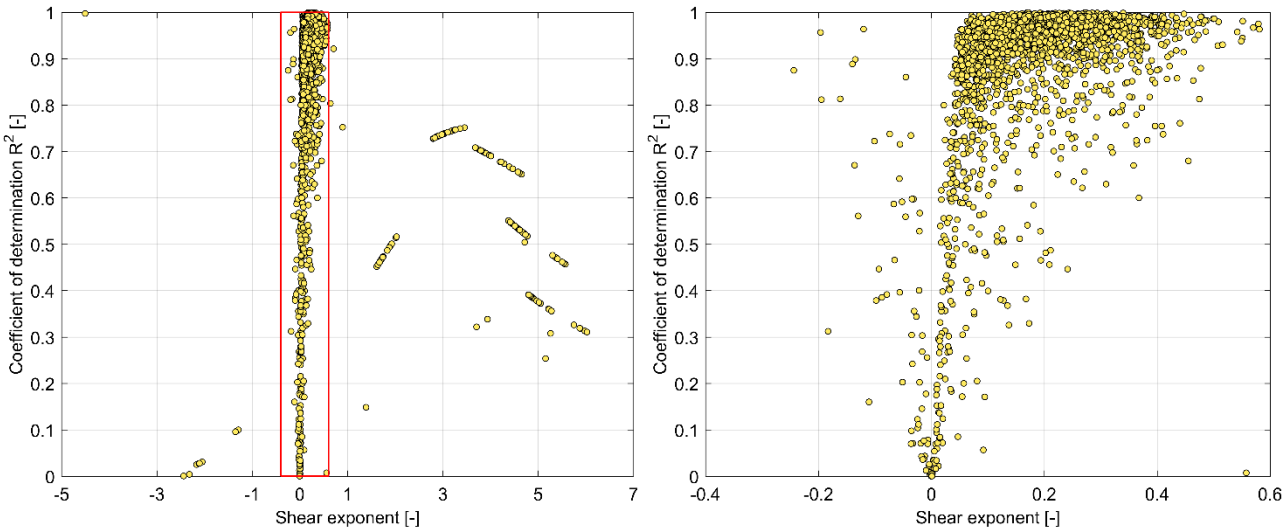

Figure 16. Goodness of fit of shear exponent from the ZP300 lidar measurements, for wind directions within the site calibration sector (230-280 deg): coefficient of determination (log fit) vs. shear exponent. Left: complete range. Right: zoom to red rectangle.

Figure 17 shows the distribution of the turbulence intensity measured by the ZP300 lidar at 58.5m agl., within the IEC wind sector. On average, the turbulence intensity is approximately 12%. For comparison, the average turbulence intensity can be expected to be within 8% to 10% at a flat site, and as low as 5% to 6% offshore.

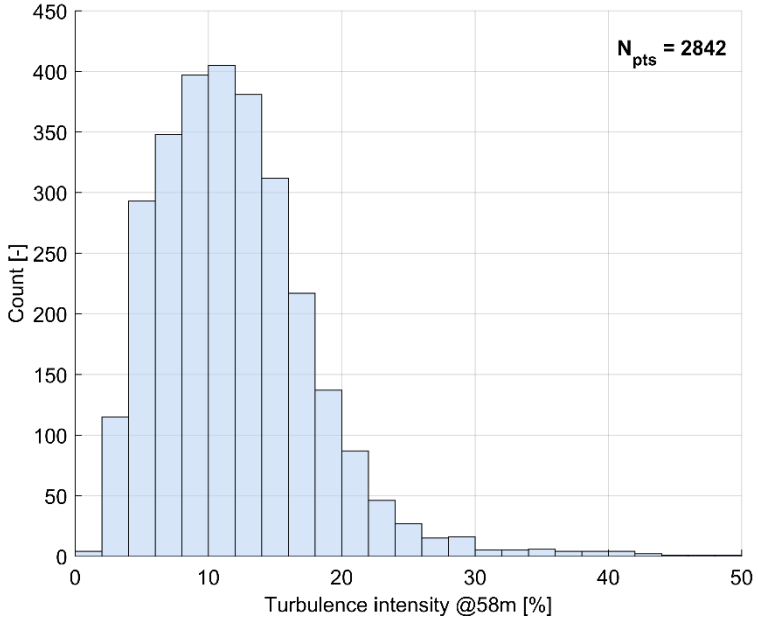

Figure 17. Histogram of turbulence intensity @58.5m agl. (hub height) measured by the ZP300 lidar, for wind directions within the site calibration sector (230-280 deg).

Chapter 4

4 Lidar performance

This section briefly reports on the performance of the two nacelle lidar systems (4BWI and ZDM) during the campaign. All graphs are based on 10-minute data.

4.1 Time series of raw signals

Figure 18 shows the time series of the LOS wind velocities measured by the 4BWI (left) and ZDM (right) lidars, prior to applying any filtering other than quality control of real-time data (see Chapter 5). This demonstrates that the two nacelle lidars have been in continuous operation during the entire concurrent measurement period.

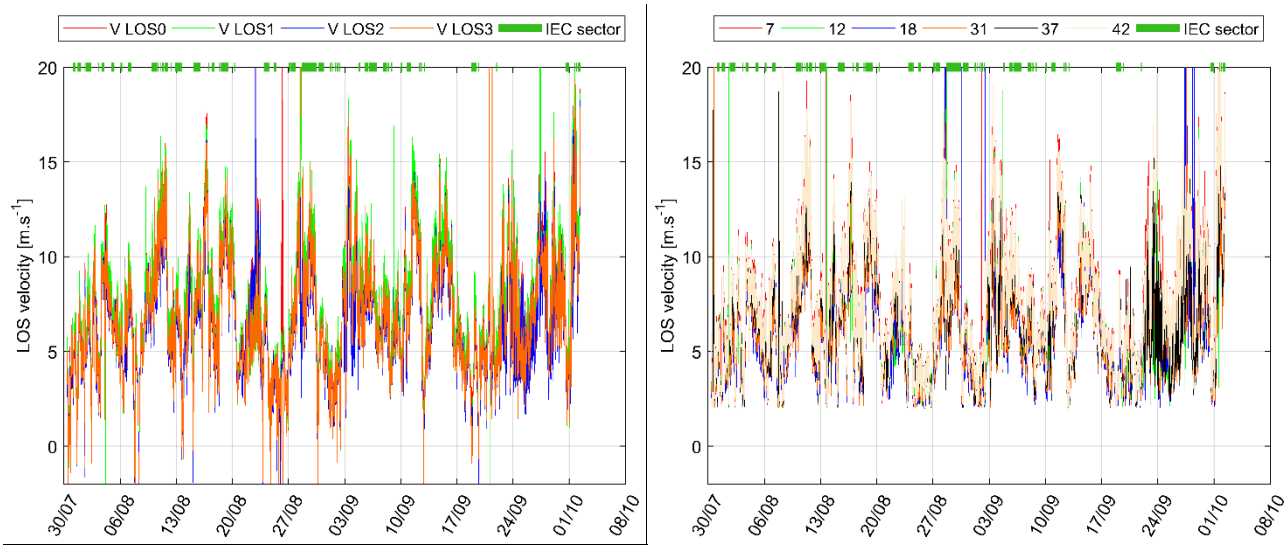

Figure 18. Time series of unfiltered lidar-measured LOS velocities @208m range. Left: for the four LOS of the 4BWI. Right: for six LOS (azimuthal sectors) of the ZDM.

The time series of the two lidar backscatter signals – Carrier-to-Noise Ratio (CNR) for the 4BWI and "Backscatter" (power of signal) for ZDM – @208m range are displayed in Figure 19. Essentially, these two lidar backscatter signals characterize the intensity of the light returned by atmospheric particles (aerosols).

The CNR of the 4BWI remained between -25dB and -15dB for most of the time, while the backscatter of the ZDM usually took values between 0 and 0.5 (in SI unit).

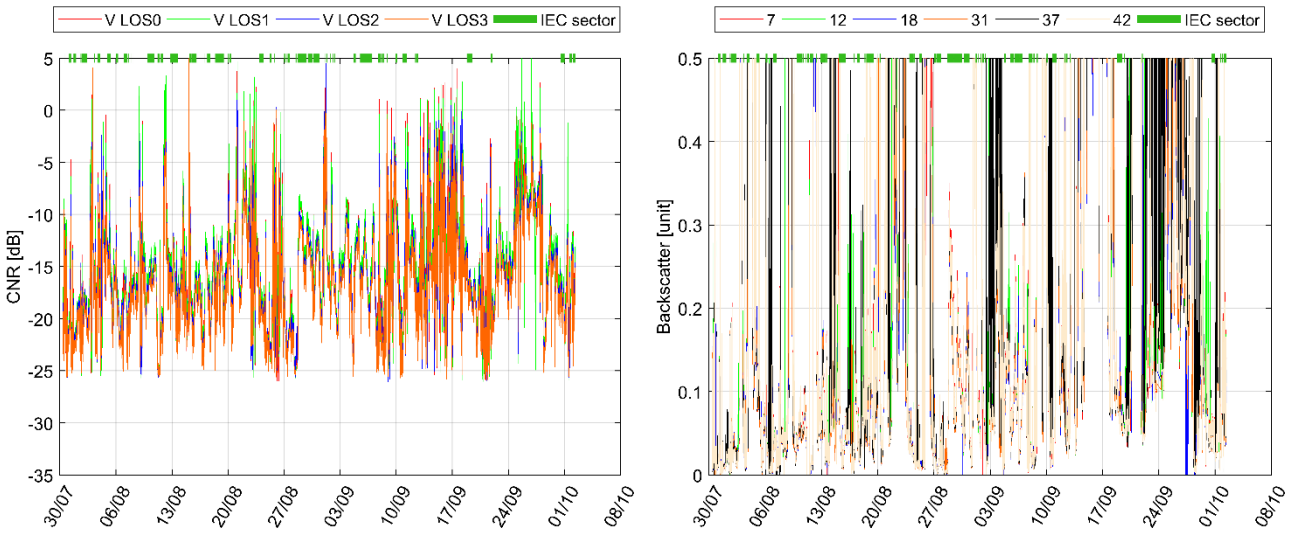

Figure 19. Time series of (unfiltered) power in lidar backscatter signal @208m range. Left: CNR for the four LOS of the 4BWI. Right: backscatter (in SI unit) for six LOS (azimuthal sectors) of the ZDM.

4.2 Tilt and roll

The two lidar – and therefore their inclinometers – have not been calibrated. During installation, while the turbine was at stand still, the static inclination angle readings were not reported but can be estimated from Figure 21 and Figure 23 to:

- For the 4BWI (inclinometers on optical head): -0.3° tilt and -0.25° roll;
- For the ZDM (inclinometers on heat sink of lidar pod) -0.1° tilt and -0.25° roll.

Note that a negative tilt angle means the lidar optical axis is looking downwards.

Figure 20 shows the histogram of the tilt angle (prior to applying any filtering other than quality control of real-time data). The lidars tilt angles are higher than their static values – i.e. the tilt when the turbine is stopped – for most of the time since the thrust on the rotor (when the turbine is operating) is making the turbine tower and therefore the nacelle bend backwards. Indeed the tilt increases with the wind speed, up to rated speed (maximum thrust), as shown in Figure 21. The 10-minute tilt average has been used to get the actual position of the beam in the wind characteristic reconstruction (see chapter 6).

Figure 22 shows the histogram of the roll angle. The lidars' roll has been lower than the static -0.25° value for most of the time since the rotation of the rotor (when the turbine is operating) is making the turbine nacelle roll slightly to one side. Indeed this effect increases with the wind speed, up to rated speed, as shown in Figure 23.

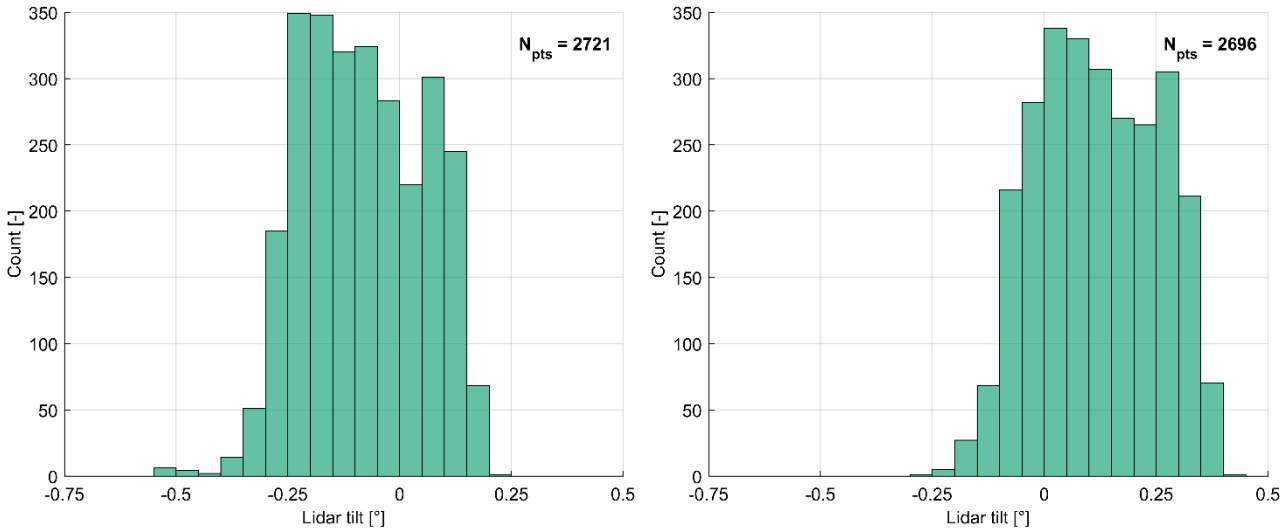

Figure 20. Histogram of lidar tilt, for wind directions within the site calibration sector (230-280 deg). Left: 4BWI. Right: ZDM.

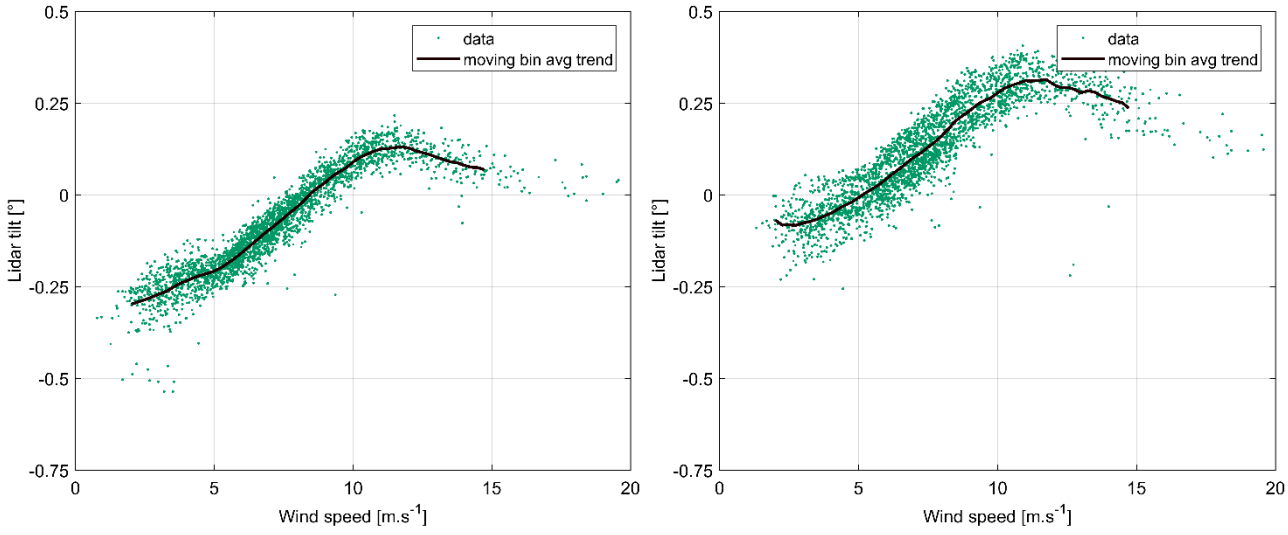

Figure 21. Lidar tilt vs. ZP300 wind speed @58.5m agl., for wind directions within the site calibration sector (230-280 deg). Left: 4BWI. Right: ZDM.

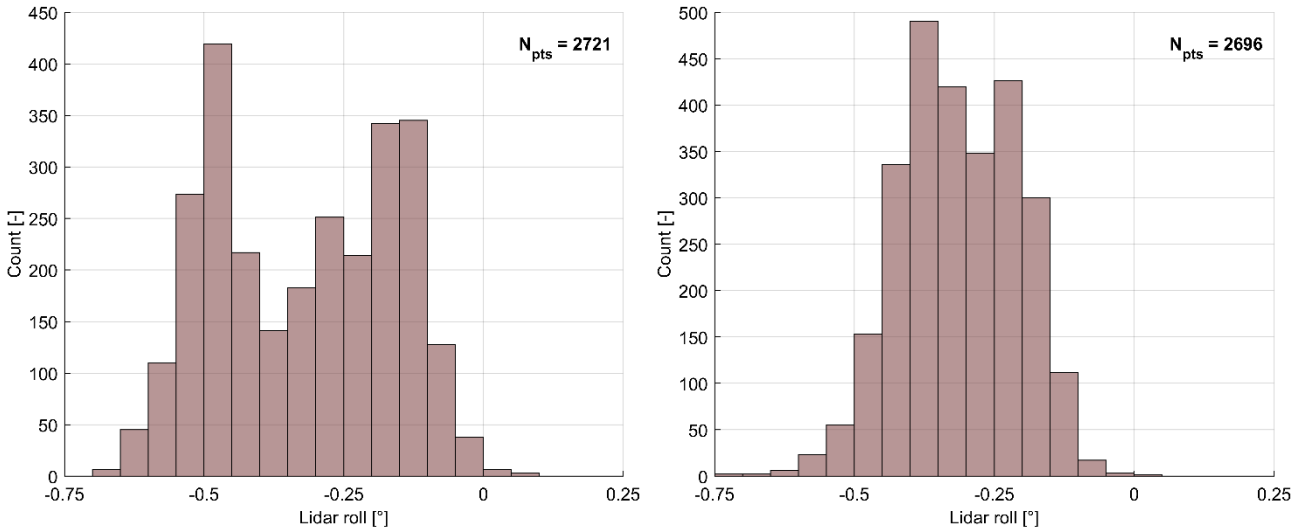

Figure 22. Histogram of lidar roll, for wind directions within the site calibration sector (230-280 deg). Left: 4BWI. Right: ZDM.

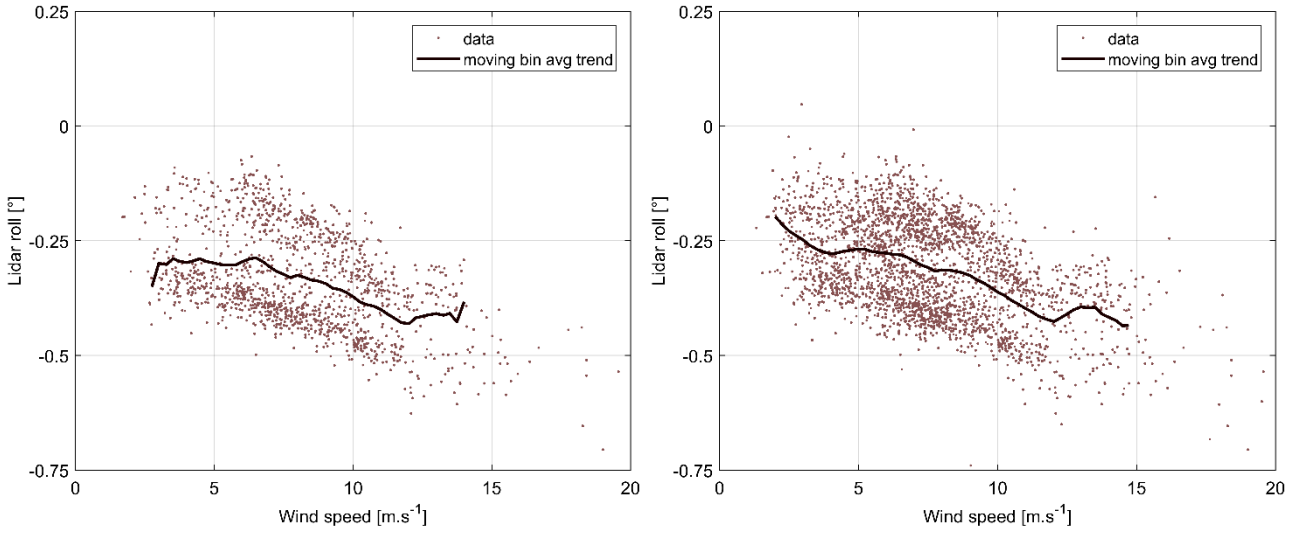

Figure 23. Lidar roll vs. ZP300 wind speed @58.5m agl., for wind directions within the site calibration sector (230-280 deg). Left: 4BWI. Right: ZDM.

Chapter 5

5 Lidar data processing and quality control

This chapter describes the processing of the raw nacelle lidar data and their quality control. The processing of the raw lidar data was performed differently from the methods embedded on the systems and designed by the lidar manufacturers. The processing performed on the two lidars uses in-house (DTU) developed algorithms and codes, which have previously been demonstrated within the UniTTe project (see [2], [4]).

5.1 Lidar data processing

5.1.1 Quality control for 4-beam Wind Iris

The time series of real-time raw data (not filtered) from the 4BWI were graphed for the entire campaign, by blocks of 10 minutes. The measurement data we analysed were: LOS velocity (V_{los}), CNR and spectral width of V_{los} (denoted dRWS). The data was plotted only for real-time measurements indicated as valid by the embedded flag, i.e. when the parameter "RWS_status" = 1.

This flag proved to be insufficient as obvious outliers remained. Such outliers were investigated and several types of reasons were identified. The outliers are due to either: the presence of hard targets (not the case in the Hill of Towie campaign); erroneous processing by the LOS velocity estimator, usually at very low CNR. We have therefore implemented some further quality control of the 1Hz LOS data before computing the 10-minute statistics. The quality control of the 4BWI is described in this paragraph.

One reason for those outliers was found in another campaign (see [10]) to be due to one of the LOS hitting a met mast. Hitting a hard target (HT) can have an effect on three parameters:

1) a very high CNR at the range gate of the hard target;
2) a low LOS speed;
3) a low spectral width (dRWS) (typically, the hard target is not fully hit by the lidar beam)

Nevertheless the absolute value of those three parameters can vary during the campaign due to the varying wind and aerosols conditions. Therefore we have defined hard target events as relative values between the different LOS. Furthermore, all three conditions are always clearly detectable. Thus three combinations of parameters were applied to detect hard target events. We considered that one of the lidar LOS (LOS i) was hitting a hard target if at least one of the three following flags were raised. Those flags were evaluated for all the 1Hz data.

Flag HT1: Low LOS speed and high CNR

True for LOS i when, for all other LOS j ($j \neq i$):

1. $abs(RWS_i) < 0.2\, avg\left(RWS_j\right)$
and
2. $avg\left(RWS_j\right) > 2\, ms^{-1}$
and
3. $CNR_i > avg\left(CNR_j\right) + 2\, std\left(CNR_j\right) + 1dB$

Flag HT2: High CNR and large spectral width

True for LOS i when, for all other LOS j ($j \neq i$):

1. $CNR_i > avg\left(CNR_j\right) + 2\, std\left(CNR_j\right) + 1dB$
and
2. $dRWS_i > avg\left(dRWS_j\right) + 3\, std\left(dRWS_j\right)$

Flag HT3: low LOS speed and large spectral width

True fo rLOS i when, for all other LOS j ($j \neq i$):

1. $abs(RWS_i) < 0.2\, avg\left(RWS_j\right)$
and
2. $avg\left(RWS_j\right) > 2\, ms^{-1}$
and
3. $dRWS_i > avg\left(dRWS_j\right) + 3\, std\left(dRWS_j\right)$

We also observed that some outliers characterised by very high LOS speed (up to 40-50ms^{-1}) and low CNR (erroneous processing by the LOS velocity estimator) were not caught by any of those flags. In order to detect and eventually discard those erroneous data, a fourth flag has been defined as follow:

Flag E: high LOS and low CNR

1. $CNR_i < -25\, dB$
and
2. $RWS_i > 15\, ms^{-1}$

The real time data, for each LOS, were filtered so that:

- RWS_status=1;
  And
- Flag HT1=0
  And
- Flag HT2=0
  and
- Flag HT3=0
  And
- Flag E=0.

The 10-minute statistics used in the rest of the analysis were evaluated from the quality-controlled time series. In order to know how much data was remaining in each 10-minute period after applying those filters, we have defined a 10-minute LOS availability parameter as the ratio between the number of data remaining after quality control and the measurement attempts.

5.1.2 Quality control and statistics for ZephIR Dual Mode

The quality control (QC) of the ZDM raw data (RAW.zph files) was performed using the LOS velocity and the spectral data (FFT data, recorded at ~50Hz) as primary inputs. The ZDM lidar does not flag the high resolution RAW data. For confidentiality reasons, we will only list the measurement issues that the QC processing allows to handle and flag in order to discard them from the measurement statistics:

- **Blade blockage (fully)**: characterised by a very high backscatter signal, even in cases where the blade is located far from the focus points, the volume averaging weighting function has an infinitely long tail which yields large backscatter signals.
- **Low Doppler** (empty Doppler power spectrum).
- **Calm filter**: LOS velocity measurements are not accurate enough at very low speeds (or when the wind direction is orthogonal to the LOS direction).
- **Partial blade blockage (glint)**: handling of glints is achieved by discarding azimuthal sector just before and just after a full blade blockage is detected (first filter).

Note that the two months of high-frequency ZDM spectral data corresponds to approximately 300GB. Post-processing the ZDM's spectral data is computationally expensive; here it took approximately three days using an automated processing script (Processor Intel Core™ 2Duo P9600 2.67GHz, RAM of 4GB).

The statistics of the ZDM measurement data were obtained by:

- Defining 48 averaging azimuthal sectors, see Figure 5;
- Computing for each range and azimuthal sector:
  - the mean, standard deviation, minimum and maximum values of:
    - LOS velocities,
    - tilt and roll angles,
    - spectral spread
  - Computing the LOS availability, as the number of valid measurements (after QC) divided by the number of measurement attempts.

5.2 Lidar data availability

The following figures show the lidars' LOS availability as a function of:

- Average CNR and backscatter for the 4BWI (LOS3) and the ZDM (LOS 12; hub height, right side) respectively; see Figure 24.
- LOS velocity: LOS 3 for the 4BWI and LOS 12 for ZDM; see Figure 25.

Identical plots for the other LOS are shown in Annex A.

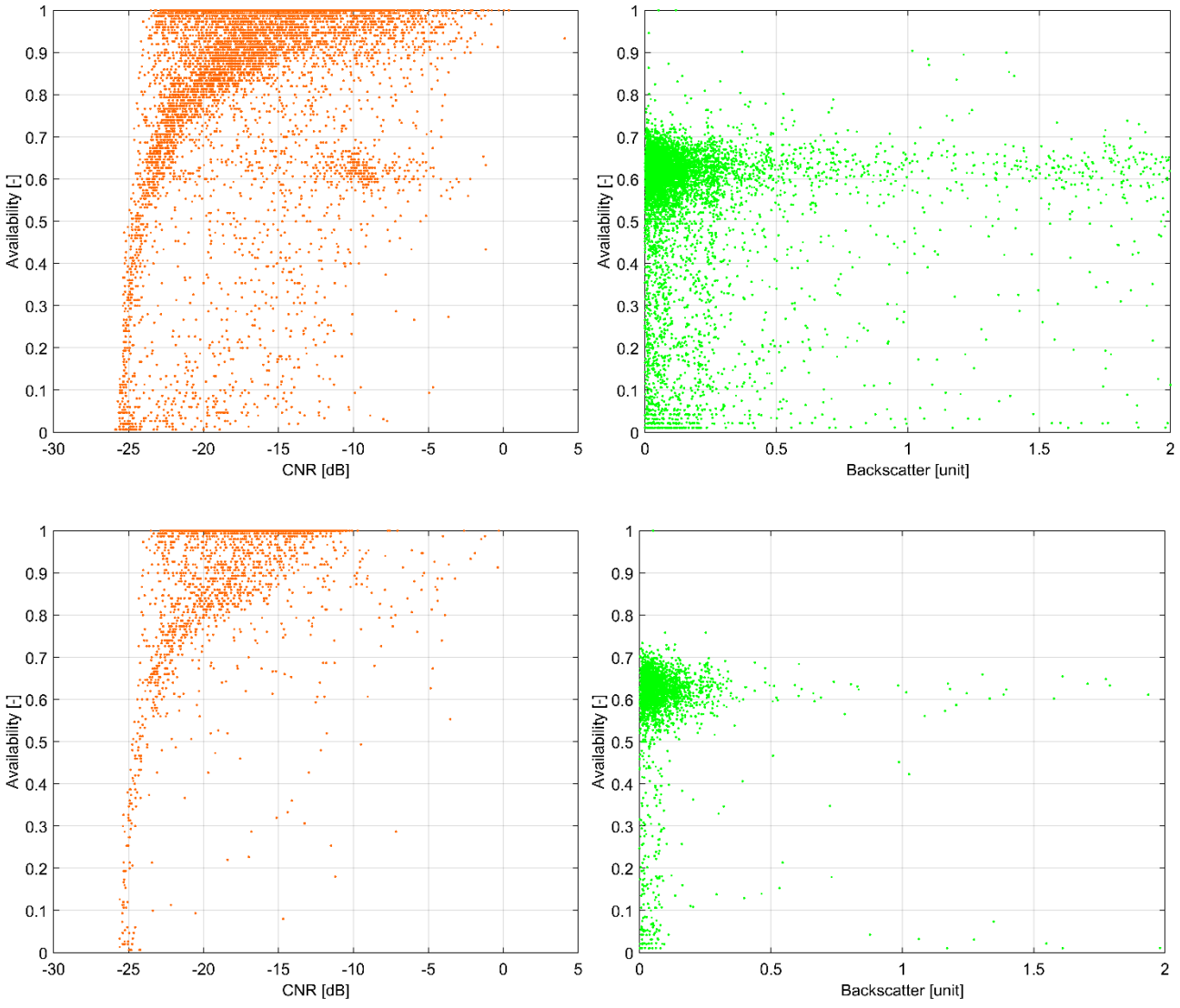

Figure 24. Lidar LOS availability as a function of mean CNR/backscatter. Left: 4BWI (LOS 3). Right: ZDM (LOS 12). Top: for all sectors. Bottom: for the site calibration sector.

For the 4BWI, the LOS availability drops rapidly for CNR below -20dB approximately. Above -20dB, there is no clear dependence between availability and CNR. We have therefore chosen to apply a filter on both parameters (CNR and availability) for each LOS. For the ZDM, the LOS availability is usually contained between 0.5 and 0.7, and there is no clear dependence between availability and backscatter.

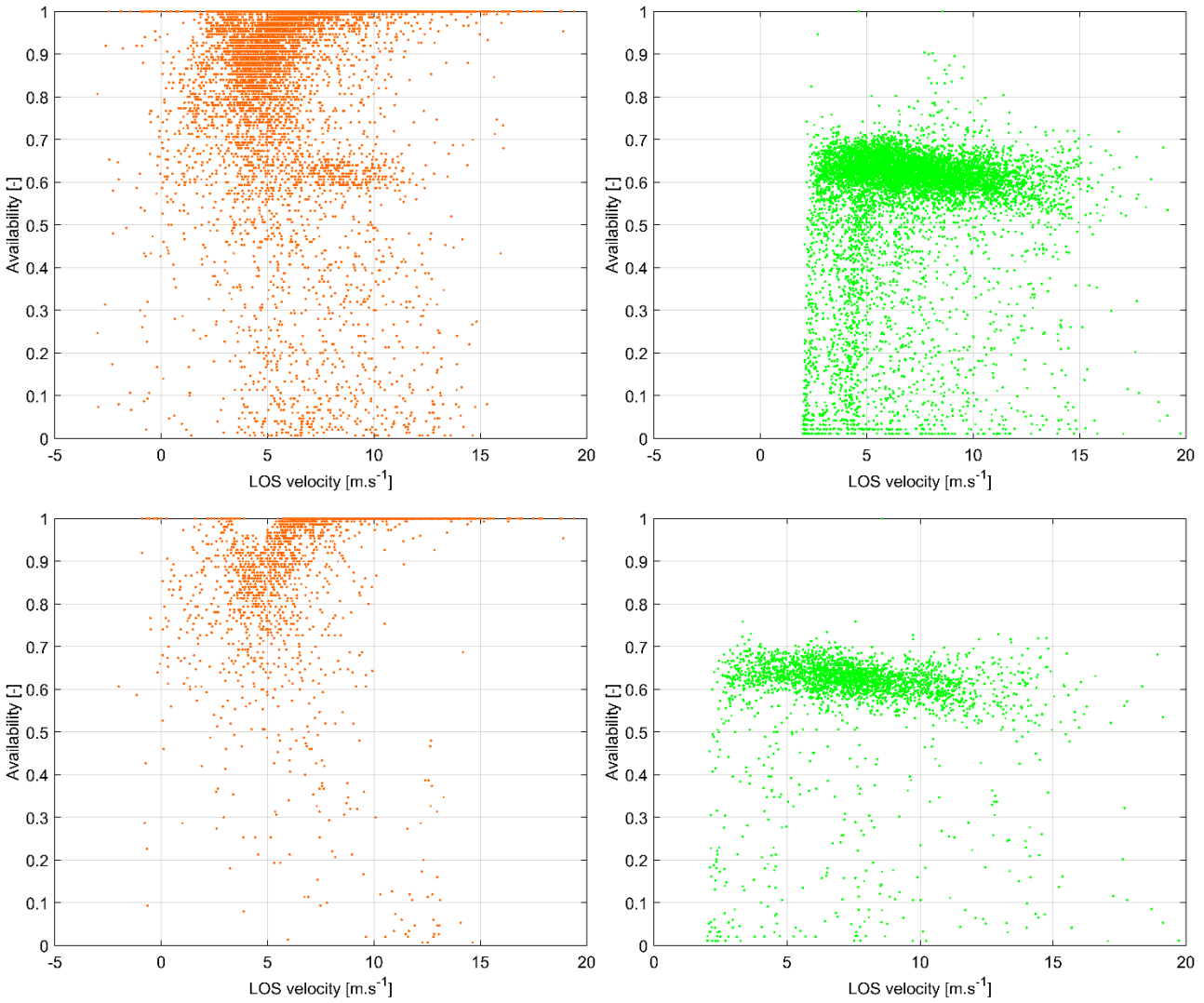

Figure 25. Lidar LOS availability as a function of LOS velocity. Left: 4BWI (LOS 3). Right: ZDM (LOS 12). Top: for all sectors. Bottom: for the site calibration sector.

For the 4BWI, there is a small tendency of the availability to increase with LOS velocity. This is due to the increase in turbine rotor speed, allowing the beam to get through the rotor more often. For ZDM, the tendency is opposite. Indeed, the combination of very high measurement frequency of the ZDM and higher rotor speed has the consequence that the blades block the lidar beam more often.

This shows that the dependency of the LOS availability on the rotor speed is directly related to the ratio of time scales between lidar measurements (1sec and 20ms for 4BWI and ZDM respectively) and the rotor rotational speed (approximately or 15-20 rpm corresponding to a timescale of 3 secs).

It is also clear that the LOS availability depends on the beam and thus on the position of the lidar itself on the nacelle: the availability is higher for LOS pointing upwards (LOS 0 and 1 for 4BWI, LOS 7 and 42 for ZDM) than downwards (LOS 2 and 3 for 4BWI; LOS 31 and 37 for ZDM). In the Hill of Towie campaign, both lidars were placed for practical reasons close to the rotor (<3m), which is not ideal as it yields frequent blade blockage.

The filters applied on the availability were therefore chosen as a compromise to ensure high quality data but not to discard the low wind speed range, which is necessary for the power curve measurement.

5.3 Data filtering

The filtering of the 10-minute data was performed according to the following criteria:

- Time filter: start time is 2017-07-30 09:30. Data acquired prior to this date where the 4BWI was not powered adequately are rejected.
- Turbine yaw between 230° and 280° (site calibration sector);
- Wind direction measured by ZP300 lidar @58.5m agl. between 230° and 280°;
- Turbine status: shutdown duration equal to 0 sec (maximum value is 600 secs);
- Nacelle lidars
    - 4BWI, for all four LOS at each selected range
        - LOS availability > 70% at each LOS and each range;
        - Average CNR > -23 dB;
        - Inclinometers availability > 0.9;
        - (extra) hard target filter: with $\Delta CNR_i = max\,(CNR_i) - avg(CNR_i)$ the amplitude of CNR values during one period, if $\Delta CNR_i > avg\left(\Delta CNR_j\right)_{j \neq i} + 15dB$ then the 10-minute period is filtered out.
    - ZDM lidar:
        - LOS availability > 40% at each LOS and each range;
        - Number of attempts (“count”) to measure an azimuthal sector > 80.

The final dataset is obtained by joining (same time periods) the filtered datasets corresponding to the wind field reconstruction (see Chapter 6):

- Using the “wind” model (see Section 6.2.1) and both the 4BWI and ZDM measurements at the 208m range;
- Using the combined “wind-induction” model (see Section 6.2.2) and both the 4BWI and ZDM measurements at three ranges close the turbine rotor – respectively 48m, 64m and 85m lidar ranges.

The detailed analysis of the filters and their impact on data selection are presented in Table 9. The main observations from this analysis are that:

1) About 30% of the data is within the site calibration sector, both in terms of turbine yaw position and wind direction as measured by ZP300;
2) If the 4BWI had been powered adequately from the data of installation (5th July), the unfiltered datasets would contain 1/3 more data (26.9% of data removed by time filter in ZDM).
3) Looking at each individual lidar case, the lidar filters discard (sequential filtering)
    a. for the 4BWI, 3% and 5% respectively for the wind and wind-induction models;
    b. for the ZDM, 5% and 6% respectively for the wind and wind-induction models;
4) The joining of all datasets (two lidars with two different reconstruction models each) removes 8% and 4% more data for the 4BWI and ZDM respectively (about 1/3 of what was left before joining).

Table 9. Analysis of data filters for the 4-beam Wind Iris and Zephir Dual mode lidars.

	4-beam Wind Iris						
	Individual filtering			Sequential filtering			All data
	Valid data	Filtered data		Valid data	Filtered data		
	[-]	[-]	[%]		[-]	[%]	[-]
Time filter	9673	0	0,0%	9673	0	0,0%	9673
Turbine yaw	3037	6636	68,6%	3037	6636	68,6%	
Turbine status	8801	872	9,0%	2589	7084	73,2%	
Wind direction	3127	6546	67,7%	2281	7392	76,4%	
	using wind model @208m range						
LOS availability	7187	2486	25,7%	2084	7589	78,5%	
CNR	8240	1433	14,8%	2053	7620	78,8%	
(extra) Hard target	9613	60	0,6%	2038	7635	78,9%	
Inclinometers avail.	8913	760	7,9%	2038	7635	78,9%	
	using wind-induction model @48,64,85m ranges						
LOS availability	7059	2614	27,0%	1863	7810	80,7%	
CNR	7449	2224	23,0%	1712	7961	82,3%	
(extra) Hard target	9649	24	0,2%	1707	7966	82,4%	
Inclinometers avail.	9050	623	6,4%	1707	7966	82,4%	
Joining datasets	-	-	-	943	8730	90,3%	
Result	943 (9,7 % valid data)						
	ZephIR Dual Mode						
	Individual filtering			Sequential filtering			All data
	Valid data	Filtered data		Valid data	Filtered data		
	[-]	[-]	[%]		[-]	[%]	[-]
Time filter	9611	3539	26,9%	9611	3539	26,9%	13150
Turbine yaw	3953	9197	69,9%	3043	10107	76,9%	
Turbine status	12161	989	7,5%	2597	10553	80,3%	
Wind direction	4227	8923	67,9%	2290	10860	82,6%	
	using wind model @208m range						
LOS availability	6933	6217	47,3%	1781	11369	86,5%	
Count LOS attempts	9940	3210	24,4%	1583	11567	88,0%	
	using wind-induction model @48,64,85m ranges						
LOS availability	9469	3681	28,0%	2035	11115	84,5%	
Count LOS attempts	8703	4447	33,8%	1536	11614	88,3%	
Joining datasets	-	-	-	943	12207	92,8%	
Result	943 (7,2 %)						

Chapter 6

6 Wind field reconstruction

The wind field characteristics (hub height horizontal wind speed, vertical shear, yaw misalignment, etc) were reconstructed using the model-fitting method described in [4]. The method was adapted in order to account for the terrain complexity by integrating a terrain (elevation) correction into the wind field reconstruction algorithms.

6.1 Hub coordinate system

The wind field reconstruction is performed in this study in the hub coordinate system (CS).

The hub CS $(\mathcal{H}, \overrightarrow{x_{\mathcal{H}}}, \overrightarrow{y_{\mathcal{H}}}, \overrightarrow{z_{\mathcal{H}}})$ is a right-handed Cartesian orthonormal system with its origin at the center of the rotor plane (longitudinal direction). The x-axis of the hub CS is closely aligned with the rotor axis, which in reality is inclined by some degrees. The x-axis points downwind (i.e. measurements located upstream of the rotor plane correspond to negative $x_{\mathcal{H}}$ coordinates). $(\overrightarrow{x_{\mathcal{H}}}, \overrightarrow{y_{\mathcal{H}}})$ defines a horizontal plane.

6.2 Models

Two reconstruction models were used in this analysis, they are the same as those applied in [4].

6.2.1 Wind model

The wind model used in this study makes three assumptions on the spatial variability of the wind field.

First, it assumes that the wind vector $\vec{V} = [u,\ v,\ w]$ is horizontal, i.e. that the vertical wind component w is zero. Thus the wind vector becomes two-dimensional ($\vec{V} = [u,\ v,\ 0]$). Here, u and v are the longitudinal and transverse wind speeds, respectively.

Secondly, it assumes that the wind speed $V = \sqrt{u^2 + v^2}$ is the horizontally homogeneous (the same at a given height above terrain). The wind model characterises the vertical shear with the power law and a shear exponent. Third, the relative wind direction θ_r – also called yaw misalignment – is considered homogeneous.

The wind model is parameterized by three wind characteristics: the hub height wind speed V_{hub}, the relative wind direction θ_r and the shear exponent α. It is defined as follow:

$$V(z_{\mathcal{H}}) = V_{hub}\left(\frac{z_{\mathcal{H}} + H_{hub}}{H_{hub}}\right)^{\alpha},$$

where V_{hub} is the wind speed at hub height $(z_{\mathcal{H}} = 0)$ and α is the shear exponent. And we have:

$$u(z_{\mathcal{H}}) = V(z_{\mathcal{H}})\cos\theta_r\ ;\ u(z_{\mathcal{H}}) = V(z_{\mathcal{H}})\sin\theta_r.$$

For each 10-minute period, the three wind characteristics are fitted to the nacelle lidar LOS speeds.

This wind model was fitted to the nacelle lidars LOS speeds measured at 208m upstream, so that the hub height wind speed could be compared to the ZP300 wind speed measurement.

6.2.2 Wind-induction model

The wind-induction model includes the variation (deceleration) of the wind speed with the distance upstream from the turbine rotor.

The induction model (one-dimensional) we used results from the vortex-sheet theory (vortex cylinder) applied to the actuator disk model of a wind turbine rotor. The analytical expression for the induction model is given by:

$$u\left(\xi = \frac{x_{\mathcal{H}}}{R_{rot}}\right) = u_{\infty}\left(1 - a_{ind}\left[1 + \frac{\xi}{\sqrt{1+\xi^2}}\right]\right).$$

Here, a_{ind} is the axial induction factor (directly related to the thrust forces exerted by the turbine on the wind flow), u_{∞} is the longitudinal component of the free stream wind speed – infinitely far away from the rotor –, R_{rot} is the rotor radius and $\xi = \frac{x_{\mathcal{H}}}{R_{rot}}$ is the non-dimensional longitudinal distance from the rotor plane.

The induction model is combined with the wind model by assuming that only the longitudinal wind speed contributes to the generation of thrust. Consequently the transverse wind speed v remains constant when approaching the rotor. The final expression for the model flow field wind speed thus becomes:

$$V(x_{\mathcal{H}}, z_{\mathcal{H}}) = V_{\infty}\left(\frac{z_{\mathcal{H}} + H_{hub}}{H_{hub}}\right)^{\alpha} = \left(\frac{z_{\mathcal{H}} + H_{hub}}{H_{hub}}\right)^{\alpha}\sqrt{u_{\infty}^2\left(1 - a_{ind}\left[1 + \frac{\xi}{\sqrt{1+\xi^2}}\right]\right)^2 + v_{\infty}^2},$$

where $V_{\infty} = \sqrt{u_{\infty}^2 + v_{\infty}^2}$ is the free stream wind speed at hub height, θ_r is the relative wind direction (or yaw misalignment), $u_{\infty} = V_{\infty}\cos\theta_r$ and $v_{\infty} = V_{\infty}\sin\theta_r$ are the axial and transverse components of the free stream wind vector.

For each 10-minute period, the four wind characteristics (V_{∞}, θ_r, α, a_{ind}) are fitted to the nacelle lidar LOS speeds. The wind induction model was applied to simultaneous measurements at three nacelle lidar ranges (upstream distance): 48, 64 and 85m, corresponding approximately to 0.55, 0.75 and 1.0 rotor diameter.

Note: the two models can be adapted in order to include extra parameters such as veer or an inflow angle. Inflow angles (i.e. vertical wind components) can be significant in complex terrain. However, it is clear that the retrieval of the inflow angles is very inaccurate for these two nacelle lidars: the contamination of the lidar LOS velocity is very insufficient since the lidar beams create a small angles (here <10°) with the horizontal plane.

6.3 Terrain correction

Furthermore, both the wind and wind-induction models were applied with two different assumptions:

1) the terrain height variations between the lidar measurement position and the turbine position were ignored and the model fitting was assuming that the lidar axis (which, together with the lidar geometry, defined the height of each LOS above the ground) was at the same height (hub height + height above nacelle) above the ground at any distance upstream of the turbine;

2) The terrain height variation was accounted for in the model fitting. The actual height of the each LOS, at each measurement distance, was calculated based on an elevation map of the terrain around the turbine (Source: SRTM dataset 1 arc-second resolution (~30m)).

The height of the LOS relative to the ground affects directly the fitting to the vertical shear parameter (see Sections 6.2.1 and 6.2.2). The terrain correction was therefore implemented by using terrain data as extra inputs to the fitting routine. Figure 26 displays a flow chart describing the model-fitting wind field reconstruction methodology (more explanations can be found in [4]) and showing at which step of the algorithm the terrain correction was integrated.

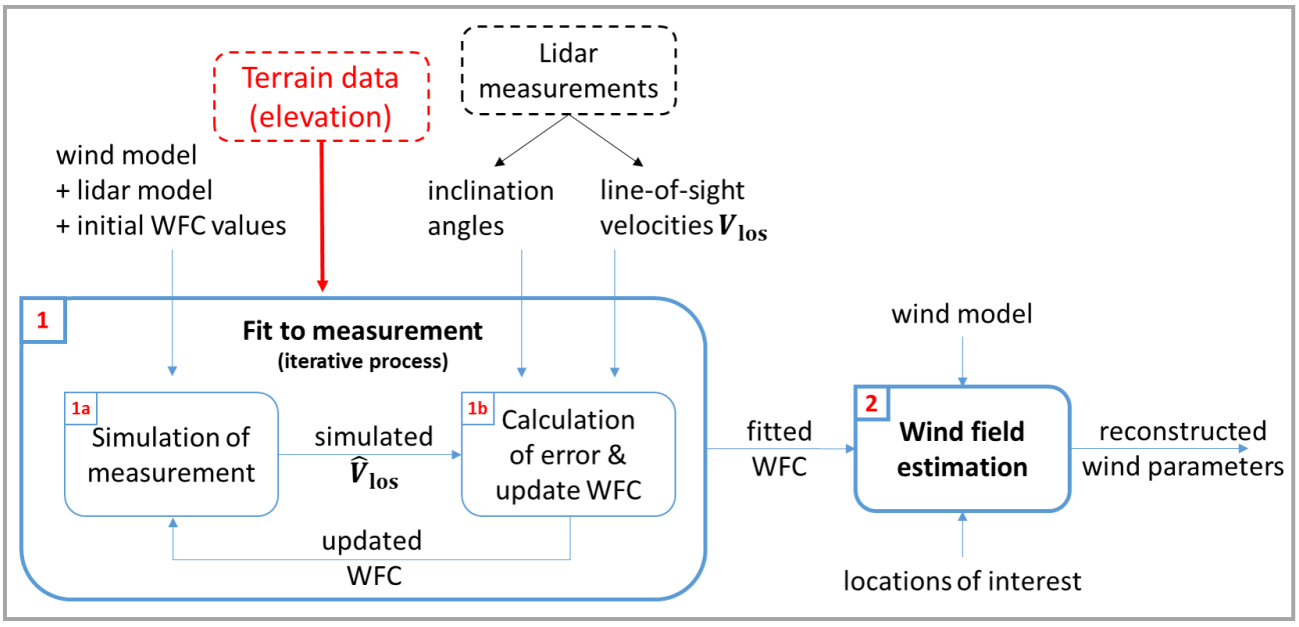

Figure 26. Flow chart of the model-fitting Wind Field Reconstruction methodology including the terrain correction.

The principles of the terrain correction algorithm are as follows:

- Elevation profiles are extracted from the map at the center 10°-wide direction sectors. The resulting 36 elevation profiles start at the turbine position. We chose to use a distance up to approximately 500m.
- For each 10-minute period
    - Take the yaw direction from the SCADA;
    - Find the direction sector in which each used LOS lies. Note: this means the terrain correction is not a single elevation difference for all beams, but beam dependent (typically, beams on the "left" and "right" from the lidar point of view are corrected independently).
    - Find the elevation difference Δz at the measurement locations (i.e. horizontal distance along the beam direction). Note: hence, in the case where several ranges are used (e.g. with the wind-induction model), the terrain correction is different at each range.
- Correct the vertical coordinate $\mathrm{z}_{\mathcal{H}}$ (hub CS) by computing $\mathrm{z}_{\mathcal{H},\mathrm{corr}} = \mathrm{z}_{\mathcal{H}} + \Delta z$.
- In the wind model (combined wind-induction, respectively), replace $\mathrm{z}_{\mathcal{H}}$ by $\mathrm{z}_{\mathcal{H},\mathrm{corr}}$.

Chapter 7

7 Results on horizontal wind speed

This chapter shows the results of the wind speed estimate from both the 4BWI and ZDM nacelle lidar systems. For each lidar, both the reconstructions with the wind model and the wind-induction model (see resp. sections 6.2.1 and 6.2.2 in chapter 6) are demonstrated. In each case, the lidar wind speed at hub height is compared to the ZP300 wind speed measurements (at the 58m range, with or without correcting for the site calibration depending on cases) and a linear regression is performed. The analysis is based on the 10-minute average values. For proper comparison of the results from the different methods, the exact same dataset has been used (see filtering in 5.3) throughout the whole analysis.

See also Annex B and Annex C for the results where each lidar dataset is analysed independently.

7.1 Wind model

The wind model was fitted to the lidar measurements at 208m – close to the distance from the turbine to the ZP300 (measured to 220m, see section 2.2.2). Neither the ZP300's nor the nacelle lidars' measurements were here corrected with the site calibration since all three systems measured at a similar distance (208m for nacelle lidars, 220m for ZP300) from the turbine.

Figure 27 shows the comparison between the 4BWI (left) and ZDM (right) lidar estimates and the ZP300 measurements. The terrain correction implemented in the WFR was used. The nacelle lidar horizontal wind speed is:

- For the 4BWI, 2.2% higher than the ZP300 measurements on average, with a coefficient of determination of R^2=0.982;
- For the ZDM, 0.3% higher than the ZP300 measurements on average, with a coefficient of determination of R^2=0.985;

Figure 28 shows the same comparison except that the estimation of the horizontal wind speed from the nacelle lidars does not account for the terrain height variations relative to the lidar optical axis (equivalent to assuming flat terrain). Here, the two nacelle lidars overestimate the wind speed by 6% and 4.3%, respectively for 4BWI and ZDM, with a higher scatter. As the terrain difference at this distance is about 15m, this result is not surprising but demonstrates the ability of the developed terrain correction to improve the nacelle lidar estimates (Figure 27) with a satisfying level of accuracy. It also shows how critical it can be for nacelle lidars to feature carefully implemented terrain corrections. Such a terrain correction shall be made mandatory in the future power performance testing standards (ongoing work IEC 61400-50-3 document by TC88). Naturally, it is desirable to use the terrain map with the highest resolution and quality (to be controlled) possible.

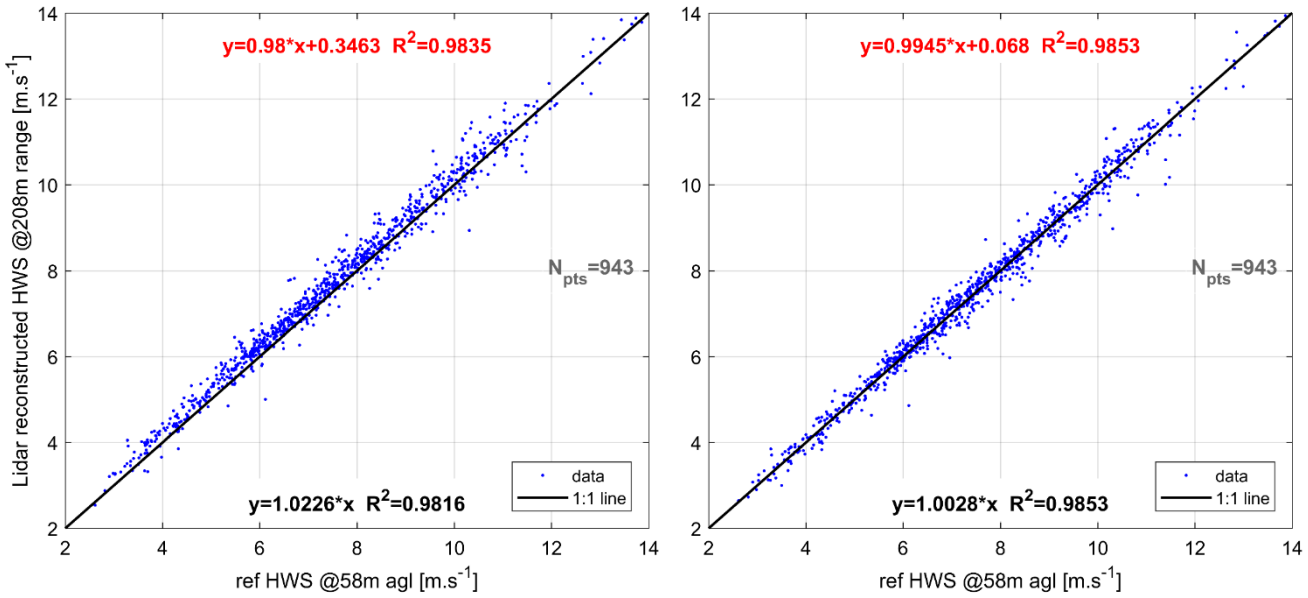

Figure 27. Comparison of the nacelle lidar wind speed estimates using the wind model at 208m with the ground-based ZP300 profiling lidar measurements. The actual height of the LOS relative to the terrain is accounted for (the terrain correction is used in the reconstruction). Left: 4BWI. Right: ZDM.

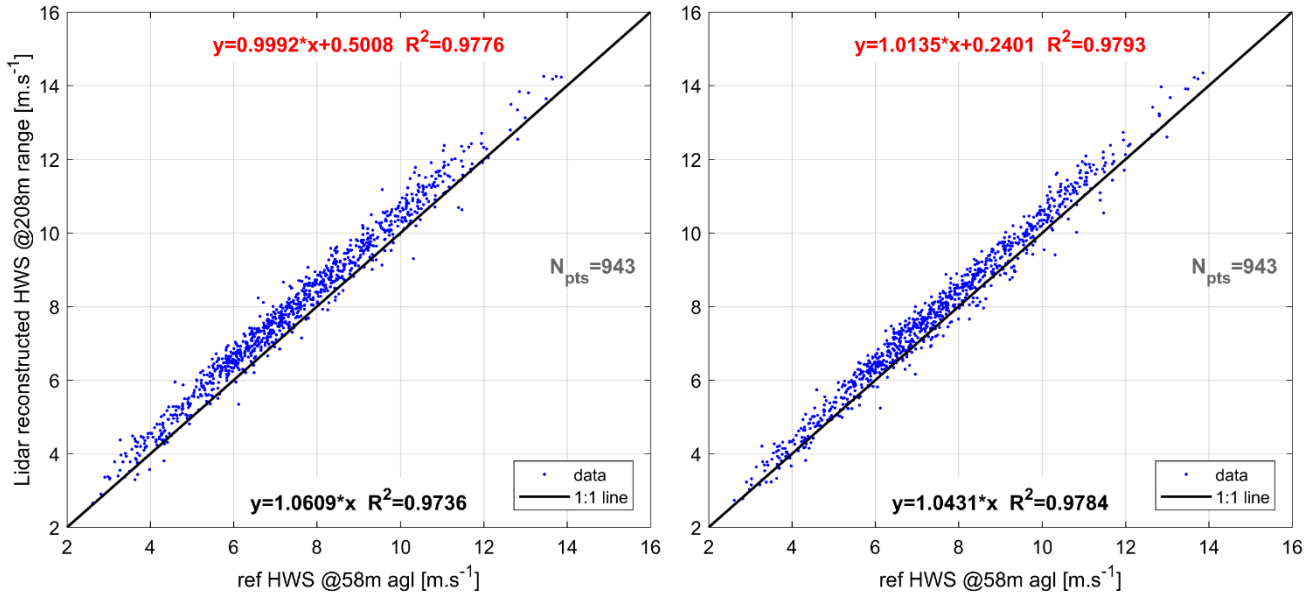

Figure 28. Comparison of the nacelle lidar wind speed estimates using the wind model at 208m with the ground-based ZP300 profiling lidar measurements. The terrain variations are ignored (no terrain correction used in the reconstruction). Left: 4BWI. Right: ZDM.

7.2 Wind induction model

7.2.1 Results

Contrary to the simple wind model, the wind-induction model is fitted to lidar measurements within 48m to 85m (0.5 to $1D_{rot}$) upstream of the turbine. The effect of the terrain on the flow within this relatively short distance is expected to be smaller than the effect at 208m upstream as the terrain variations are smaller and with it the flow evolution.

In this case, we assume that the wind flow within 1D of the rotor is identical to the wind at the turbine location if there was no turbine except for the rotor induction effect. This effect is accounted for in the wind-induction model. Therefore the free stream wind speed estimated with this reconstruction should be compared to the wind speed expected at the turbine location if there was no turbine. Such wind speed is, in principle, given by the reference wind speed measurements (from the ZP300) corrected with the site calibration.

From the model fitting method we can consider two types of wind speeds for this comparison:

1) the "free wind speed" at hub height which is a direct output of the fit (V_∞ in section 6.2.2). Note this is an artificial wind speed that cannot be measured directly. In this case the free wind speed provided from the lidar measurements and the reconstruction algorithm is compared to the ZP300 wind speed corrected with the site calibration (Table 1). Again, in each case, the models were fitted with (Figure 29) and without (Figure 30) terrain correction.

2) the wind speed estimated at hub height at 208m upstream, using the wind-induction model and the fitted values for the four model parameters (free wind speed, shear, yaw misalignment and induction factor). This remains an artificial wind speed (that cannot be measured directly). Since the terrain complex effects on the flow are ignored, this manipulation only enables us to account for the fact that at 208m upstream the flow is not truly free of the rotor induction effect. Such comparison implicitly assumes that the turbine induction affects the nacelle lidars and ZP300 measurements in the same manner – which is not the case since the yaw is not always aligned with the turbine-ZP300 direction.

Figure 29 shows the comparison between the 4BWI (left) and ZDM (right) lidar V_∞ estimates and the ZP300 measurements. The terrain correction implemented in the WFR was used. The ZP300 measurements were corrected with the site calibration (see [7]). The nacelle lidar free stream wind speed is:

- For the 4BWI, 0.4% higher than the ZP300 measurements on average, with a coefficient of determination of R^2=0.978;
- For the ZDM, 1.1% lower than the ZP300 measurements on average, with a coefficient of determination of R^2=0.979;

Figure 30 shows the same comparison except that the terrain height variations relative to the lidar optical axis are not accounted for (equivalent to assuming flat terrain). Here, the two nacelle lidars free wind speed estimates are 1.2% higher and 0.2% lower, respectively for 4BWI and ZDM, with an almost identical scatter. As the terrain difference at this distance is small, the terrain correction only affected the lidar measurements by approximately 0.8%.

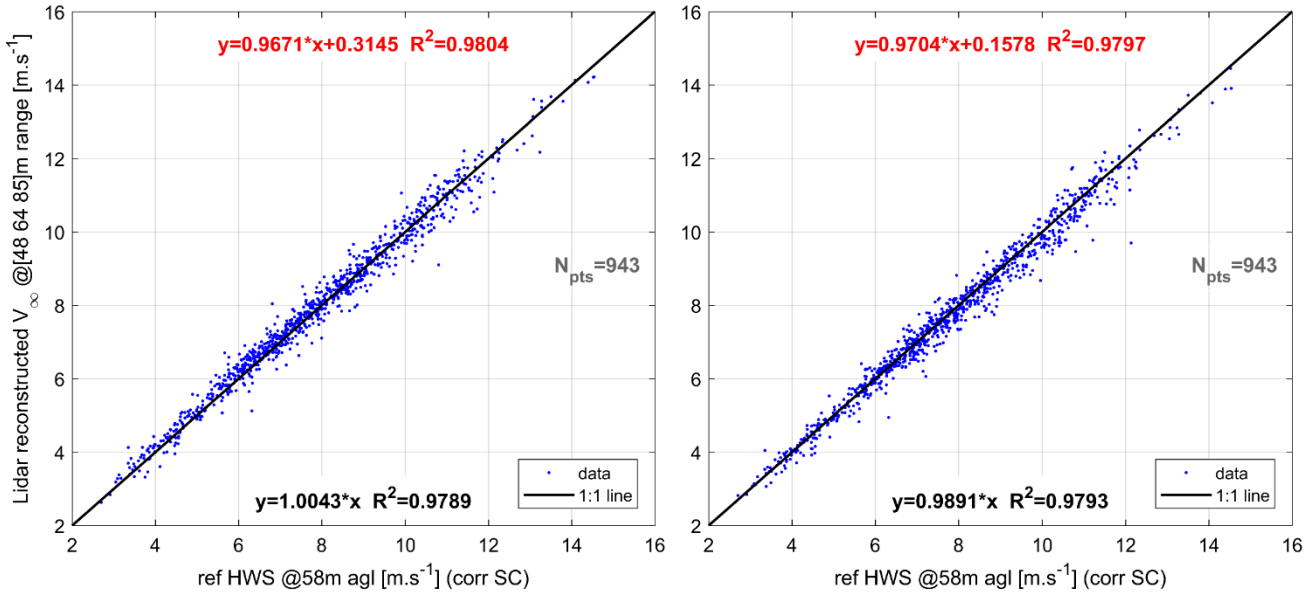

Figure 29. Comparison of the nacelle lidar free wind speed estimates using the wind-induction model with the ground-based ZP300 profiling lidar measurements. The actual height of the LOS relative to the terrain is accounted for (the terrain correction is used in the reconstruction). Left: 4BWI. Right: ZDM.

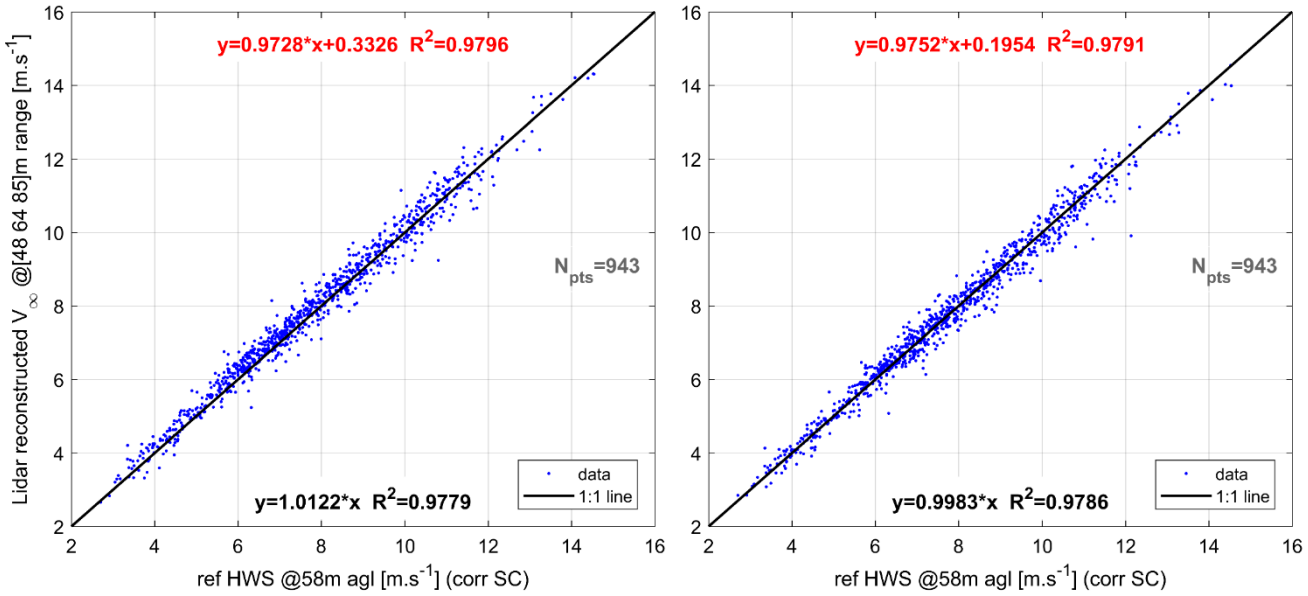

Figure 30. Comparison of the nacelle lidar free wind speed estimates using the wind-induction model with the ground-based ZP300 profiling lidar measurements. The terrain variations are ignored (no terrain correction used in the reconstruction). Left: 4BWI. Right: ZDM.

7.2.2 Discussion on the site calibration and ground-based lidar wind measurements

The (original) site calibration used to correct the ZP300 lidar measurements of wind speed was performed six years prior to this campaign, in 2011.

The site calibration campaign was conducted with compliance to the former edition of the IEC 61400-12-1 ([5]). This means the site calibration made use of two meteorological masts, one placed at the turbine location, and one reference mast. During the 2017 campaign, the effect of the site calibration (Table 1) on the selected dataset is an increase by approximately 4% on average on the wind speed due to the distribution of wind direction (Figure 11) concentrated mainly in the 230-260° sector.

A numerical site calibration was performed in order to compare to the measured site calibration. For the measurement sector of 230-280°, the numerical site calibration showed neither a speed-up nor a speed–down, as shown in Figure 31. The nearly invariant speed ratios in the numerical site calibration may be explained by the coarse terrain map, and to the lack of a valid roughness map for this site.

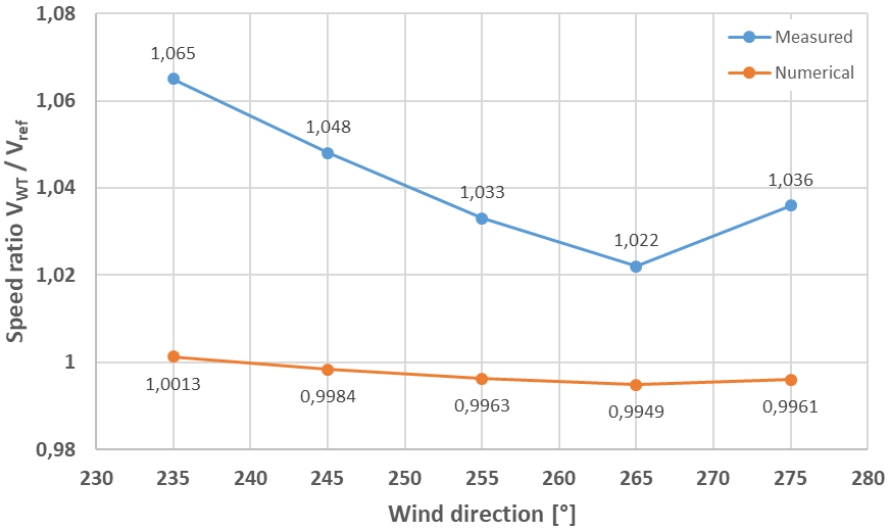

Figure 31. Numerical vs. measured site calibration results.

The ZP300 ground-based lidar used in this analysis as reference instrument was placed at the exact same location as the mast. However, the measuring principles of the ZP300 lidar for wind speed retrieval assumes horizontal flow homogeneity. These assumptions are reasonable in flat terrain but much less in complex sites, see [11] (they are formally always violated in any case). Complex flow corrections attempts have been made using simple (basic) CFD models – see [12] for ZP300 profilers, or [13] for WindCube profilers – but were not used in this campaign. Such CFD-based corrections should be considered carefully as they have been shown to improve the results only in some situations only ([12], [14]). In not-so-uncommon situations they can degrade the quality of the wind speed estimates.

In the case of the Hill Of Towie 2017 campaign, the ZP300 lidar beam probed locations separated by a rather small horizontal distance of approximately 60m (58m range/height with 60° full cone angle). On such a short separation, the variability of the wind flow is less likely to present large inhomogeneities providing reasonable confidence in the reference wind speed measurements from ZP300.

Chapter 8

8 Results on secondary wind characteristics

This chapter presents succinctly the results on "secondary" wind characteristics – as the primary interest in PCV in the wind speed – estimated from the two nacelle lidars measurements. These secondary characteristics are the wind shear and the wind yaw misalignment (also called relative wind direction) at hub height.

In this chapter, all the results presented made use of the terrain correction algorithm implemented in the wind field reconstruction codes (Figure 26). See also Annex B and Annex C for the results where each lidar dataset is analysed independently.

8.1 Vertical wind shear

The vertical wind shear is assumed to follow a power law. The nacelle lidar shear exponent estimate has been compared to the shear exponent derived from fitting the wind speed measured by the ZP300 lidar at 11 heights. Note that in some periods, the ZP300 was unable to provide wind speed at all eleven heights. As a consequence, the two plots contain 887 data points (instead of 943).

8.1.1 Wind model

Figure 32 shows the results where the wind model is fitted to the lidar measurements at 208m. On average, the lidar estimates of the wind shear exponent are within 4% of the ZP300 fitted values, with linear coefficients of determination R^2 of 0.73 and 0.85 for the 4BWI and ZDM respectively.

The lower observed scatter in the ZDM-estimated shear exponent estimates can be attributed to the fact that three different heights are probed – vs. two heights for the 4BWI – and with a larger span (vertical opening angle between the bottom and top pairs of beams of respectively 10° for the 4BWI and approximately 20° for the ZDM, see measurement trajectories in Figure 4 and Figure 5).

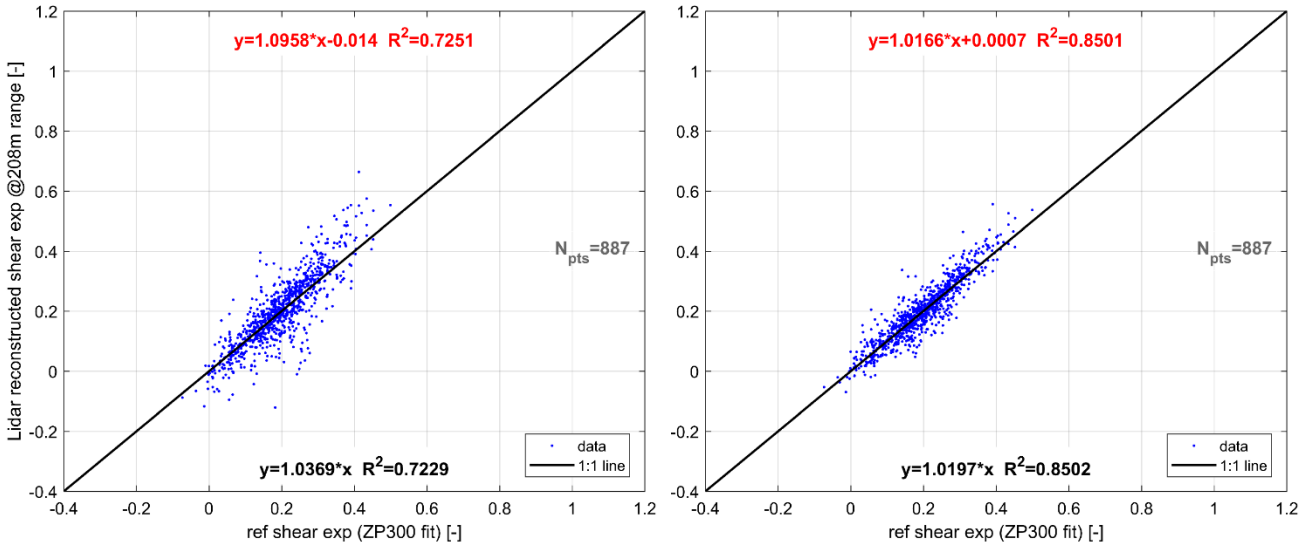

Figure 32. Comparison of the nacelle lidar wind shear estimates using the wind model at 208m with the ground-based ZP300 profiling lidar measurements. The actual height of the LOS relative to the terrain is accounted for (the terrain correction is used in the reconstruction). Left: 4BWI. Right: ZDM.

8.1.2 Wind-induction model

Figure 33 shows the results where the wind-induction model is fitted to lidar measurements within 48m to 85m (0.5 to 1D_{rot}) upstream of the turbine.

On average, the lidar estimates of the wind shear exponent are 4% lower and 13% higher than the ZP300 fitted values, respectively for the 4BWI and ZDM. The scatter is significantly higher than in the case where the wind model was used (Figure 32), with R^2 values of 0.6 and 0.7. Most likely, the reason for poorer quality in the comparisons are due to the lower span of probed measurement heights (see measurement trajectory in Figure 5), caused by the use of short-range measurements as inputs to the WFR algorithms.

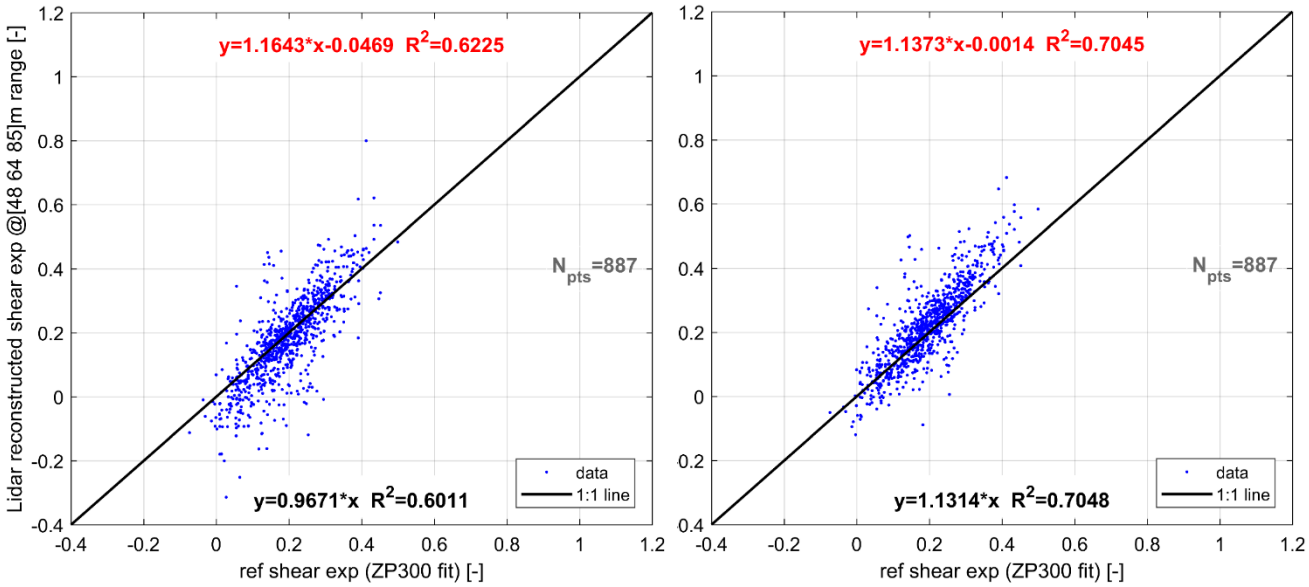

Figure 33. Comparison of the nacelle lidar wind shear estimates using the wind-induction model with the ground-based ZP300 profiling lidar measurements. The actual height of the LOS relative to the terrain is accounted for (the terrain correction is used in the reconstruction). Left: 4BWI. Right: ZDM.

8.2 Yaw misalignment

The wind yaw misalignment is analysed by plotting it as a function of wind speed. A moving bin-averaged trend line was also computed. The yaw misalignment estimates from the two nacelle lidars is directly output by the WFR algorithms, while the "reference" yaw misalignment is taken as the difference between the wind direction measured by the ZP300 lidar @58.5m agl and the turbine yaw position.

8.2.1 Wind model

Figure 34 displays the nacelle lidar-estimated yaw misalignment using the wind model at 208m. For both the 4BWI and ZDM lidar systems, the observed trend and scatter of the yaw misalignment are consistent with the values obtained from the difference between ZP300 wind and SCADA yaw directions.

Overall, this is an excellent result provided that all three lidar systems may have offsets in the direction retrieval due to:

- For the nacelle lidars, the difficulty of aligning the optical centreline to the axis of the rotor;
- For the ground-based lidar, the uncertainty in the North offset input in the configuration of the ZP300 software and used in the wind direction reconstruction.

According to the two nacelle lidars, the turbine yaw misalignment is on average approximately +4°. Note: in verification trials, the SCADA yaw misalignment fed into the turbine controller is commonly considered to require corrections when it exceeds 5°.

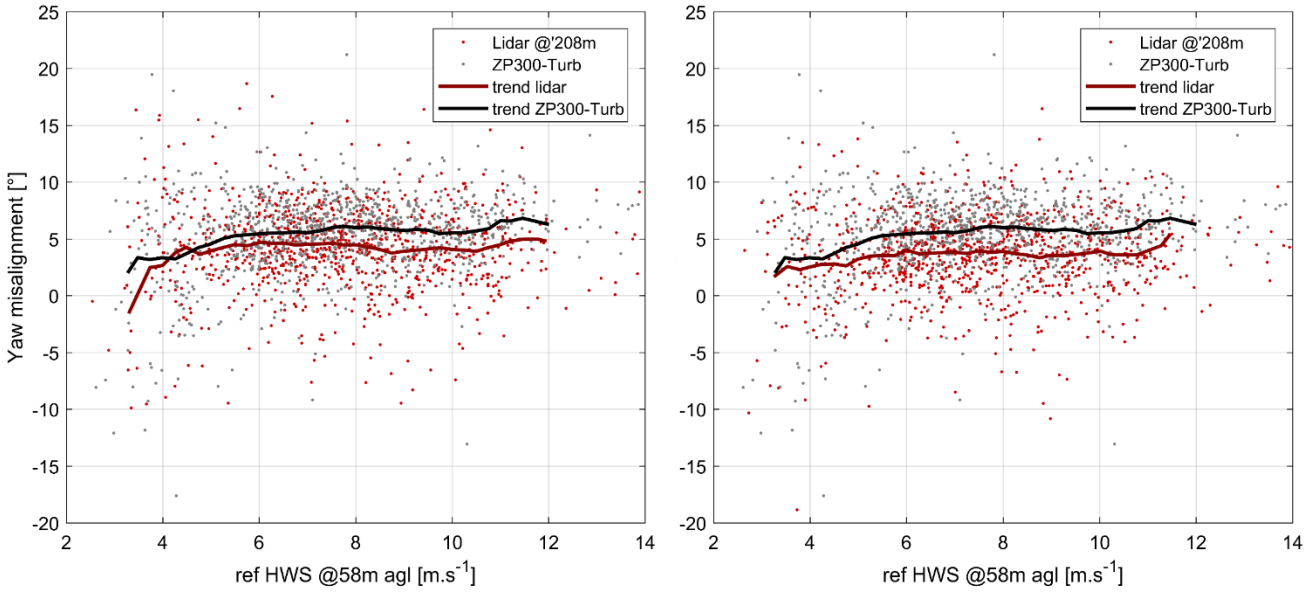

Figure 34. Scatter plots of yaw misalignment estimated from the nacelle lidar wind speed estimates using the wind model at 208m, and using the ground-based ZP300 profiling lidar measurements of wind direction. The actual height of the LOS relative to the terrain is accounted for (the terrain correction is used in the reconstruction). Left: 4BWI. Right: ZDM.

8.2.2 Wind-induction model

Figure 35 displays the nacelle lidar-estimated yaw misalignment using the wind-induction model and lidar measurement at three distances close to the rotor (48m, 64m and 85m). For both the 4BWI and ZDM lidar systems, the observed trend and scatter of the yaw misalignment are also consistent with the values obtained using the ZP300 wind and SCADA yaw directions.

It is worth noting that the scatter in yaw misalignment is lower than when using the wind model (Figure 34). This is another benefit of using short-range nacelle lidar measurements.

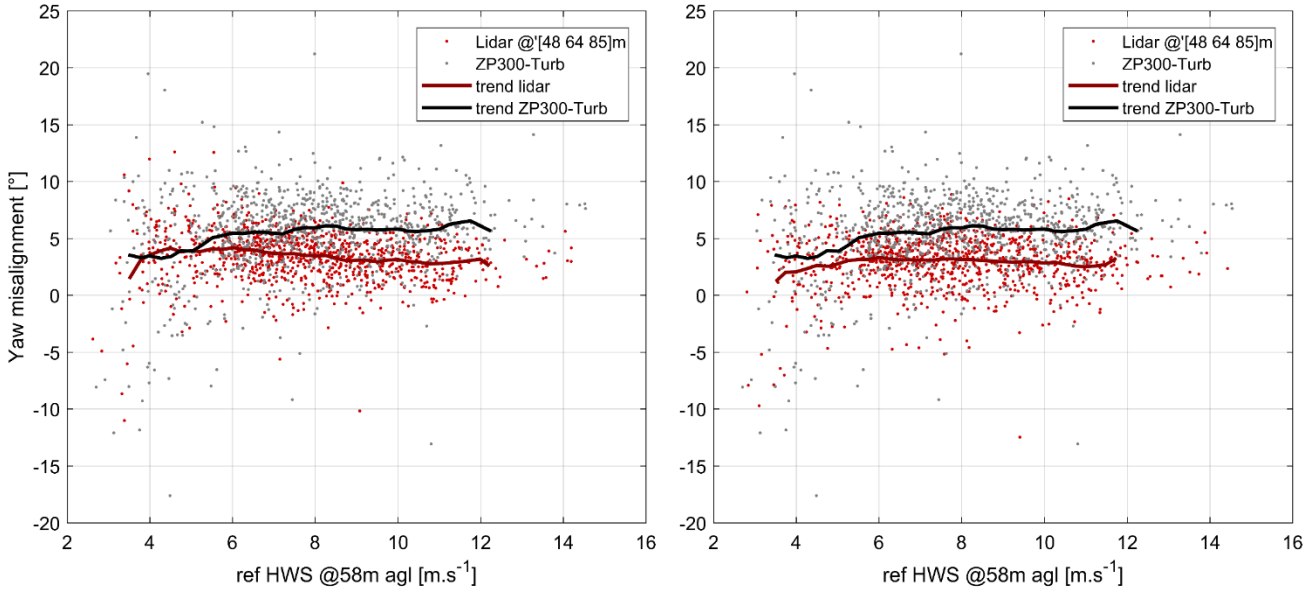

Figure 35. Scatter plots of yaw misalignment estimated from the nacelle lidar wind speed estimates using the wind-induction model, and using the ground-based ZP300 profiling lidar measurements of wind direction. The actual height of the LOS relative to the terrain is accounted for (the terrain correction is used in the reconstruction). Left: 4BWI. Right: ZDM.

Chapter 9

9 Model fitting residuals

The “model adequacy” of the wind and combined wind-induction models is analysed in this chapter using the so-called LOS velocity fitting residuals. The results are presented through histograms of two residual statistics: the mean bias (MB) and the root mean squared error (RMSE). More details and definitions can be found in [2].

Essentially, an “adequate” model shows average MB centered on and close to zero, while the RMSE should be as small as possible. Note that in this chapter, all the results presented made use of the terrain correction algorithm implemented in the wind field reconstruction codes (Figure 26).

9.1 Wind model

Figure 36 and Figure 37 show the distributions of MB and RMSE respectively. Here the wind field reconstruction algorithms employ the wind model and the nacelle lidar measurements at 208m.

The MB is in the order of 5×10^{-4} ms^{-1} for both the 4BWI and ZDM lidars. The distributions are well centered on zero (unbias model). The spread is larger in the case of the ZDM than 4BWI. The RMSE:

- for the 4BWI, takes values up to 0.2 ms^{-1} with an average of approximately 0.05 ms^{-1};
- for the ZDM, takes values up to 0.25 ms^{-1} with an average of approximately 0.08 ms^{-1}.

Here the terrain correction was used. In the cases where it is not applied (graphs not shown), the MB show comparable distributions, while the RMSE values are significantly larger (+0.03 ms^{-1} on average).

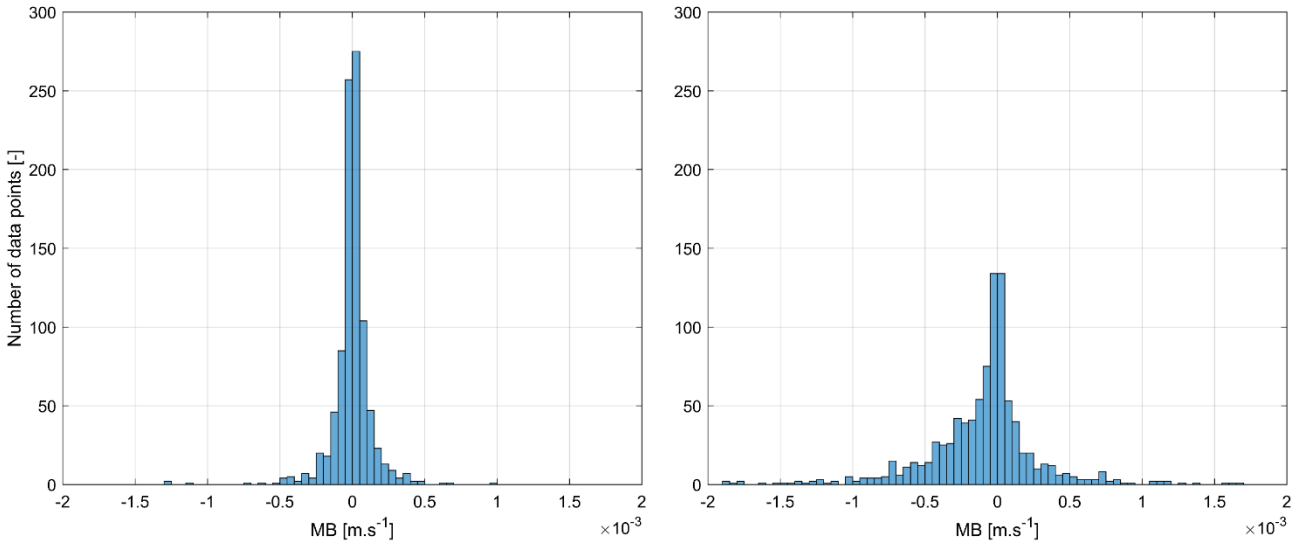

Figure 36. Histograms of mean bias (MB) of LOS velocity residuals, for the case where the nacelle lidar reconstruction uses the wind model at 208m. The actual height of the LOS relative to the terrain is accounted for (the terrain correction is used in the reconstruction). Left: 4BWI. Right: ZDM.

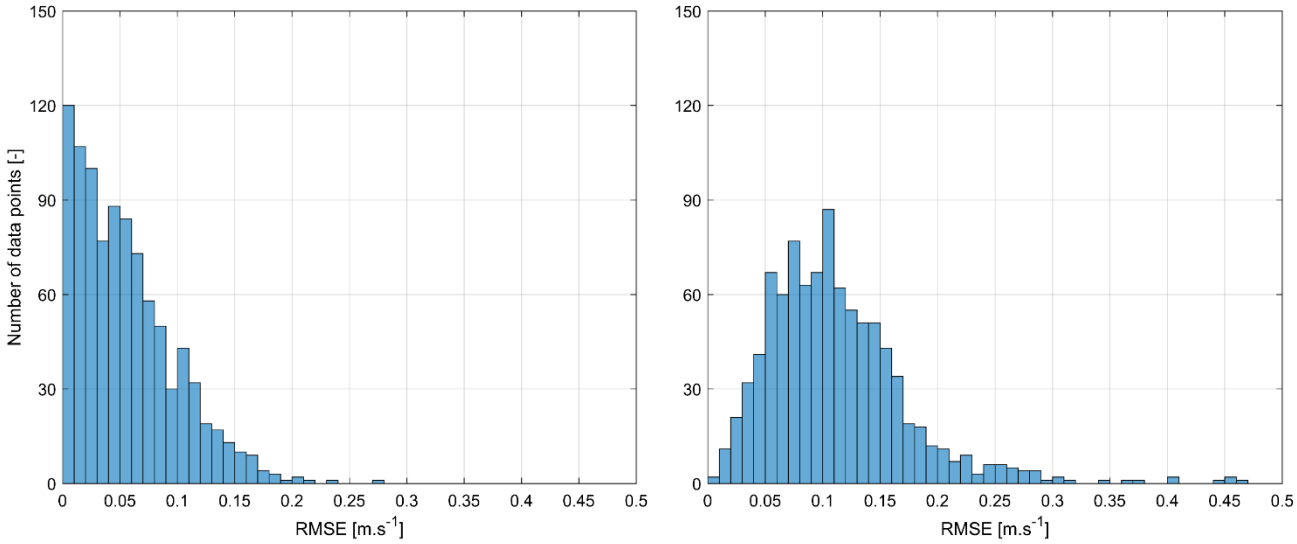

Figure 37. Histograms of root mean squared error (RMSE) of LOS velocity residuals, for the case where the nacelle lidar reconstruction uses the wind model at 208m. The actual height of the LOS relative to the terrain is accounted for (the terrain correction is used in the reconstruction). Left: 4BWI. Right: ZDM.

9.2 Wind-induction model

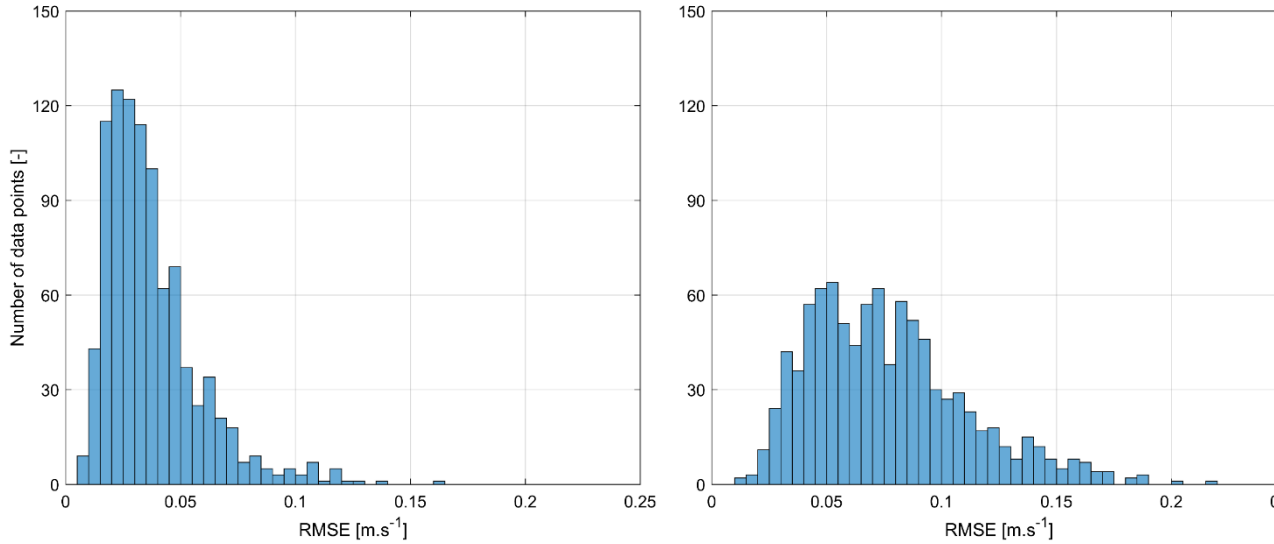

Figure 39 show the distributions of MB and RMSE respectively. Here the wind field reconstruction algorithms employ the combined wind-induction model and the nacelle lidar measurements at three distances close to the rotor (48m, 64m, 85m).

The MB is in the order of 5×10^{-5} ms^{-1} for both the 4BWI and ZDM lidars – i.e. one order of magnitude lower than for the wind model. The distributions are well centered on zero (unbias model). The spread is here again larger in the case of the ZDM than 4BWI. The RMSE is reduced by almost 50% compared to the case where the wind model was used, with:

- for the 4BWI, RMSE values up to 0.1 ms^{-1} with an average of approximately 0.03 ms^{-1};
- for the ZDM, RMSE values up to 0.15 ms^{-1} with an average of approximately 0.06 ms^{-1}.

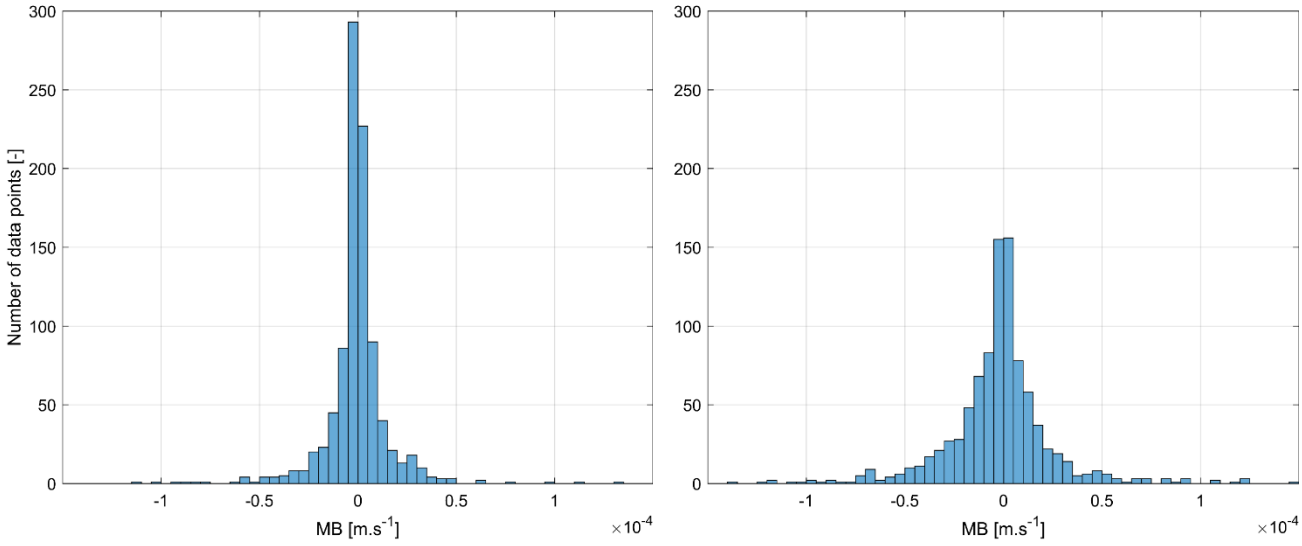

Figure 38. Histograms of mean bias (MB) of LOS velocity residuals, for the case where the nacelle lidar reconstruction uses the wind-induction model. The actual height of the LOS relative to the terrain is accounted for (the terrain correction is used in the reconstruction). Left: 4BWI. Right: ZDM.

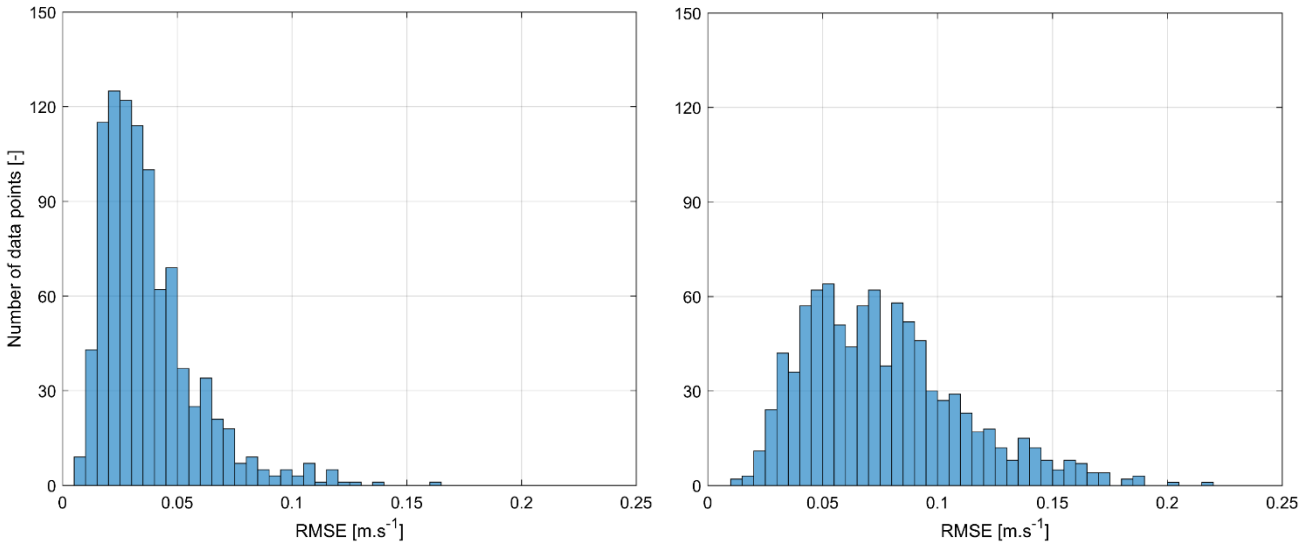

Figure 39. Histograms of root mean squared error (RMSE) of LOS velocity residuals, for the case where the nacelle lidar reconstruction uses the wind-induction model. The actual height of the LOS relative to the terrain is accounted for (the terrain correction is used in the reconstruction). Left: 4BWI. Right: ZDM.

Chapter 10

10 Power curve

This chapter shows the power curves obtained with the wind speed resulting from the different measurement techniques and results presented in Chapter 7: the ZP300 hub height wind speed measurements, the two nacelle lidars (4BWI and ZDM) estimates using the wind model and the wind-induction model.

Once again, note that the 4BWI, ZDM and ZP300 datasets used in this chapter are perfectly concurrent (exact same periods used). See also Annex B and Annex C for the results where each lidar dataset is analysed independently.

10.1 Methods

The results are based on 10-minute averaged data and are presented in power curve scatter plots, bin-averaged power curve and relative annual energy production (AEP).

Those power curves were obtained with the exact same dataset (same 10-minute periods – same wind turbine power, only the wind speed changes depending on the measurement and estimation technique). Note that the normalisation of data was performed on the wind speed using only air density corrections. The air density was derived for each 10-minute period from measurements at ground level of air temperature and pressure (extrapolated to hub height) made by the met. station embedded in the ZP300 lidar. No turbulence intensity, shear or veer normalisation was applied.

The reference power curve is the site-specific power curve as computed by the turbine manufacturer. The warranted power curve uses the specific turbine controller. It is usually computed for a narrow range of shear profiles and a given turbulence intensity. For confidentiality reasons, all power curve results are shown in non-dimensional form, both for the turbine power output and the normalised wind speed.

The AEP was calculated independently for each measurement system and technique using the extrapolated power curves (for missing bins and high wind speeds) and standard Rayleigh wind speed distributions with average wind speeds from 4 to 11 ms^{-1}. For the nacelle lidars, the relative AEP difference expressed in % was calculated in two ways:

1) Using the turbine manufacturer's power curve: $\left(AEP_{lidar} - AEP_{ref}\right)/AEP_{ref}$;
2) Using the extrapolated power curve obtained from the ZP300: $\left(AEP_{lidar} - AEP_{zp300}\right)/AEP_{zp300}$.

For more details on the data analysis procedures, we refer the reader to the IEC 61400-12-1 standard ([1]) and to the extended description in Chapter 5 of [2].

Note: no shear or turbulence intensity filters have been applied in the power curve measurements. As a consequence, they are not directly comparable to the warranted power curve; the warranted curve is only used to provide a consistent baseline reference.

10.2 Wind model

Figure 40 shows the power curve scatter plots with the ZP300 (top) and the two nacelle lidars where the wind model is used (4BWI (bottom left), ZDM (bottom right)). For the three lidar systems, the wind speed measurements are corrected using the site calibration. The reference power curve (site-specific turbine manufacturer warranted power curve) is shown on each graph with the black line.

The scatter in the ZP300 power curve can be due to the lack of correlation between the wind speed at the ZP300 and the turbine locations, the effect of the terrain on the flow, or turbulence. In flat terrain, it is common to observe a significant scatter reduction when using nacelle lidars as they measure the wind directly upstream the rotor instead of a fixed location ([1], [2]). Such a scatter reduction is not observed here, or to a lesser extent as confirmed in Figure 41. This may be due to the higher inadequacy (model uncertainty) of the wind model and flow complexity at the Hill Of Towie site, which is significantly forested and moderately mountainous.

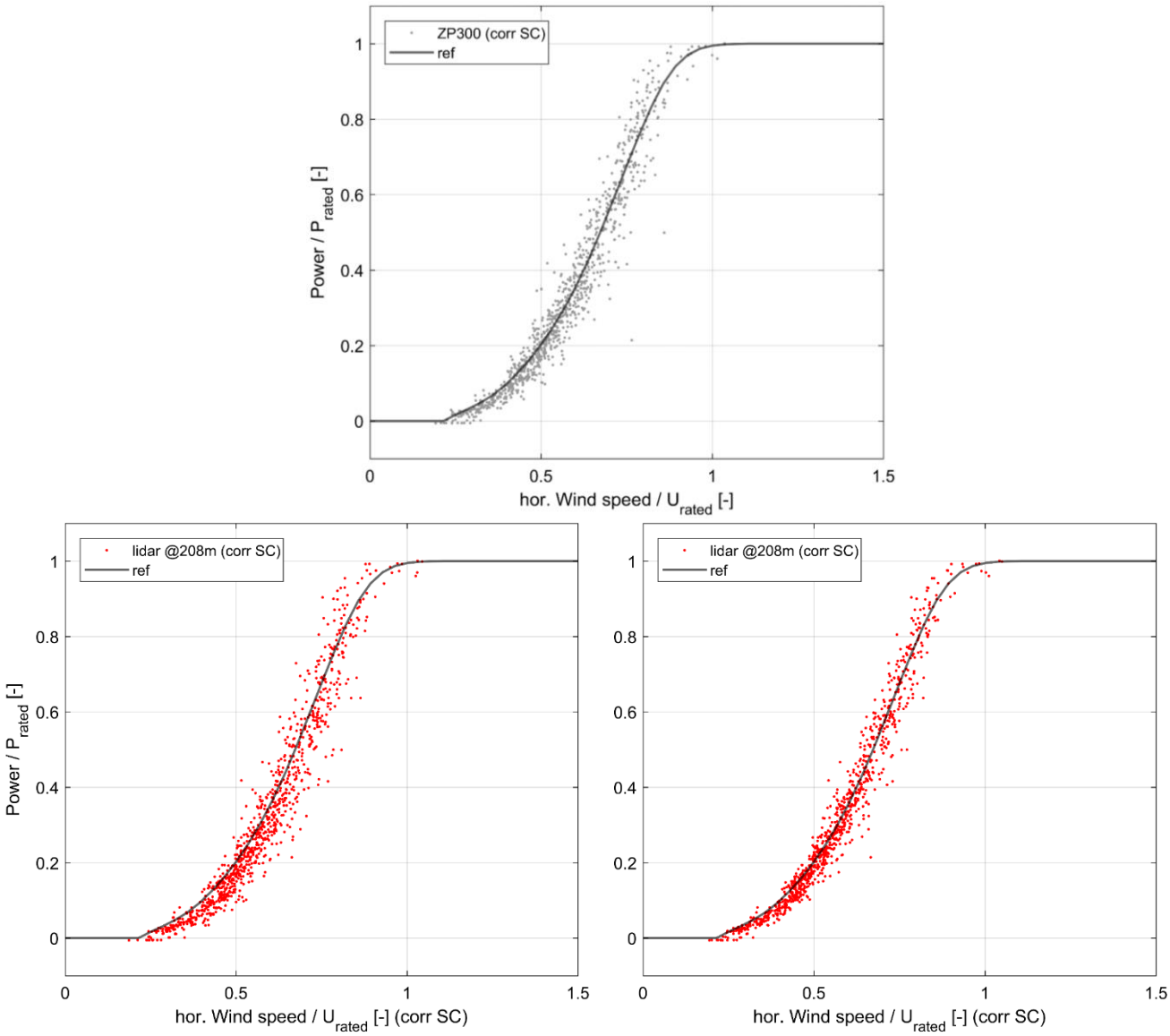

Figure 40. Power curve scatter plot. The wind speed is corrected using the site calibration and then normalised using air density measurements. Top: hub height wind speed measured by ZP300. Bottom: nacelle lidar wind speed estimate using the wind model at 208m; 4BWI (left); ZDM (right).

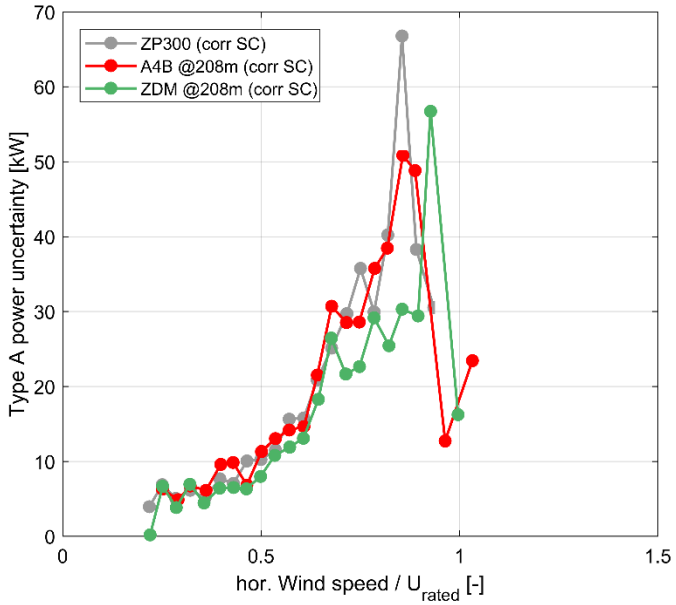

Figure 41. Type A power curve uncertainty as a function of wind speed. The nacelle lidar wind speed is estimated using the wind model at 208m.

Figure 42 displays the bin-averaged power curve obtained using the ZP300 and the nacelle lidar estimate with the wind model. The 10-minute data were grouped and averaged in wind speed bin of 0.5 ms^{-1}. The ZP300 measured power curve is visually in good agreement with the reference. At low wind speeds, it is slightly shifted to the right compared to the reference power curve. The 4BWI power curve is clearly shifted even further to the right due to the 2.2% overestimation of the wind speed compared to ZP300 (see section 7.1), while the ZDM power curve visually cannot be distinguished from the ZP300 one.

Consequently, the AEP obtained with the ZP300 and the nacelle lidars' wind speed estimate is lower than the the one computed using the reference power curve, as seen in Figure 43. For instance, at 8 ms^{-1} average annual wind speed (Rayleigh distributed), the relative AEP error is:

- For ZP300, -1.3%;
- For the 4BWI lidar, -5.2%;
- For the ZDM: -1.8%.

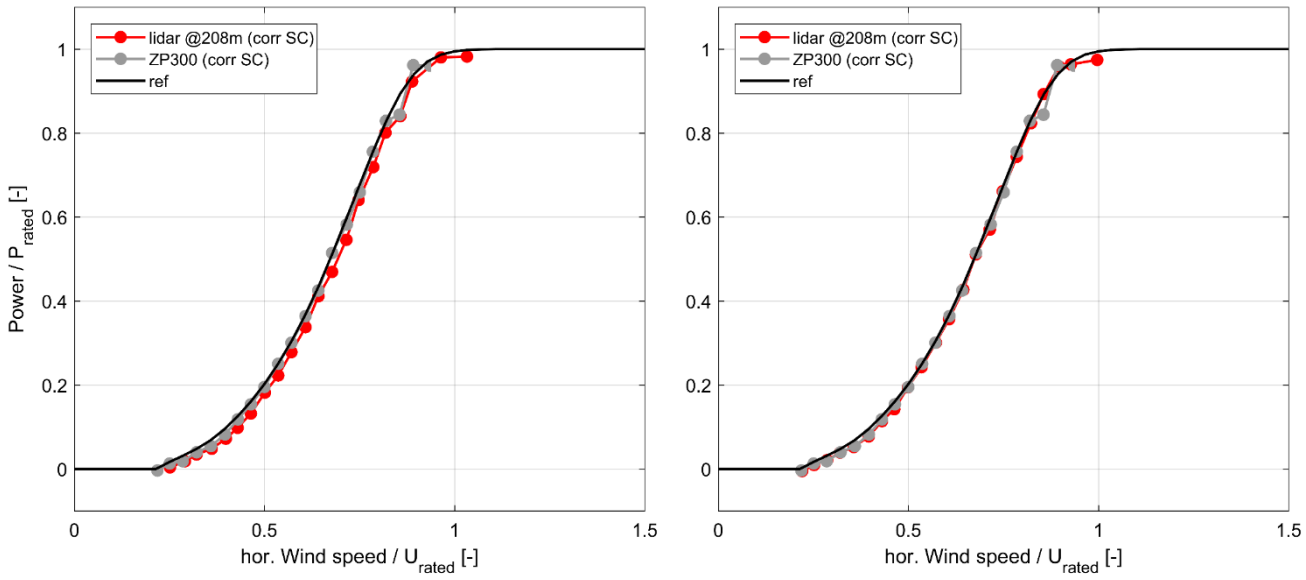

Figure 42. Power curve (bin-averaged). The nacelle lidar wind speed is estimated using the wind model at 208m. Left: 4BWI. Right: ZDM.

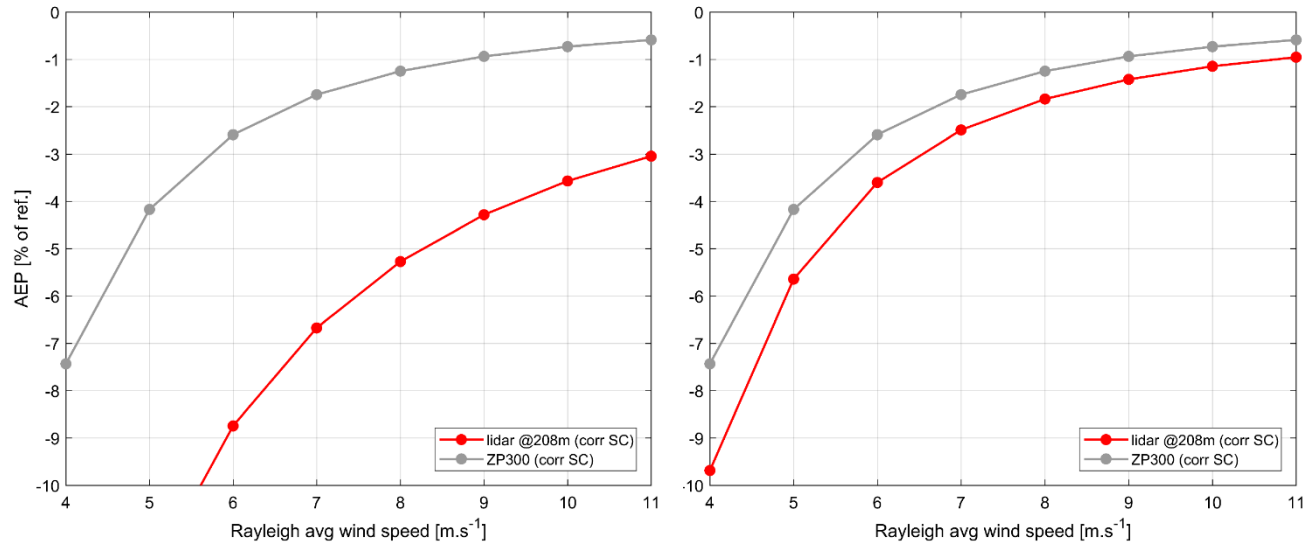

Figure 43. AEP difference relative to the reference power curve. Grey: using ZP300 power curve. Red: using power curve with nacelle lidar and the wind model at 208m. Left: 4BWI. Right: ZDM.

10.3 Wind-induction model

Figure 44 shows the power curve scatter plots with the ZP300 (top) and the two nacelle lidars where the combined wind-induction model is used (4BWI (bottom left), ZDM (bottom right)). Only the ZP300 wind speed is corrected using the site calibration. The wind speed estimate for the nacelle lidars is directly the free stream wind speed V_∞ output by the reconstruction algorithms, without any need for site calibration. Once again, the reference power curve (site-specific turbine manufacturer warranted power curve) is shown on each graph with the black line.

In [2] and [10], the scatter reduction in the nacelle lidar power curve was even greater when using the wind-induction model and lidar measurements close to the rotor than when using the wind model. Visually, the scatter reduction is hardly observed here similarly to the case of the wind model (Section 10.2), see also Figure 42. This may be due to the higher inadequacy (model uncertainty) of the wind-induction model and flow complexity at the Hill Of Towie site.

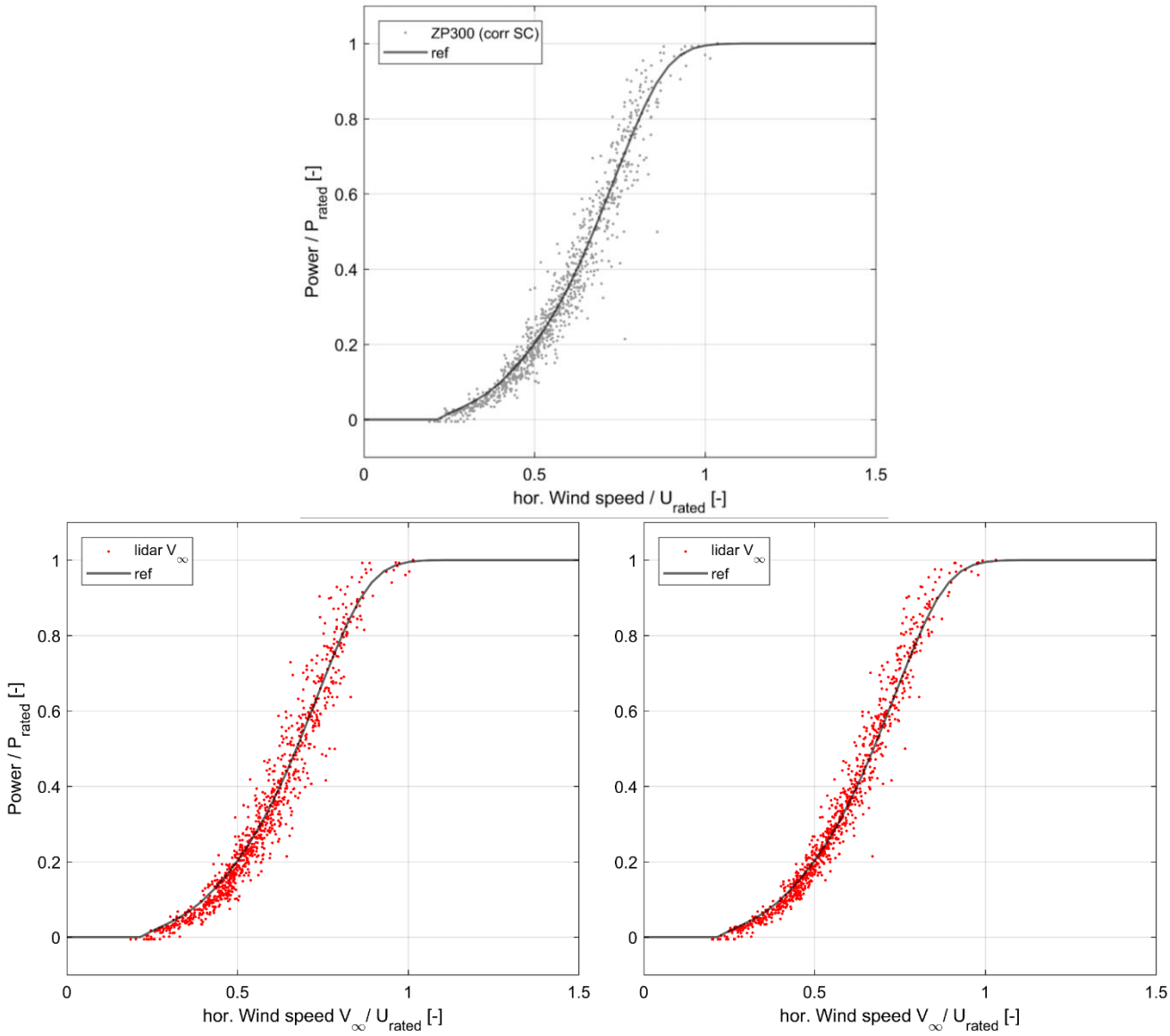

Figure 44. Power curve scatter plot. Top: hub height wind speed measured by ZP300 and corrected using the site calibration. Bottom: nacelle lidar free stream wind speed ($\mathbf{V}_\infty$) estimate using the wind-induction model at 208m; 4BWI (left); ZDM (right).

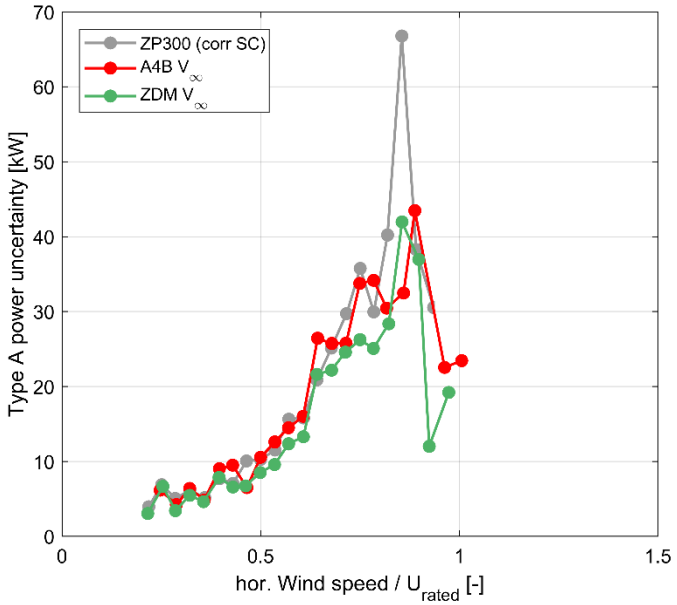

Figure 45. Type A power curve uncertainty as a function of wind speed. The nacelle lidar free stream wind speed is estimated using the wind-induction model.

Figure 46 displays the bin-averaged power curve obtained using the ZP300 and the V_∞ estimate from the two nacelle lidars. Both the 4BWI and ZDM power curves match the reference power curve well. A slight shift to the left is observed for ZDM in comparison to the ZP300 due to the 1.1% underestimation of the wind speed (see section 7.2.1), while the 4BWI power curve visually cannot be distinguished from the ZP300 one.

The AEP obtained with the ZP300 and the nacelle lidars' wind speed estimate are computed and graphed in the form of relative difference to the reference AEP (based on reference power curve) as a function of Rayleigh mean wind speed in Figure 47. For instance, at 8 ms^{-1} average annual wind speed (Rayleigh distributed), the relative AEP error is:

- For ZP300, -1.3%;
- For the 4BWI lidar, -2.0%;
- For the ZDM: +0.4%.

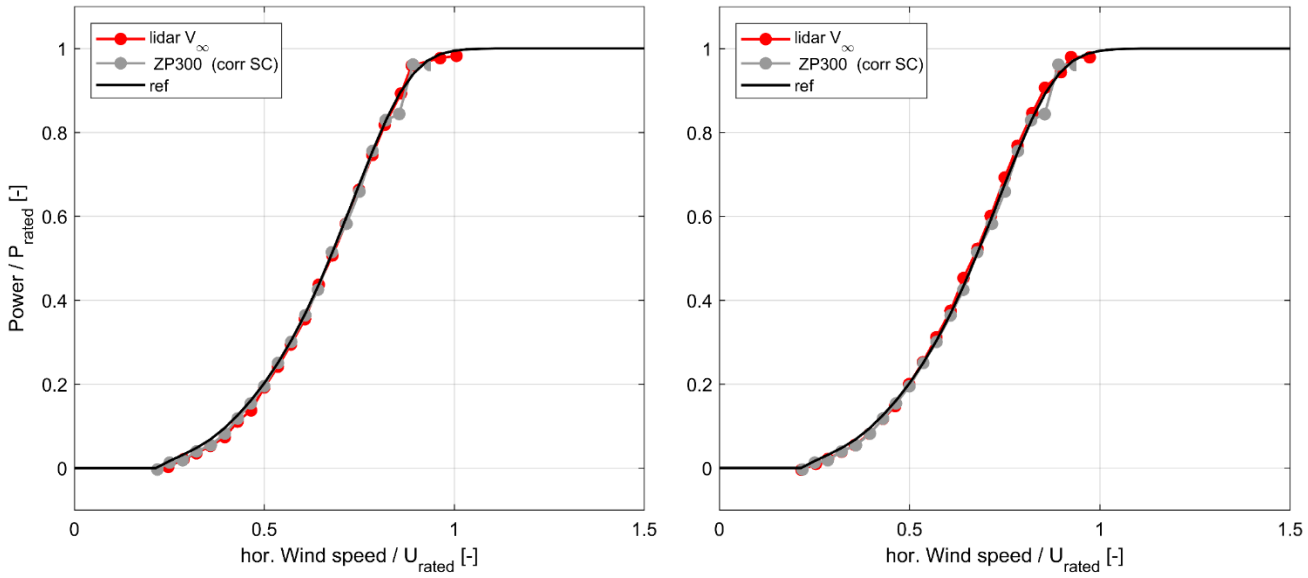

Figure 46. Power curve (bin-averaged). Only the ZP300 measured wind speed is corrected using the site calibration. The nacelle lidar free stream wind speed ($\mathbf{V}_\infty$) is estimated using the wind-induction model. Left: 4BWI. Right: ZDM.

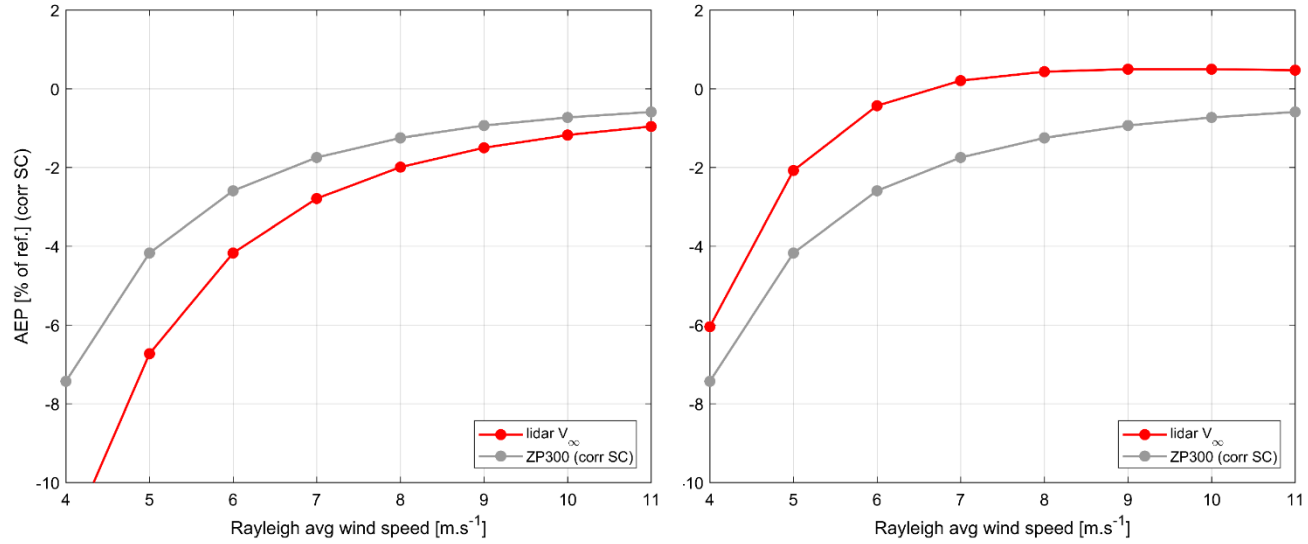

Figure 47. AEP difference relative to the reference power curve. Grey: using ZP300 power curve. Red: using power curve with nacelle lidar estimate $\mathbf{V}_\infty$ and the wind-induction model. Left: 4BWI. Right: ZDM.

Conclusion

The main purpose of this analysis was to test in complex terrain the wind field reconstruction (WFR) algorithm developed in Borraccino et al ([4]) for the specific purpose of power performance verification using nacelle-mounted lidars. The concept behind this method is to estimate the free wind speed at the turbine location based on the lidar measurements taken close to the rotor and therefore obviate the need for a site calibration. The WFR algorithms were further adapted in order to account for the topographical variations in the vicinity of the turbine.

Two nacelle lidars systems – an *Avent* 4-beam Wind Iris and *ZephIR* Dual Mode – were deployed at the Hill of Towie wind farm, a complex site in Scotland that is both hilly and forested. The new method has been evaluated by comparison to the results obtained simultaneously with measurements from a ground-based profiling lidar (ZP300) distant by 2.5 rotor diameters to the turbine. A correction for the effect of the terrain on the flow based on the site calibration performed before the erection of turbine was applied to the ZP300 measurements.

An intermediate step between the new method tested here and the reference wind sensor measurements is the wind speed estimate derived from nacelle lidar measurements at 2.5D upstream using a simple wind model. This is the approach commonly used with nacelle-mounted lidars so far, although this method still requires a site calibration of some form in complex terrain. Note however that the wind field reconstruction algorithm applied in this report is different from the default algorithm provided by *Avent* and *ZephIR*. This method gave a 2% deviation to the ZP300 measurements. The height error is significant for this site (10-15m). Consequently, it was demonstrated that the terrain correction implemented in the WFR algorithm is of critical importance in order to accurately reconstruct the wind field characteristics.

The model-fitting method using short-range lidar measurements (between 0.5 and 1 rotor diameters) and the wind-induction model showed very promising results with a difference in wind speed of about 1%. For comparison matters, the same method applied in flat terrain with a 5-beam Avent Demonstrator lidar had given a 0.6% difference in wind speed (Nørrekær Enge campaign [2]). This confers confidence in the new method.

The power curve was measured as accurately when using the two nacelle lidars and the wind-induction model as with the ground-based lidar measurements.

Annexes

Annex A. Availability of nacelle lidar LOS raw data – 4BWI and ZDM

For both 4BWI and ZDM nacelle lidars, the LOS availability is a statistics resulting from (DTU) in-house quality control of the lidar unfiltered raw data. The analysis and filtering of data is described in details in Chapter 5.

In this annex, the LOS availability is plotted:

- For the 4BWI:
  - As a function of CNR (left) and LOS velocity (right);
  - For LOS 0, 1, 2;
  - See results for LOS 3 in the graphs on the left of Figure 24 and Figure 25.
- For ZDM:
  - As a function of “baskcatter” (left) and LOS velocity (right);
  - For the other five LOS used in the report, i.e. azimuthal sectors 7 (top right), 18 (bottom right), 31 (bottom, left), 37 (mid-height, left), 42 (top, left) of the pseudo 48-beam lidar;
  - See results for LOS 12 (mid-height, right) in the graphs on the right of Figure 24 and Figure 25.

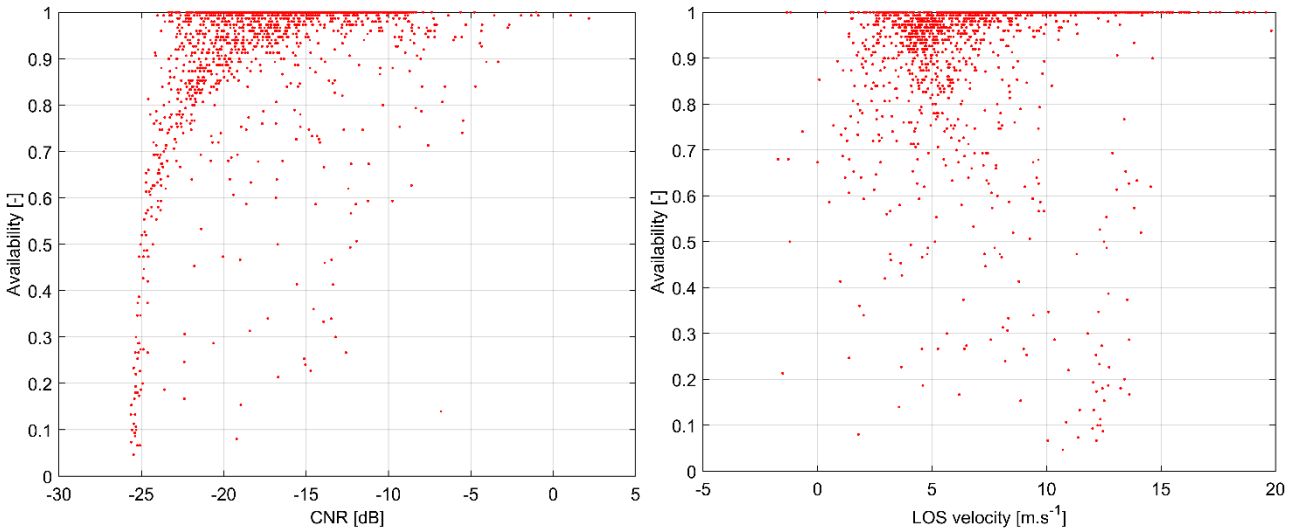

Figure A. 1. Availability of LOS 0 of 4BWI lidar as a function of mean CNR (left) and LOS velocity (right).

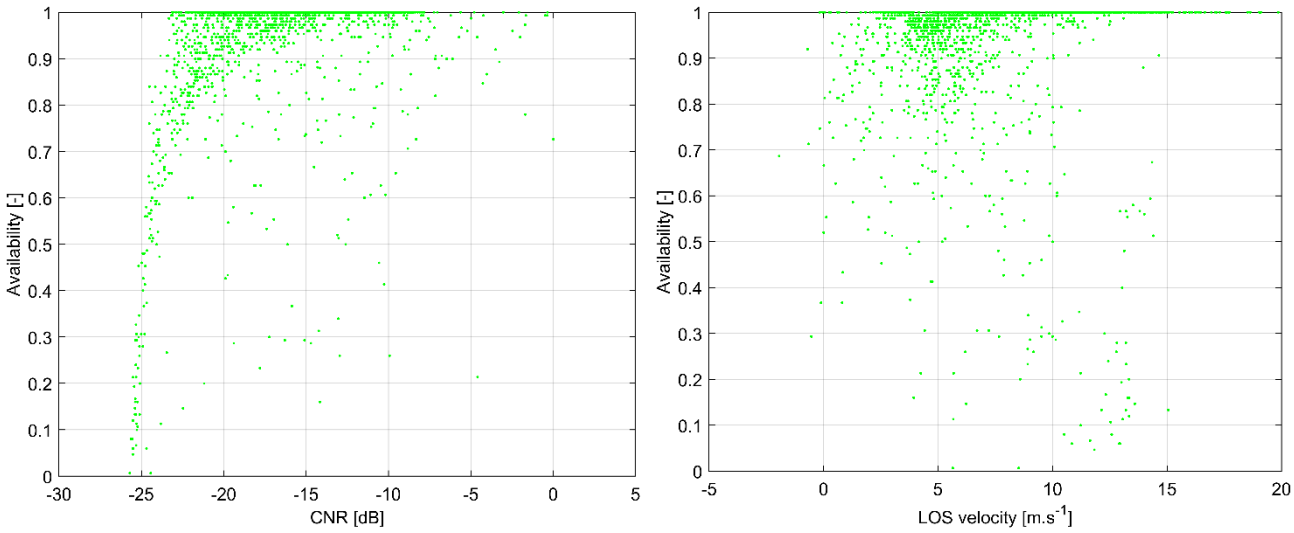

Figure A. 2. Availability of LOS 1 of 4BWI lidar as a function of mean CNR (left) and LOS velocity (right).

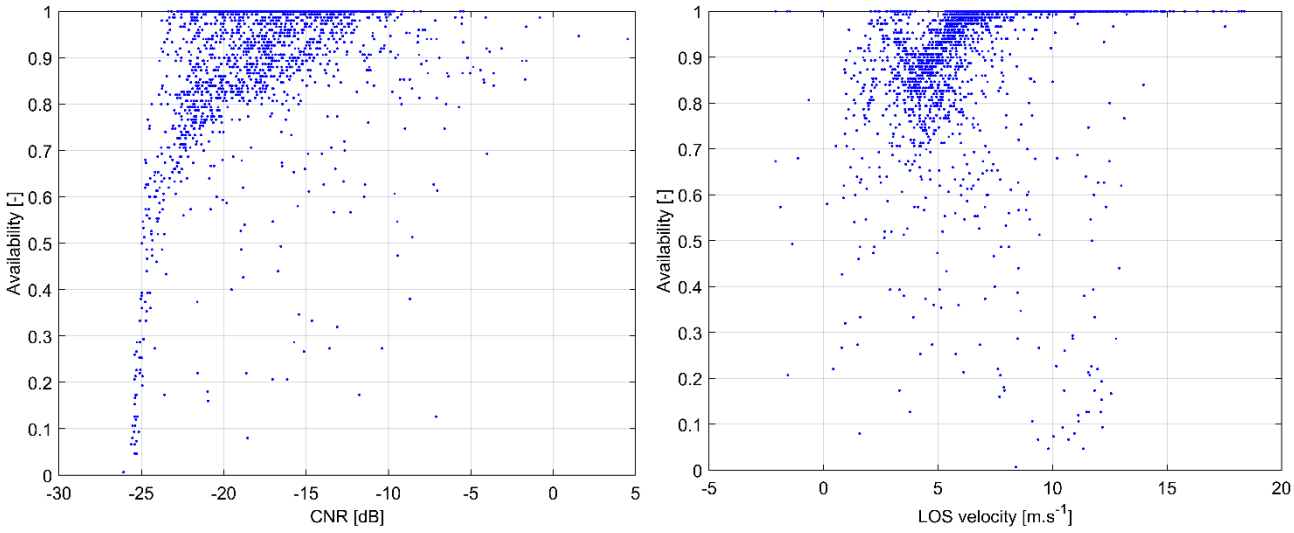

Figure A. 3. Availability of LOS 2 of 4BWI lidar as a function of mean CNR (left) and LOS velocity (right).

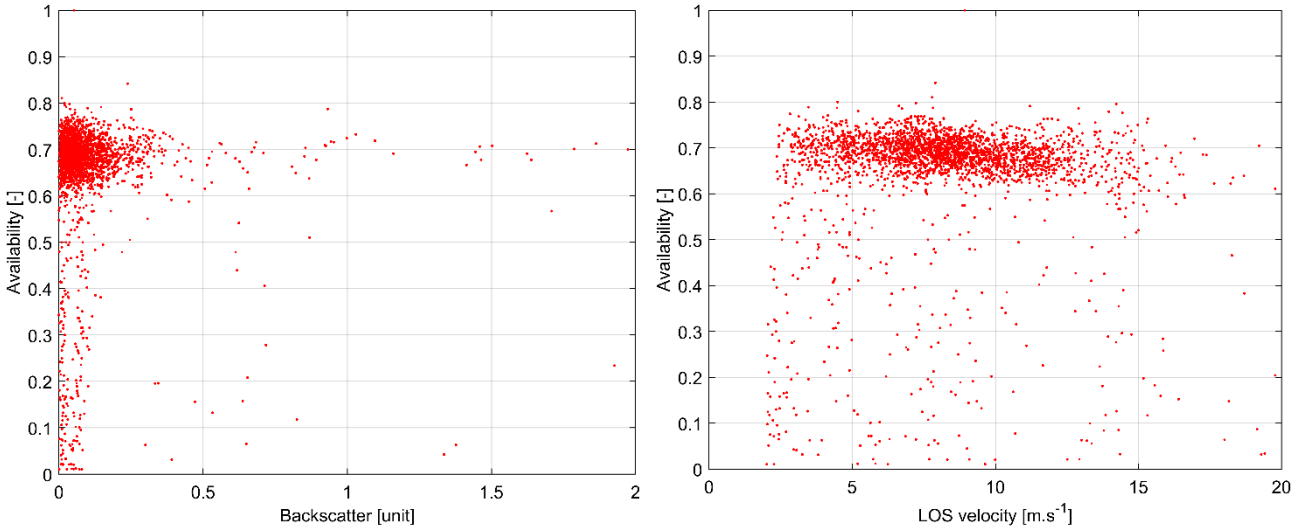

Figure A. 4. Availability of LOS 7 of ZDM lidar as a function of mean backscatter (left) and LOS velocity (right).

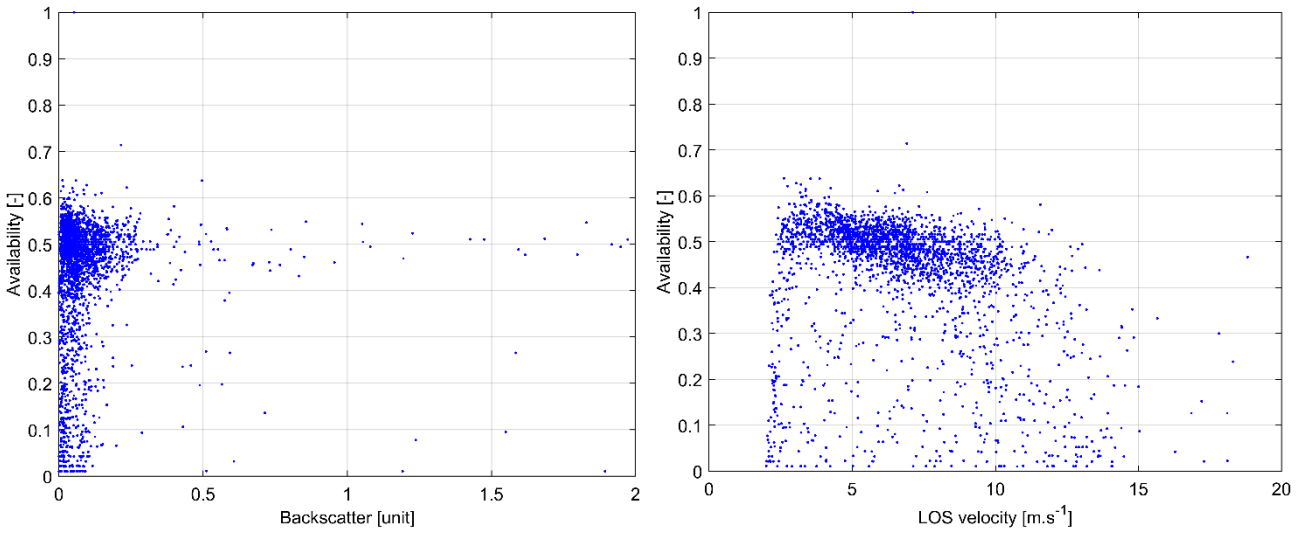

Figure A. 5. Availability of LOS 18 of ZDM lidar as a function of mean backscatter (left) and LOS velocity (right).

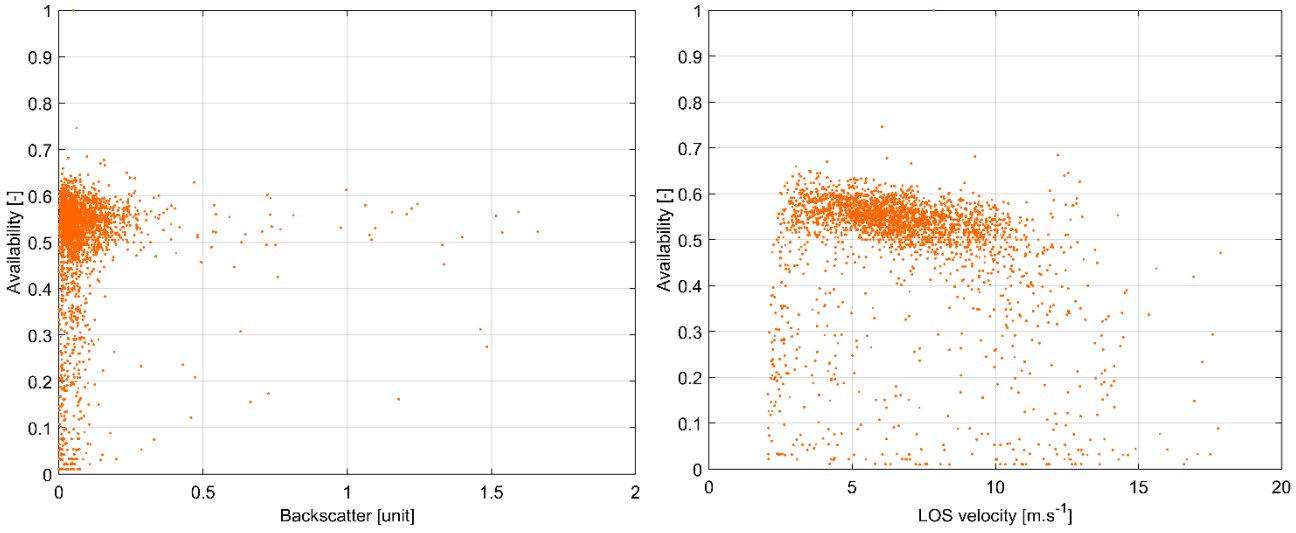

Figure A. 6. Availability of LOS 31 of ZDM lidar as a function of mean backscatter (left) and LOS velocity (right).

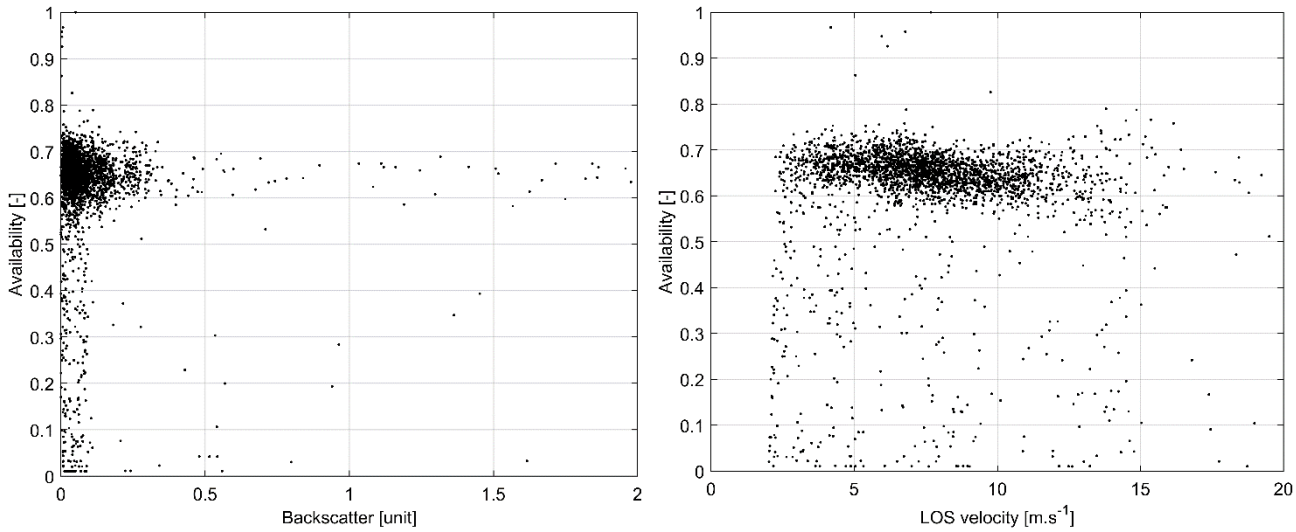

Figure A. 7. Availability of LOS 37 of ZDM lidar as a function of mean backscatter (left) and LOS velocity (right).

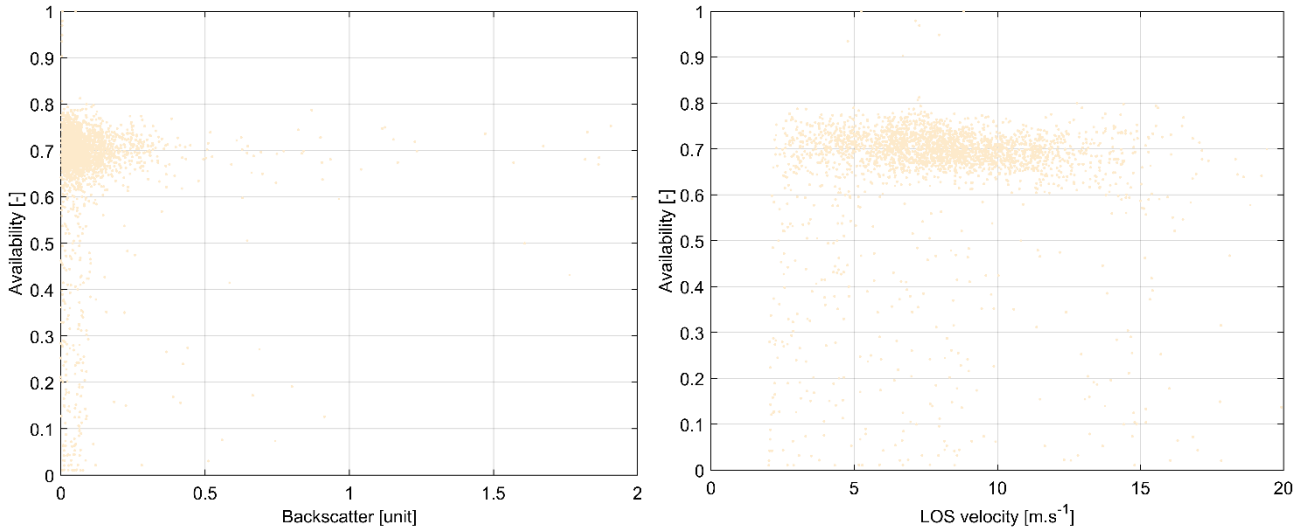

Figure A. 8. Availability of LOS 42 of ZDM lidar as a function of mean backscatter (left) and LOS velocity (right).

Annex B. Wind speed and power performance results for 4BWI dataset alone

This annex presents results obtained by treating the 4-beam Wind Iris lidar independently from the other nacelle-based system (ZDM). The results concern:

1) The wind speed comparison with the ZP300 profiling lidar measurements
2) Secondary wind field characteristics
3) The model-fitting residuals
4) The power curve

These results are provided both for the wind and the combined wind-induction models (see Section 6.2). The terrain correction implemented in the reconstruction codes is used systematically as it was shown to add value and thus necessary. More details can be found from Chapter 8 to Chapter 10.

The data filtering is entirely analogue to the one described in Section 5.3 except that the joining of dataset is made for the two reconstruction cases of the 4BWI, which allows to significantly increase the number of valid 10-minute periods (1664 data points instead of 943).

The dataset was collected from 30th July (09:30) to 2nd October 2017 (10:00).

Wind speed comparisons

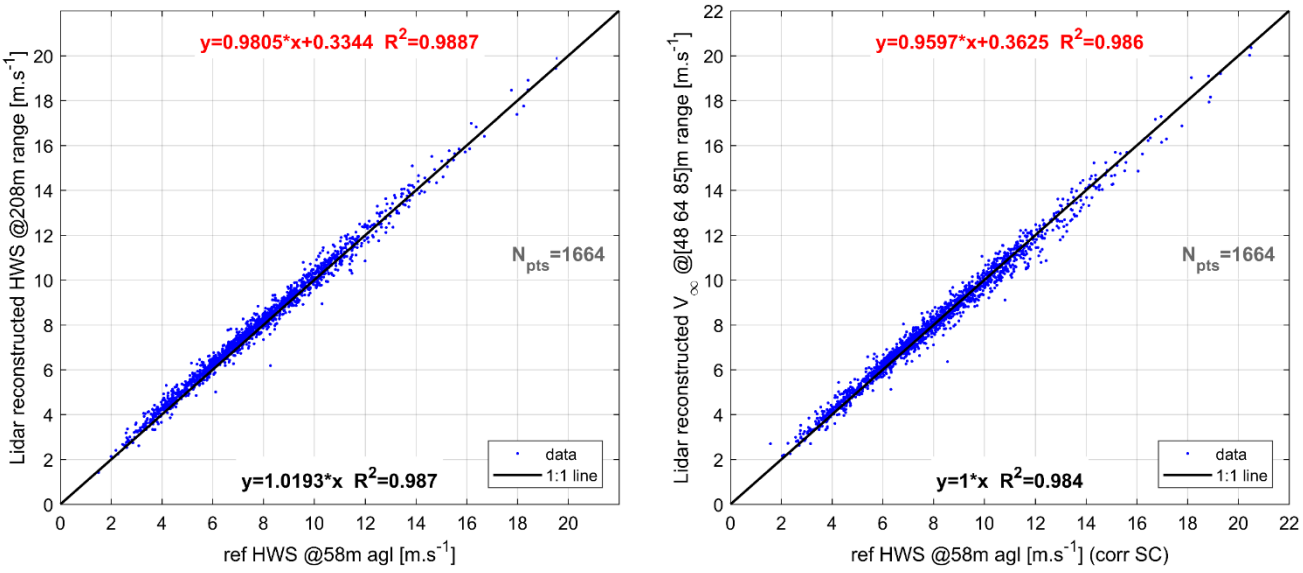

Figure A. 9. Comparison of the nacelle lidar wind speed estimates with the ground-based ZP300 profiling lidar measurements for the 4BWI dataset alone. Left: using the wind model at 208m. Right: using the wind-induction model.

Secondary wind field characteristics

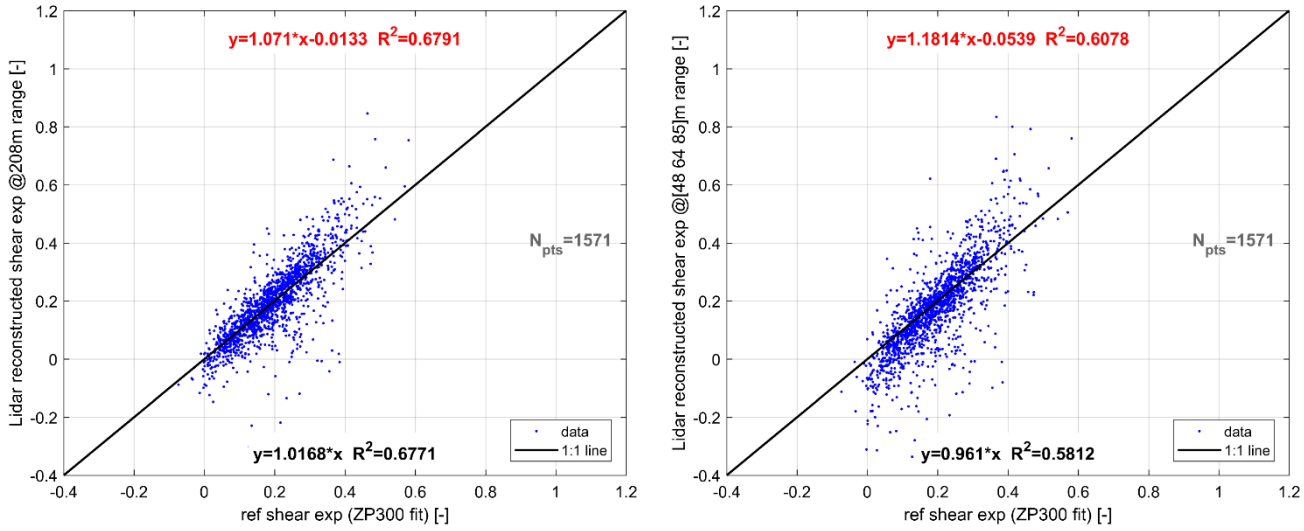

Figure A. 10. Comparison of the nacelle lidar wind shear with the ground-based ZP300 profiling lidar measurements for the 4BWI dataset alone. Left: using the wind model at 208m Right: using the wind-induction model.

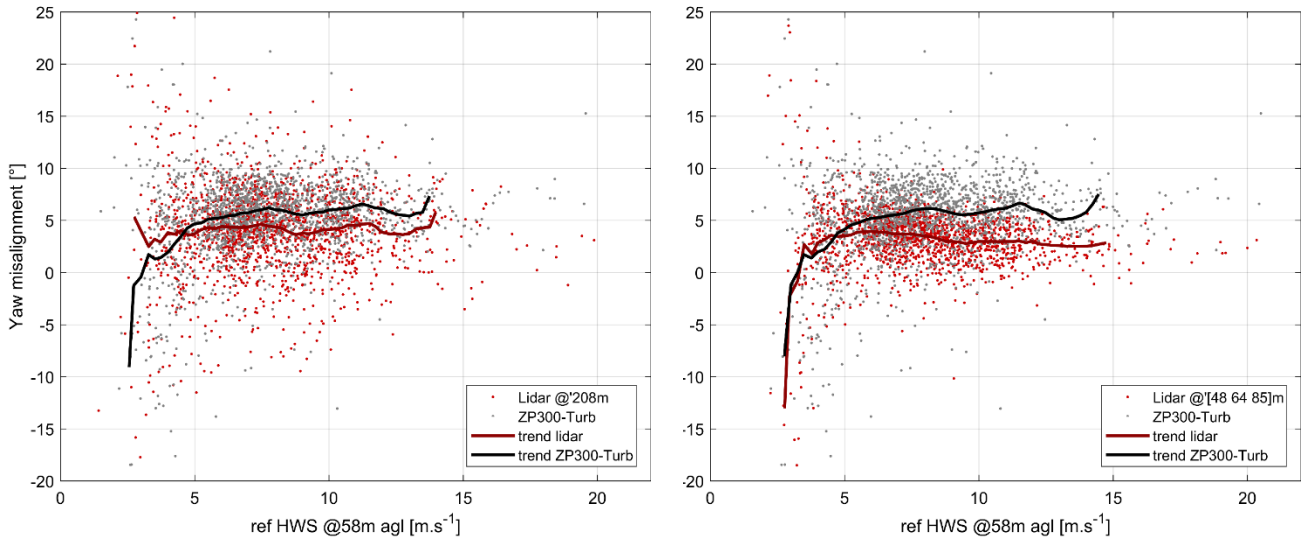

Figure A. 11. Scatter plots of yaw misalignment estimated from the nacelle lidar wind speed estimates for the 4BWI dataset alone, and using the ground-based ZP300 profiling lidar measurements of wind direction. Left: using the wind model at 208m. Right: using the wind-induction model.

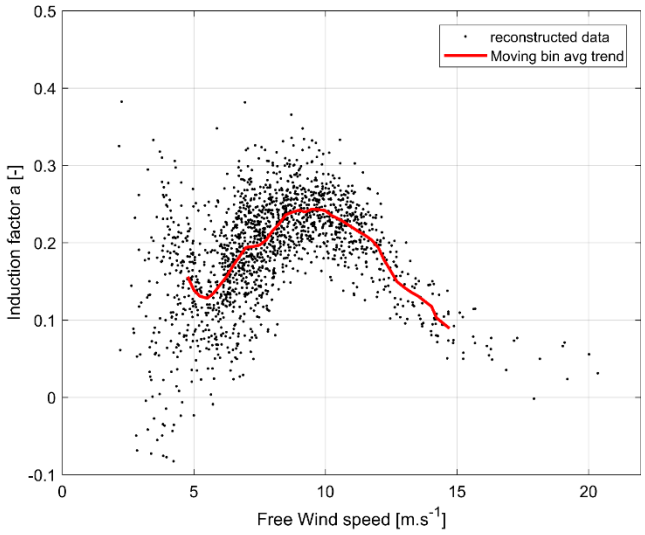

Figure A. 12. Scatter plots of induction factor estimated from the nacelle lidar wind speed estimates for the 4BWI dataset alone, using the wind-induction model.

Note: the induction factor trend line shows that at maximum thrust, the induction factor reaches values of approximately 0.25. Such a maximum value is significantly lower than observed in the Nørrekær Enge campaign. Based on CFD studies of wind flows in complex terrain (see [15], (PhD thesis)), it is expected that the induction factor is reduced in such sites.

Model-fitting residuals

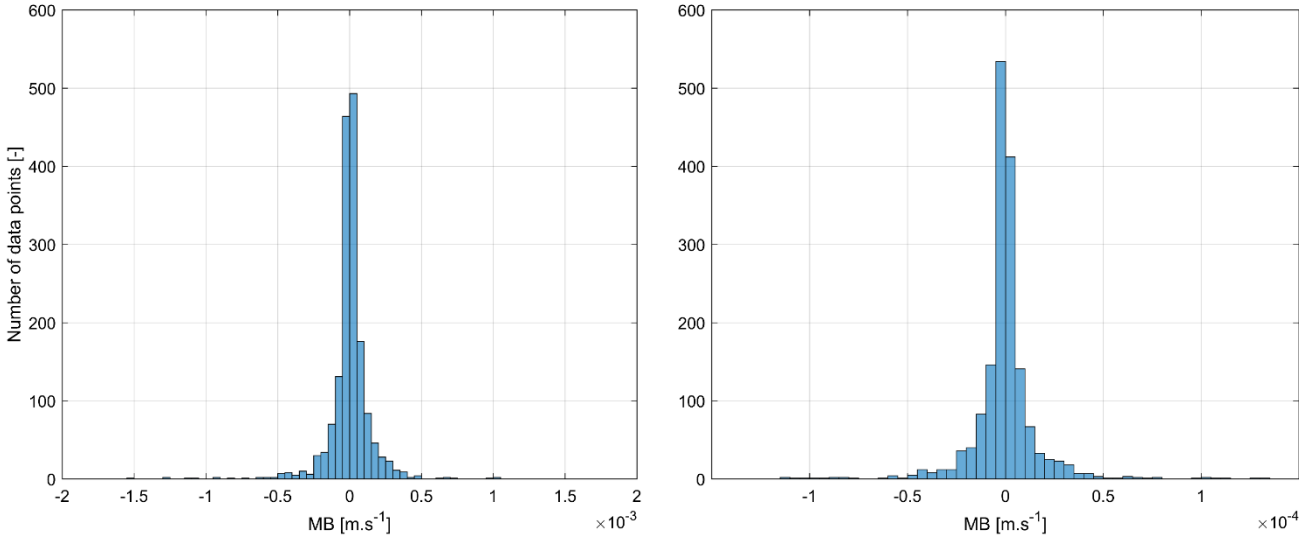

Figure A. 13. Histograms of mean bias (MB) of LOS velocity residuals for the 4BWI dataset alone. Left: using the wind model at 208m. Right: using the wind-induction model.

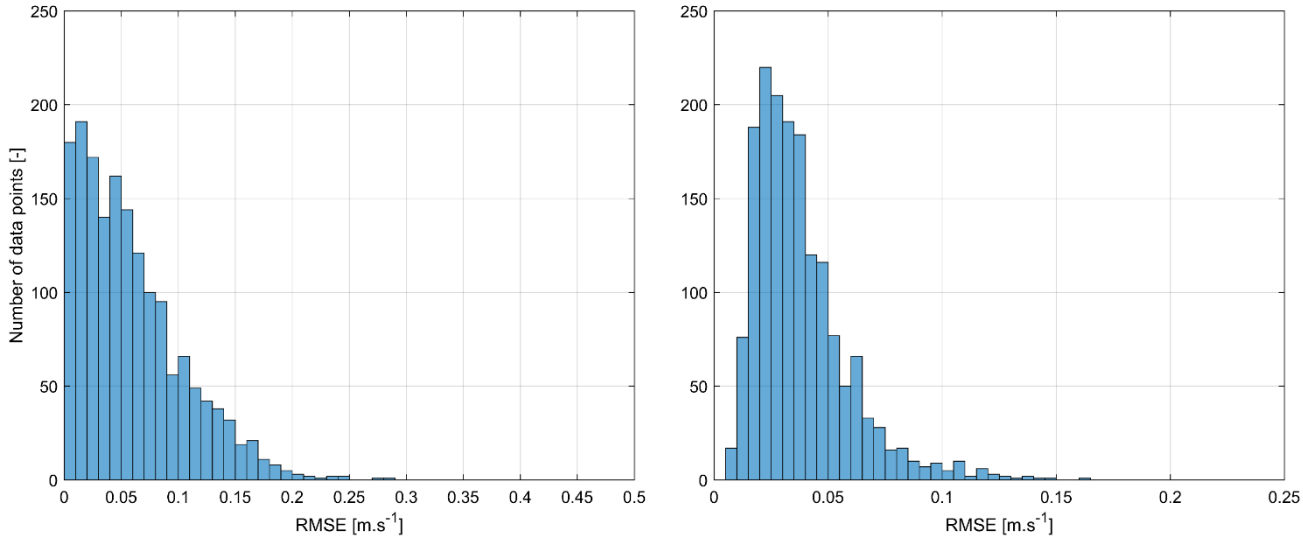

Figure A. 14. Histograms of root mean squared error (RMSE) of LOS velocity residuals for the 4BWI dataset alone. Left: using the wind model at 208m. Right: using the wind-induction model.

Power curves

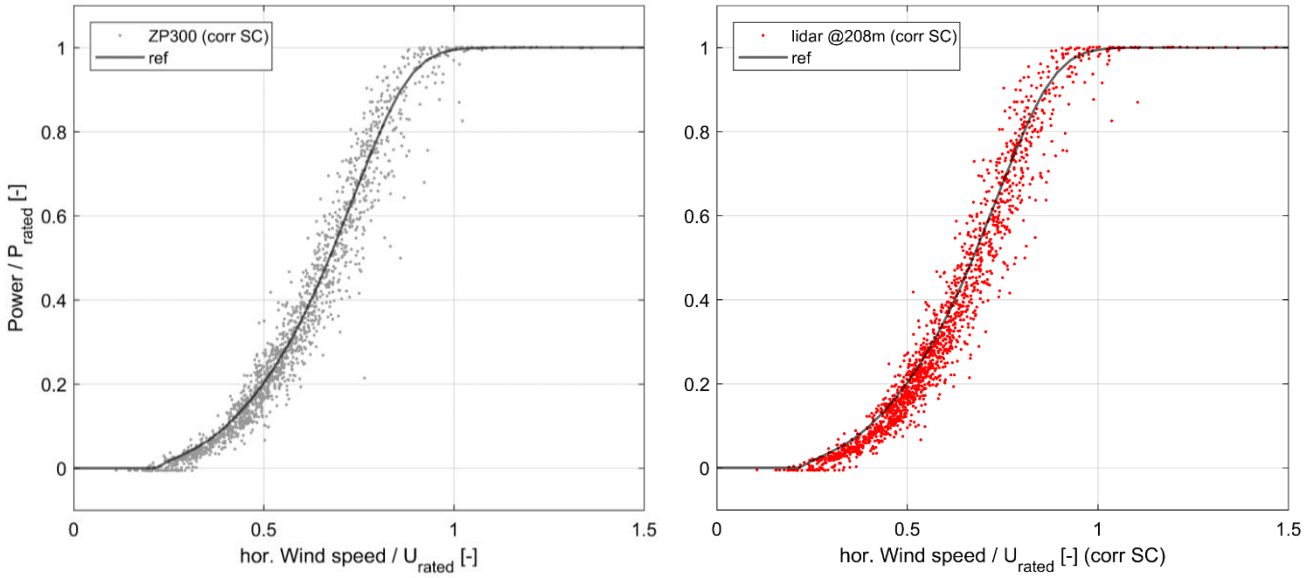

Figure A. 15. Power curve scatter plot for the 4BWI dataset alone and using the wind model at 208m. The wind speed is corrected using the site calibration and then normalised using air density measurements. Left: hub height wind speed measured by ZP300. Right: nacelle lidar wind speed estimate.

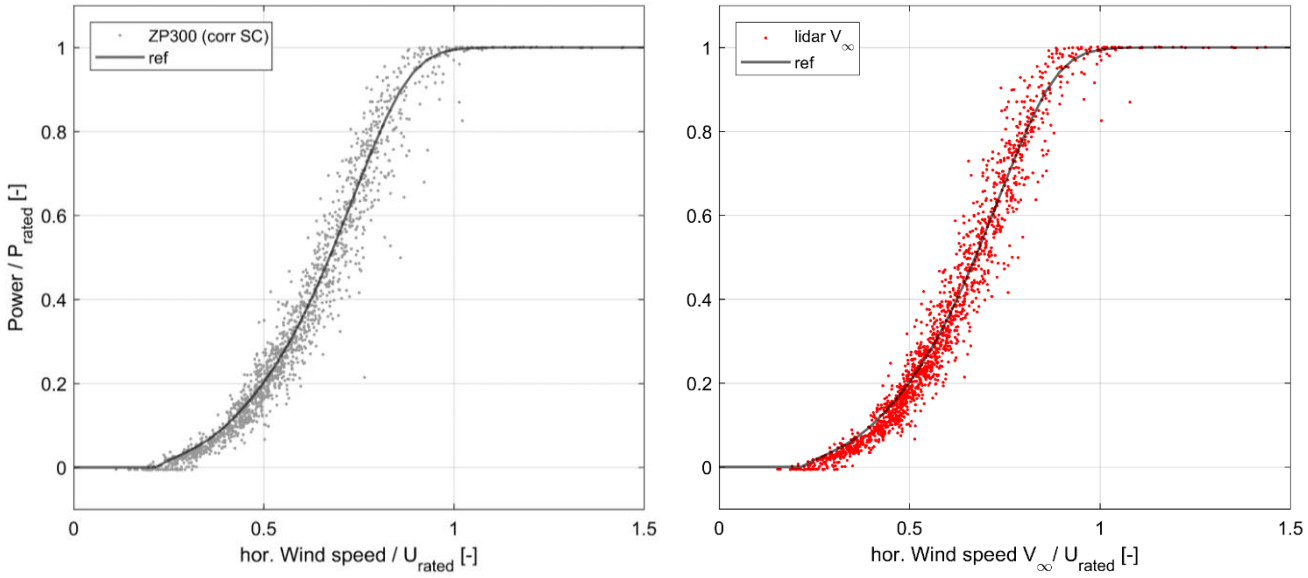

Figure A. 16. Power curve scatter plot for the 4BWI dataset alone and using the wind-induction model. The wind speed is corrected using the site calibration and then normalised using air density measurements. Left: hub height wind speed measured by ZP300. Right: nacelle lidar free stream wind speed estimate.

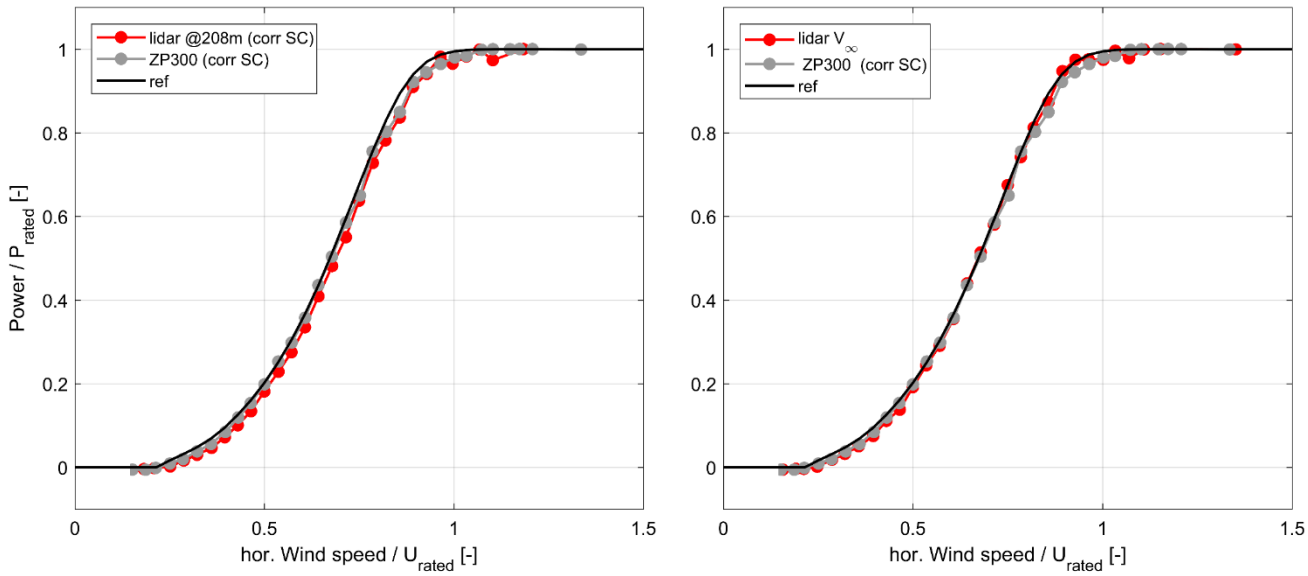

Figure A. 17. Power curve (bin-averaged) for the 4BWI dataset alone. Left: using the wind model at 208m. Right: using the wind-induction model.

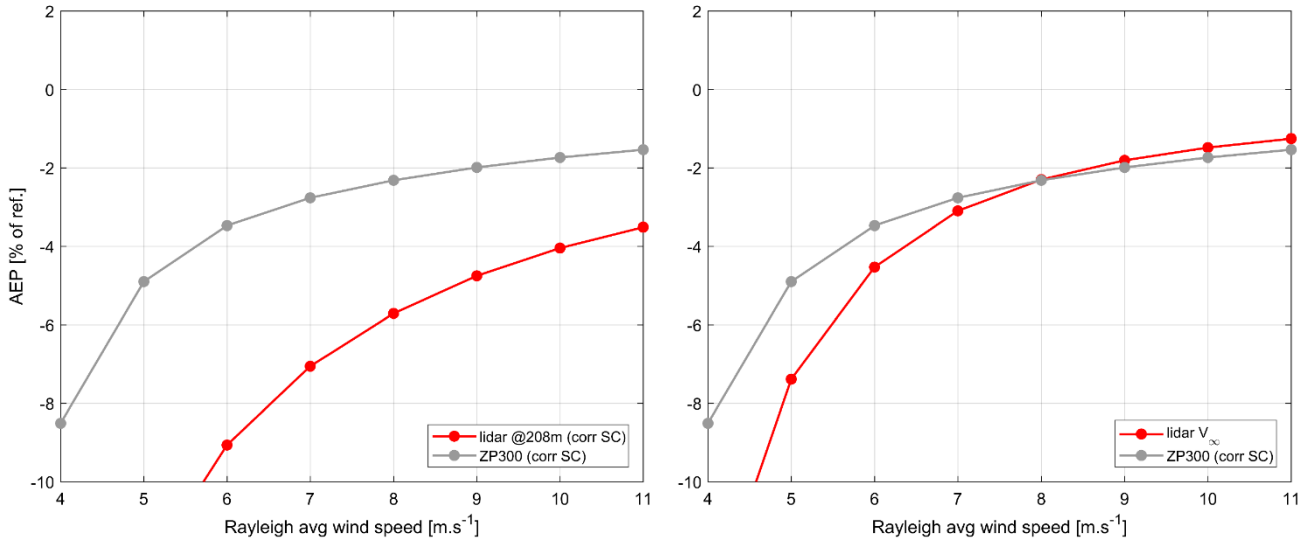

Figure A. 18. AEP difference relative to the reference power curve for the 4BWI dataset alone. Grey: using ZP300 power curve. Red: using power curve with nacelle lidar. Left: using the wind model at 208m. Right: using the wind-induction model.

Annex C. Wind speed and power performance results for ZDM dataset alone

This annex presents results obtained by treating the ZephIR Dual-Mode lidar independently from the other nacelle-based system (4BWI). The results concern:

1) The wind speed comparison with the ZP300 profiling lidar measurements
2) Secondary wind field characteristics
3) The model-fitting residuals
4) The power curve

These results are provided both for the wind and the combined wind-induction models (see Section 6.2). The terrain correction implemented in the reconstruction codes is used systematically as it was shown to add value and thus necessary. More details can be found from Chapter 8 to Chapter 10.

The data filtering is entirely analogue to the one described in Section 5.3 except that the joining of dataset is made for the two reconstruction cases of the ZDM, which allows to significantly increase the number of valid 10-minute periods (1545 data points instead of 943).

The time period of the dataset is extended, with the data being collected from 5th July (12:00) to 2nd October 2017 (10:00).

Wind speed comparisons

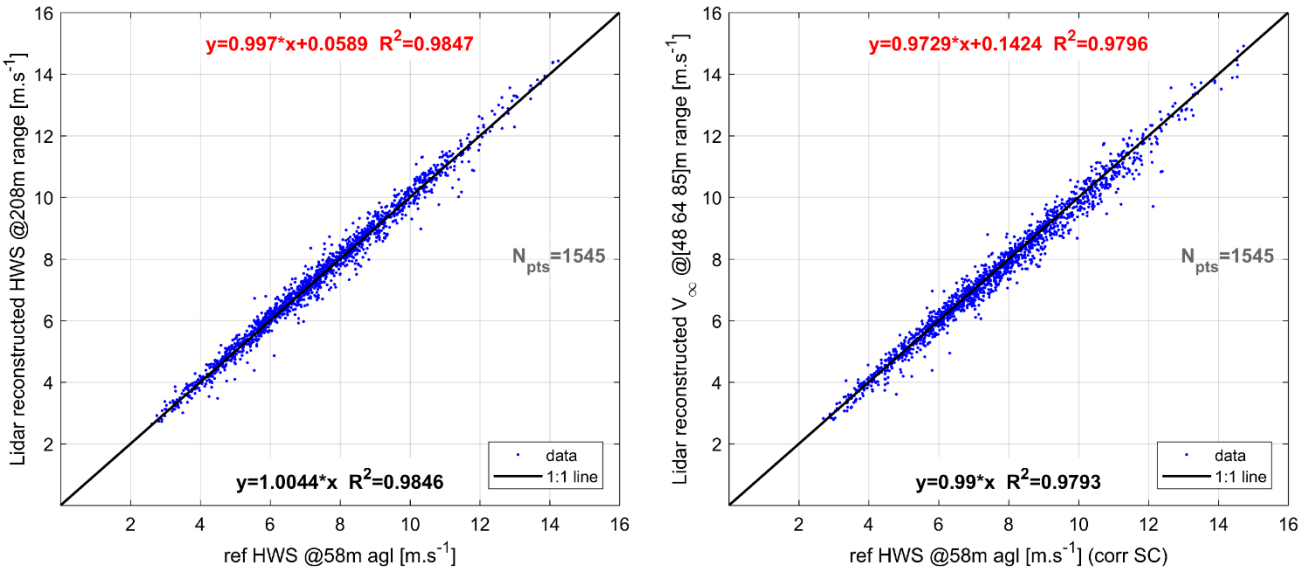

Figure A. 19. Comparison of the nacelle lidar wind speed estimates with the ground-based ZP300 profiling lidar measurements for the ZDM dataset alone. Left: using the wind model at 208m. Right: using the wind-induction model.

Secondary wind field characteristics

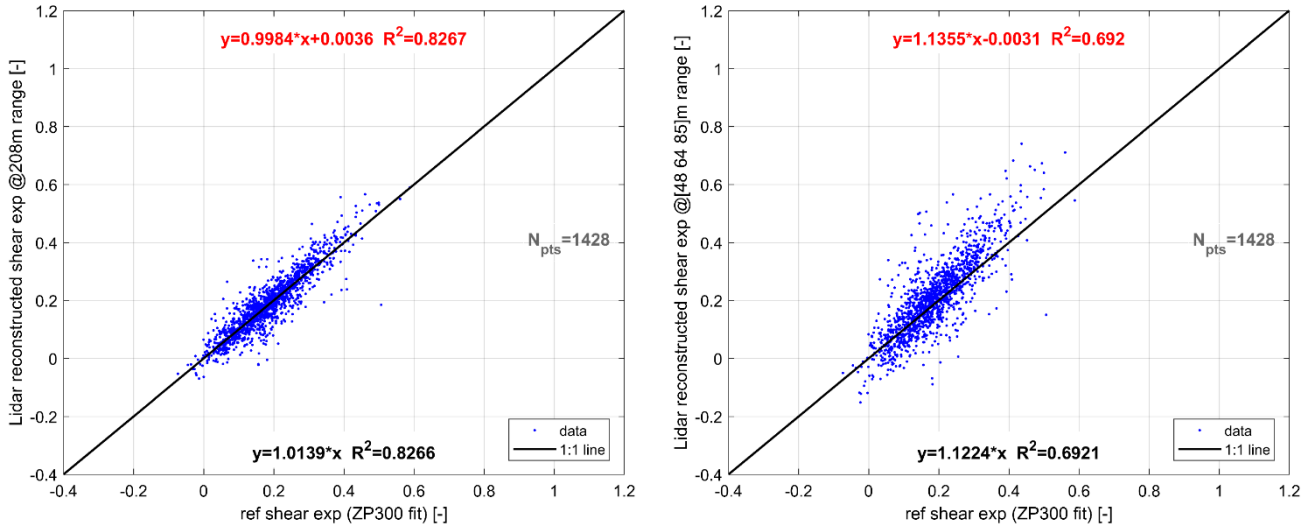

Figure A. 20. Comparison of the nacelle lidar wind shear with the ground-based ZP300 profiling lidar measurements for the ZDM dataset alone. Left: using the wind model at 208m Right: using the wind-induction model.

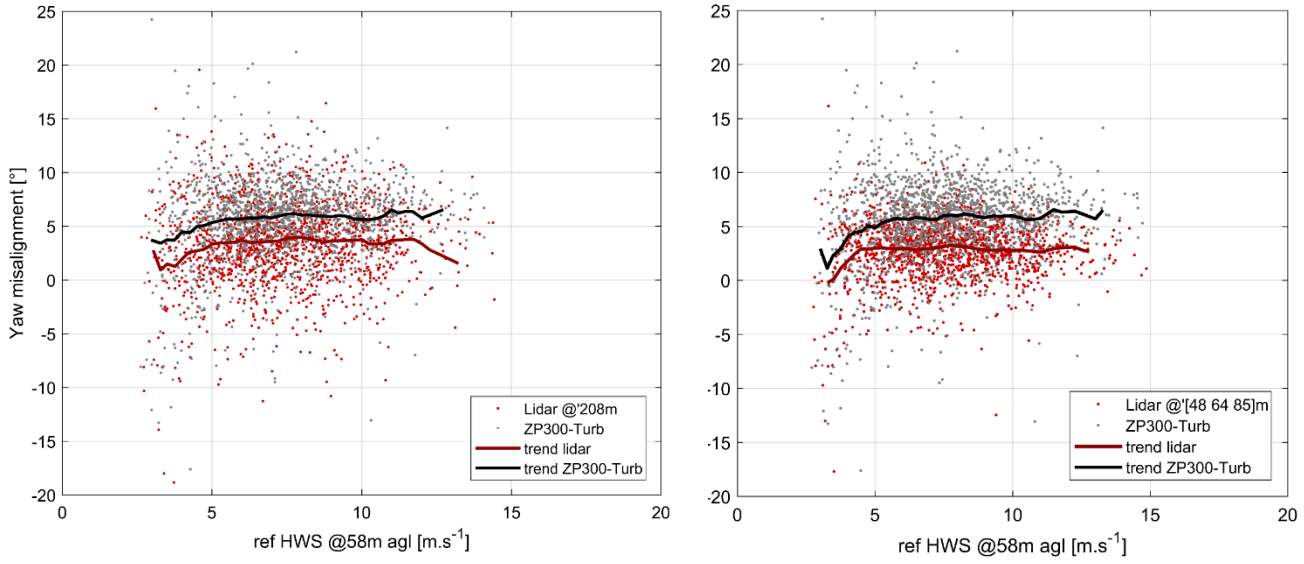

Figure A. 21. Scatter plots of yaw misalignment estimated from the nacelle lidar wind speed estimates for the ZDM dataset alone, and using the ground-based ZP300 profiling lidar measurements of wind direction. Left: using the wind model at 208m. Right: using the wind-induction model.

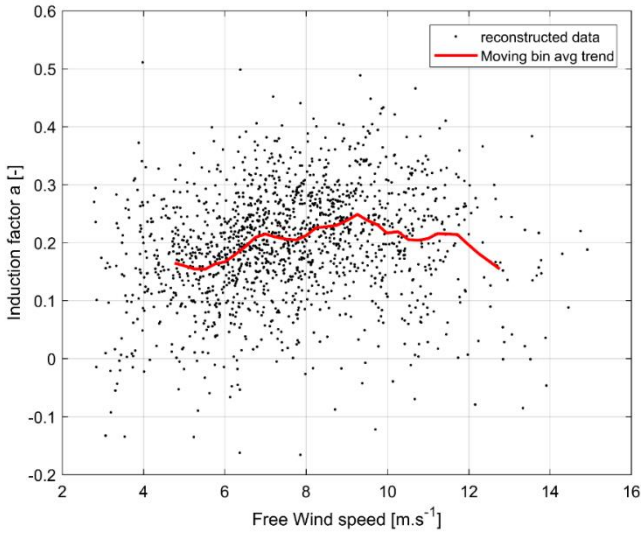

Figure A. 22. Scatter plots of induction factor estimated from the nacelle lidar wind speed estimates for the ZDM dataset alone, using the wind-induction model.

Note: the induction factor trend line shows that at maximum thrust, the induction factor reaches values of approximately 0.25. Such a maximum value is significantly lower than observed in the Nørrekær Enge campaign. Based on CFD studies of wind flows in complex terrain (see [15], (PhD thesis)), it is expected that the induction factor is reduced in such sites. Moreover, the scatter is unusually high, possibly due to the combination of:

- the "low time resolution" of the sampling of different ranges in the ZDM as configured during this campaign.
- the complexity of the wind flows in such a site: the flows changes more rapidly and the induction is less clearly defined than in flat terrain.

Model-fitting residuals

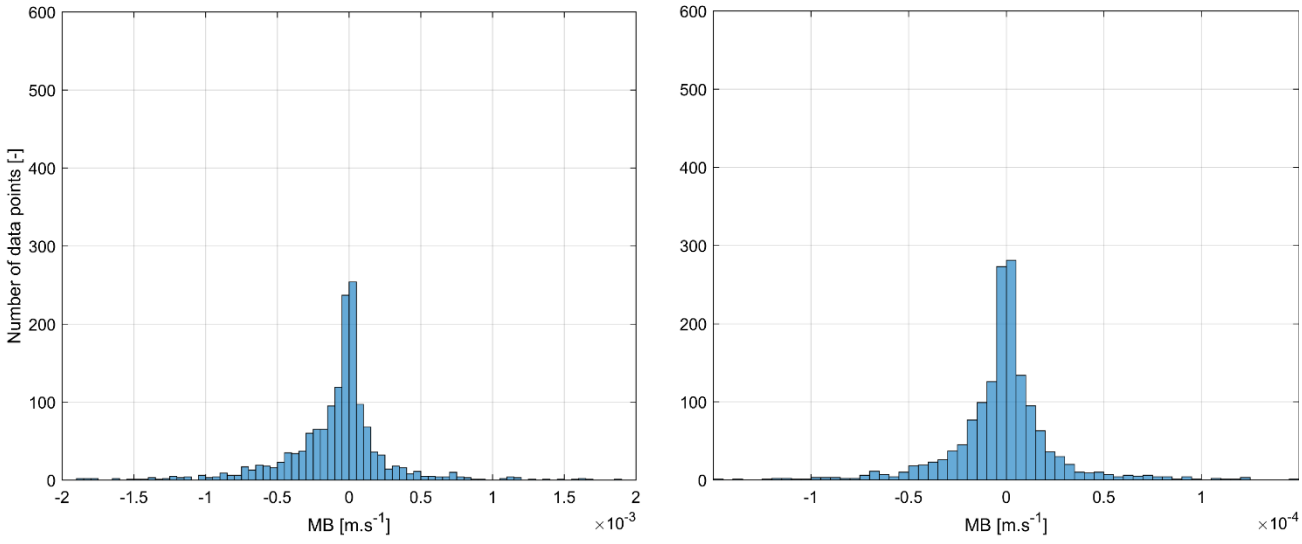

Figure A. 23. Histograms of mean bias (MB) of LOS velocity residuals for the ZDM dataset alone. Left: using the wind model at 208m. Right: using the wind-induction model.

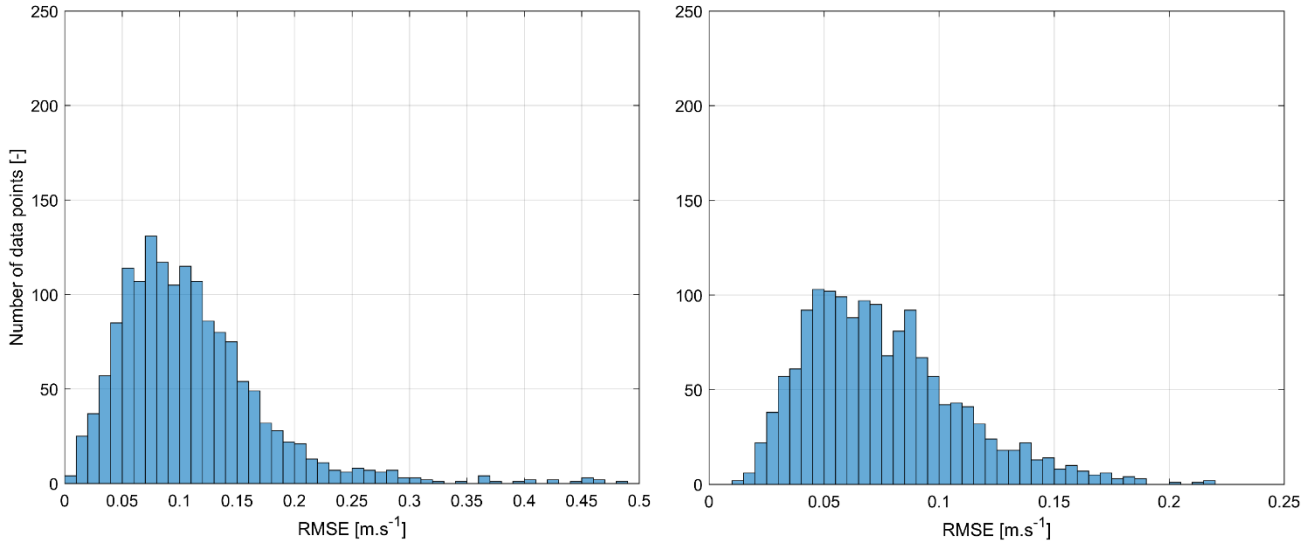

Figure A. 24. Histograms of root mean squared error (RMSE) of LOS velocity residuals for the ZDM dataset alone. Left: using the wind model at 208m. Right: using the wind-induction model.

Power curves

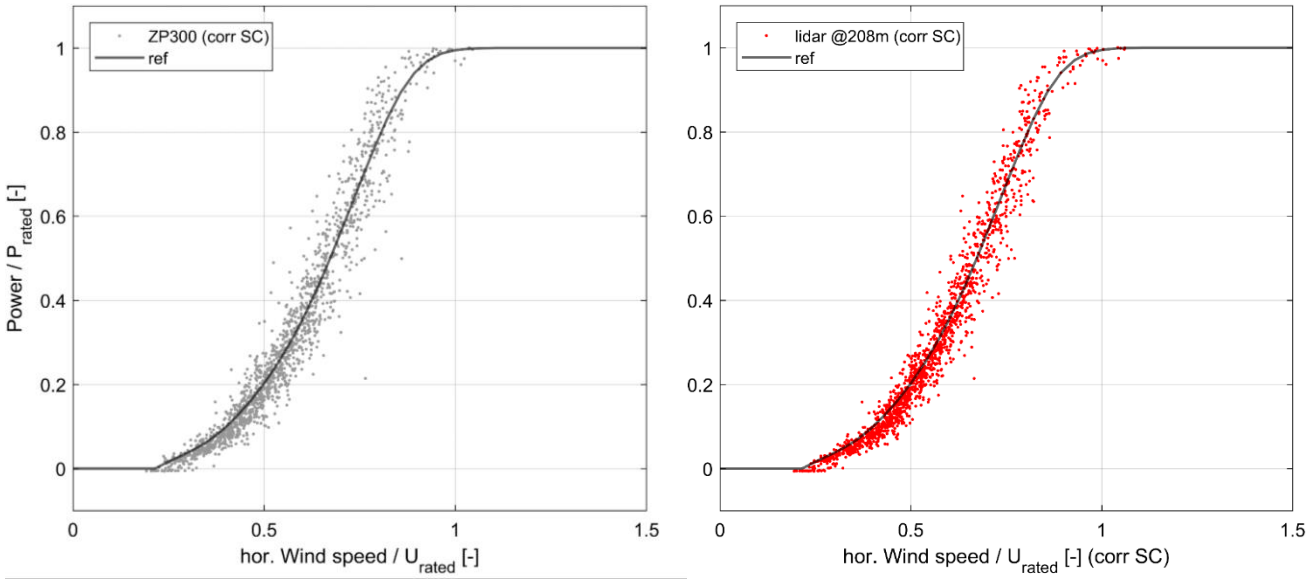

Figure A. 25. Power curve scatter plot for the ZDM dataset alone and using the wind model at 208m. The wind speed is corrected using the site calibration and then normalised using air density measurements. Left: hub height wind speed measured by ZP300. Right: nacelle lidar wind speed estimate.

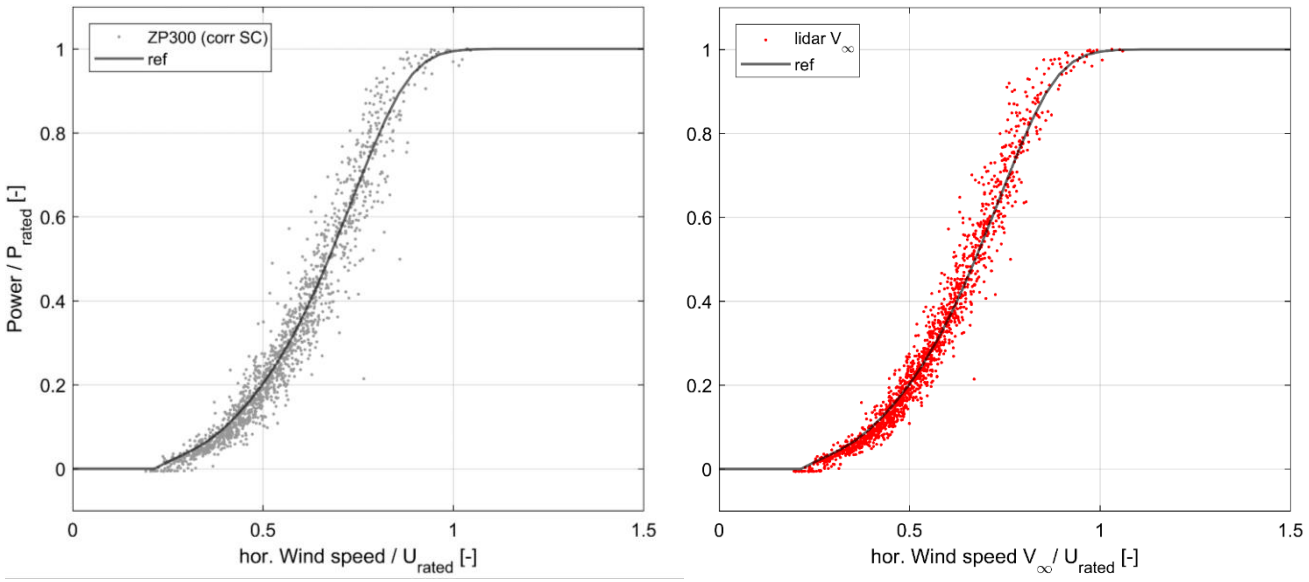

Figure A. 26. Power curve scatter plot for the ZDM dataset alone and using the wind-induction model. The wind speed is corrected using the site calibration and then normalised using air density measurements. Left: hub height wind speed measured by ZP300. Right: nacelle lidar free stream wind speed estimate.

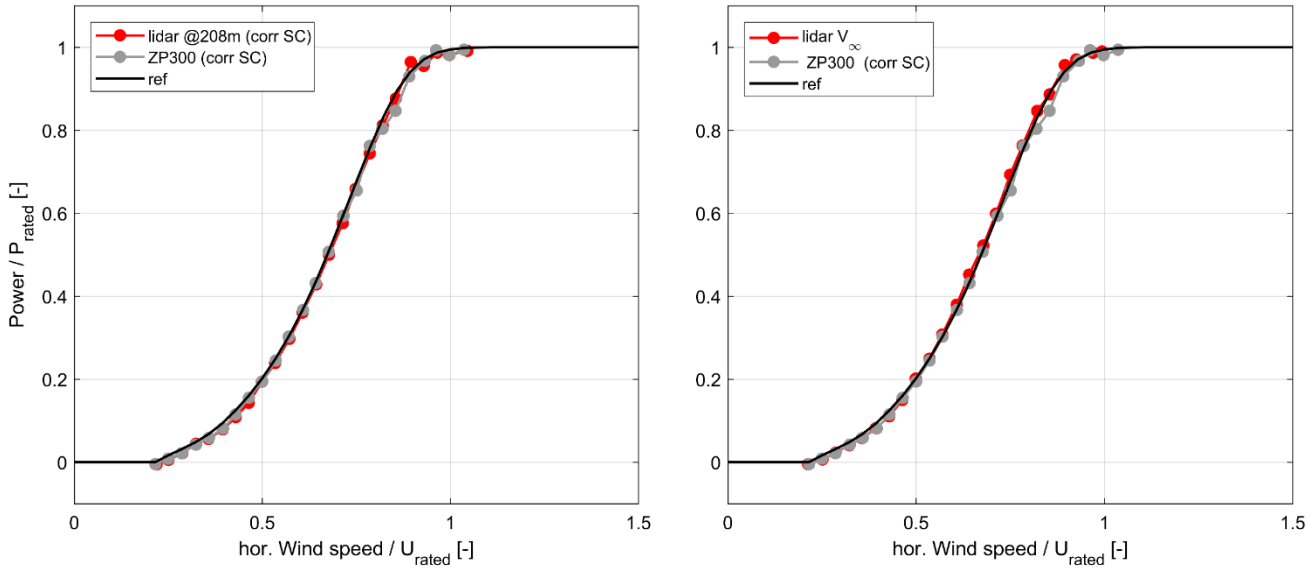

Figure A. 27. Power curve (bin-averaged) for the ZDM dataset alone. Left: using the wind model at 208m. Right: using the wind-induction model.

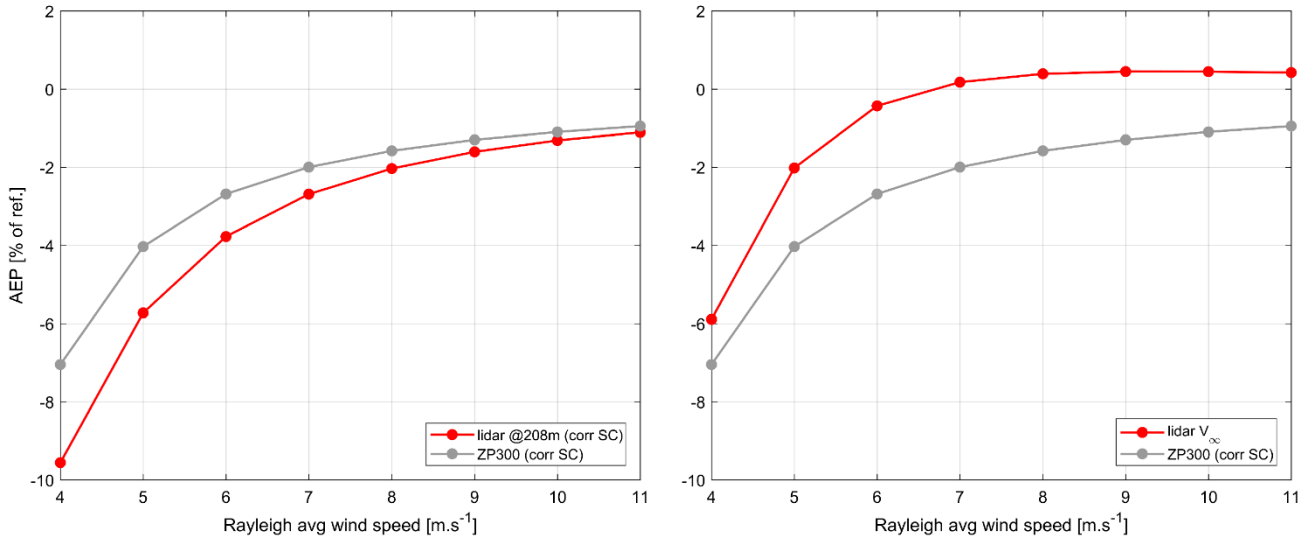

Figure A. 28. AEP difference relative to the reference power curve for the ZDM dataset alone. Grey: using ZP300 power curve. Red: using power curve with nacelle lidar. Left: using the wind model at 208m. Right: using the wind-induction model.

Annex D. Lidar-to-lidar wind speed results

This section shows the wind speed comparison obtained using the same joint datasets as in Chapter 7.

In Figure A. 29, the wind speed reconstructed from the 4BWI is plotted as function of the one reconstructed from the ZDM lidar. It shows that the mean error between the two nacelle lidar systems is 1.9% and 1.5% for the wind (left) and wind-induction (right) models respectively. The scatter is lower than when comparing individually each lidar-reconstructed wind speed to the ZP300 measurements at hub height.

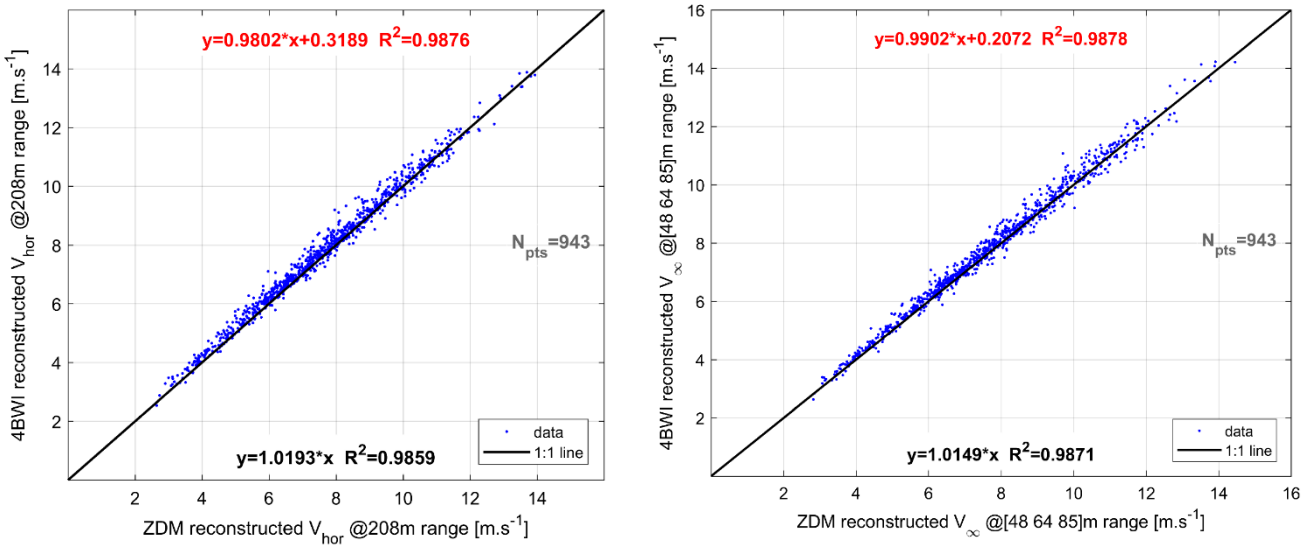

Figure A. 29. Lidar-to-lidar comparison of the wind speed estimates with the 4BWI and ZDM nacelle lidars. Left: using the wind model at 208m. Right: using the wind-induction model.

Annex E. Site calibration test with nacelle lidars

The meteorological mast remains the preferred instrumentation for performing site calibration in complex terrain, however a comparison of site calibration using lidars is of interest due to the potential to reduce campaign cost. Reports from early adopters of the methodology represents a convenient way for the industry to get inspired and avoid expensive mistakes.

With this purpose in mind, this chapter describes the site calibration tests performed in Hill of Towie before and during the UniTTe projects, and provides their results.

E.1. Goals and timeline

The goals of this part of the measurement campaign is to assess the difference between a site calibration according to the standards and one where ground-based or nacelle-mounted lidars are used. The comparisons were possible thanks to four experiments on the same turbine location:

1. Original test according to the standard: 4th July 2011 to 23rd September 2011;
2. Wind shear investigation using ground based lidar in 2013;
3. Assessment of the validity of the original test within UniTTe in 2016 using two ground-based lidars;
4. Site calibration using nacelle lidars within UniTTe in 2017.

E.2. Methods

Original site calibration

In the IEC 61400-12-1 ([3]), the site calibration method is required in complex terrain. In this method, a temporary met. mast is placed in the future position of the selected turbine, and at the same time the wind farm definitive (reference) met. mast is erected. The two masts provide simultaneous measurements for a certain amount of time, until a relationship between the wind measured by the reference mast and the temporary met. mast can be found. After, the temporary met. mast is decommissioned and the wind turbine erected in its position. The purpose of the site calibration and subsequent power performance test is to answer the question of whether the energy produced is in line with the expected generation of power with the wind speed.

In the fourth experiment, the speed up factors were obtained by nacelle lidar measurements on the same turbine that was temporarily stopped and yawed in the direction of the original reference mast.

As stated in Section 2.1, the site fails the requirements for topographical variations around the turbine under test and a site calibration is required. Figure A. 30 shows the terrain slope around the turbine under test together with the terrain requirements. Within $2D_{rot}$ from the turbine position, the terrain reaches slopes of up to 10% where the maximum slope allowed would be 3% to obviate the requirement of a site calibration.

Table B.1 – Test site requirements: topographical variations

Distance	Sector	Maximum slope %	Maximum terrain variation from plane
<2 *L*	360°	<3*	<0,04 *(H+D)*
≥2 *L* and < 4 *L*	Measurement sector	<5*	<0,08 *(H+D)*
≥2 *L* and <4 *L*	Outside measurement sector	<10**	Not applicable
≥4 *L* and <8 *L*	Measurement sector	<10*	<0,13*(H+D)*

* The maximum slope of the plane, which provides the best fit to the sectoral terrain and passes through the tower base.

** The line of steepest slope that connects the tower base to individual terrain points within the sector.

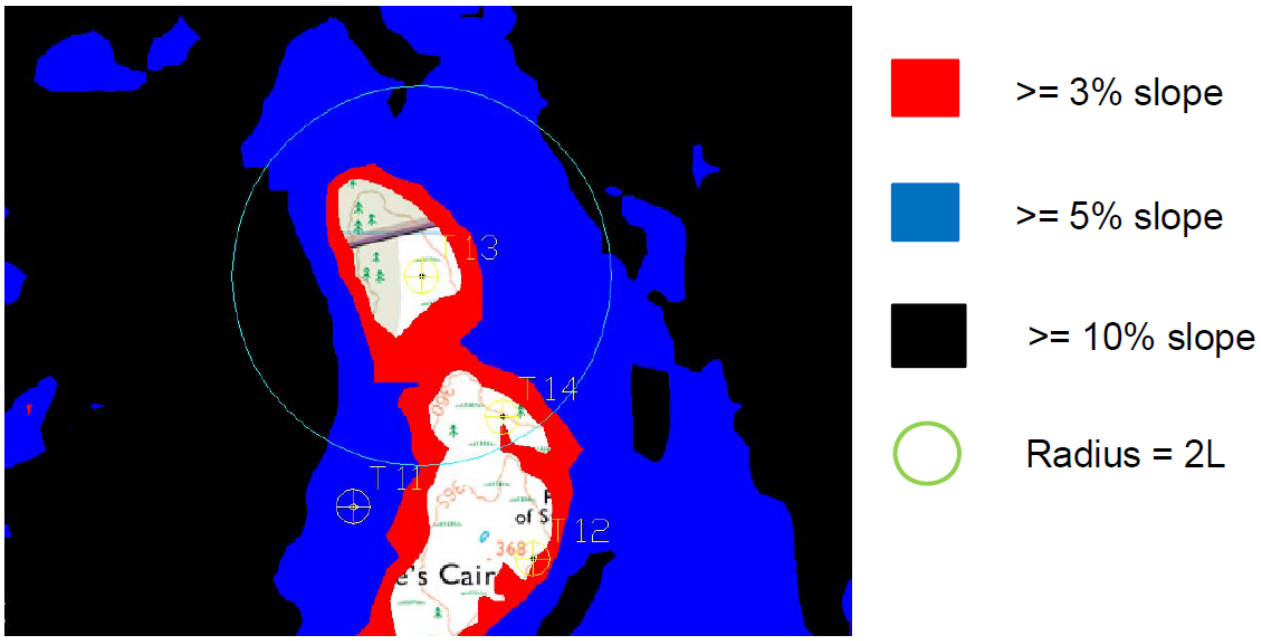

Figure A. 30. Terrain slope at the Hill of Towie site.

The next figure (Figure A. 31) shows the position of the two meteorological masts used for the site calibration test. M634 is the reference mast and M734 is the temporary mast erected at the turbine position. The site calibration was not part of the UniTTe project.

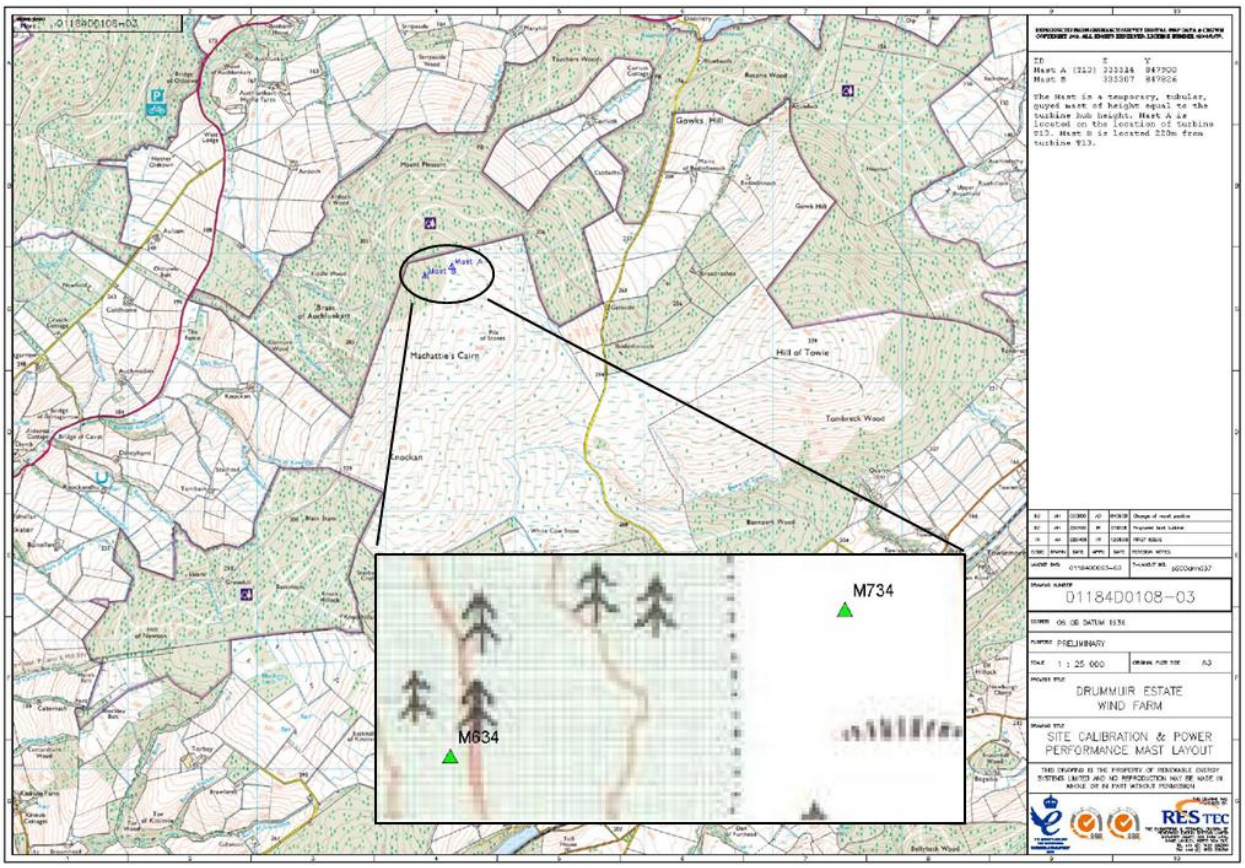

Figure A. 31. Location of the two meteorological masts used for the site calibration. M734 is at the T13 location. M634 is distant from M734 by 2.6 rotor diameters.

Investigation with ground-based lidars 2013

In the second experiment, one ground-based lidar was deployed beside the reference met. mast and then moved near the installed turbine under performance test at a distance of one rotor diameter along the ridge where the terrain effect is excepted to be similar to the turbine position (Figure A. 32). This investigation was undertaken to assess the vertical shear at the site, shear differences between turbine and mast locations and possible effect on turbine performance. This investigation was undertaken to assess the vertical shear at the site, shear differences between turbine and mast locations and possible effect on turbine performance. The investigation was not part of the UniTTe project. It should be noted that direct comparison of this dataset to the original site calibration is indicative only due to differences in instrumentation and measurement locations and the potential blockage effect from the operational wind turbine generator.

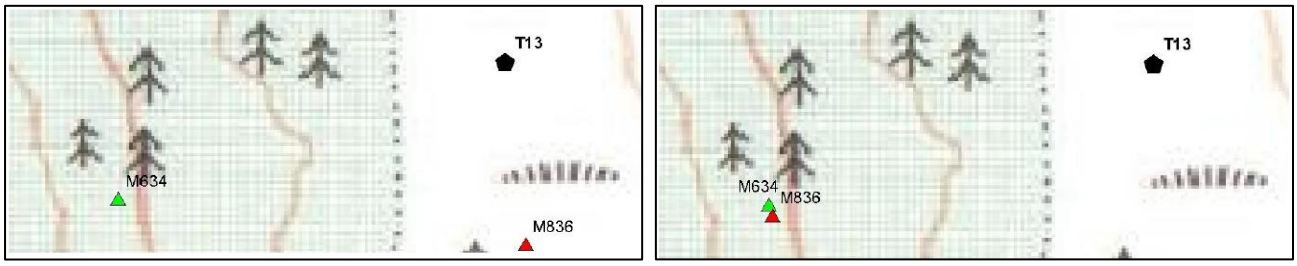

Figure A. 32. Location of the ground based lidar (red triangle) during the wind shear investigation in 2013. The lidar was located beside T13 at 1.21D along the ridge from 26/04/2013 to 30/5/2013 (left). Then it was relocated beside the M634 mast for the period 27/06/2013-22/07/2013 (right).

Investigation with ground-based lidars 2016

In the third experiment, the correction factors were obtained from two ground-based lidars – a WindCube V2 (FCR option enabled) and a ZP300 (see Figure A. 33) – measuring concurrently at the same positions as in the second experiment.

The main reason for this investigation was to detect if large changes occurred in time (for example due to forestry growth or felling) in comparison to the original site calibration results, and to which extent the speed up factors measured in 2011 could be used in 2017. This campaign was part of the UniTTe project. Comparison to the original site calibration is once again indicative in nature, however, the measurement locations are representative of those in the 2013 campaign. Although data acquired in this campaign cannot be used to guarantee the validity of the original site calibration, speedups in close agreement with the 2013 campaign provide some indication that there has been no major change in the nature of spatial variation in wind resource in the vicinity of T13 over time.

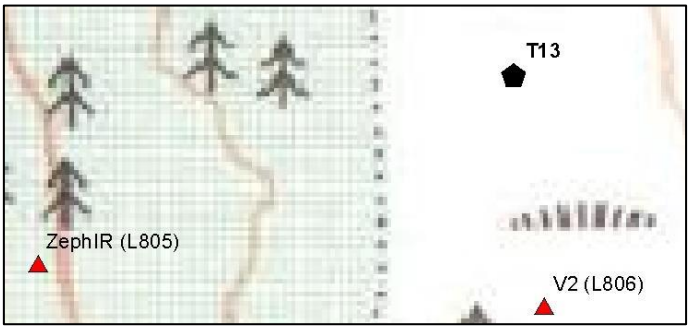

Figure A. 33. Location of the two ground-based lidars measuring concurrently.

Site calibration with nacelle lidars

The idea behind such a test is to be able to relate a measurement very close to the turbine to one at 2.5D when the turbine induction is negligible (less than 1%) in order to measure the terrain effect. Due to its capability of measuring at shorter ranges than the other nacelle lidar, the ZDM nacelle lidar was reconfigured to measure at only two ranges (10m and 208m). This could arguably be used as a measured site calibration with an increased uncertainty component (relative to IEC method) if the turbine blockage effect is not large.

After a long period of southerly winds, a week of westerly winds was forecasted towards the planned end of the UniTTe campaign in Hill of Towie. The turbine was voluntarily stopped at 11:00 on the 2nd of October 2017. The turbine was yawed remotely in the direction of the “reference mast” (a Zephir300 ground-based profiling lidar) with the help of Siemens’ personnel (Figure A. 34 and Figure A. 35).

Note that there is 16m height difference between turbine and reference mast location.

Figure A. 34. Turbine yaw and rotor position during the site calibration test viewed from the ZP300 location.

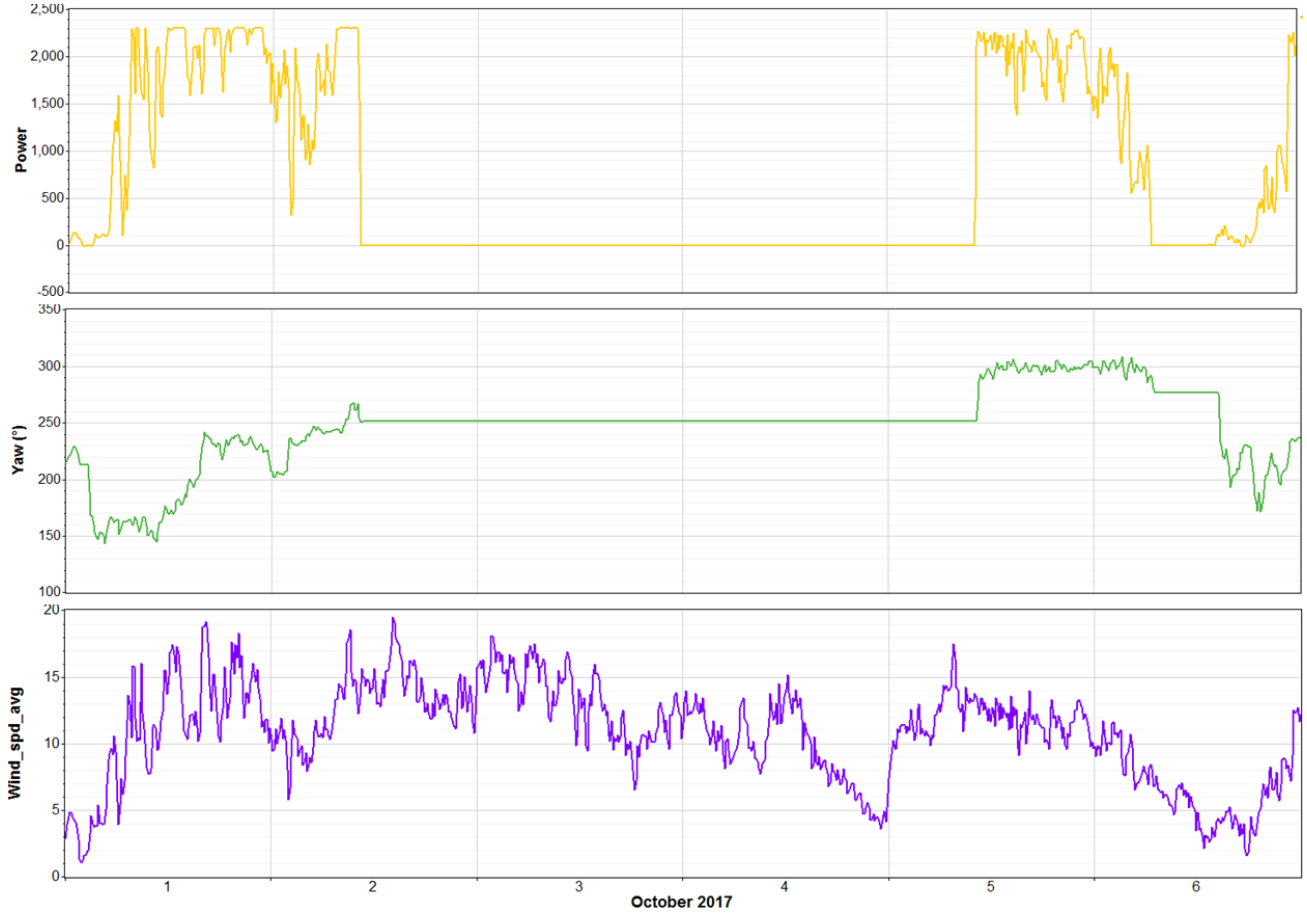

Figure A. 35. Time series of 10-minute averages of electrical power, nacelle yaw, and wind speed at hub height estimated by the ZP300 lidar during the three-day site calibration test.

The turbine was restarted at 11:00 on the 5th of October. The UniTTe project budget allowed a compensation for lost production to the turbine owner.

The wind parameters estimated by the nacelle lidar manufacturers' algorithms were used in this investigation (contrary to the studies conducted in the rest of this report).

E.3. Results

Original site calibration

The numerical results of the original site calibration are reported in Table 1. A graphical representation of these results are shown in Figure A. 36 where 10-minute wind speed ratios (on the primary (left) y axis) are plotted in function of wind direction while the bin average ratio is reported on the secondary (right) y axis. The secondary axis extent has been modified to increase the readability of the two plots.

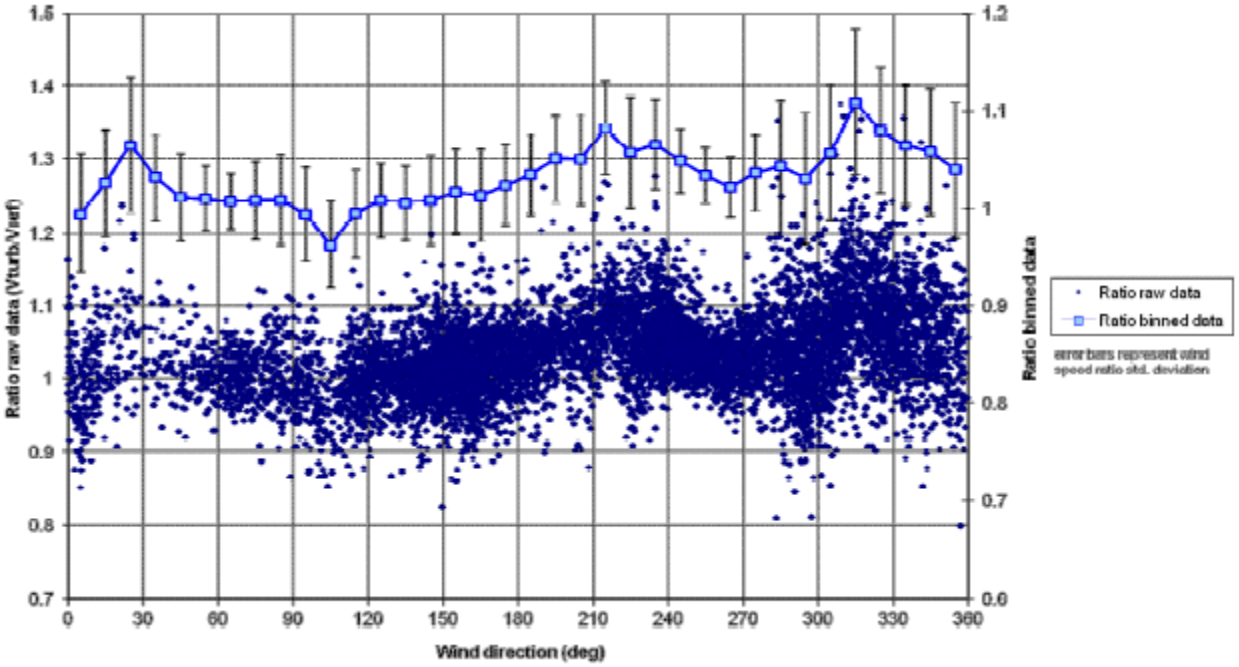

Figure A. 36. Results of the original site calibration. The wind speed ratio is obtained from the cup anemometer measurements on the turbine and reference masts.

More information such as instrumentation, duration of campaign and detailed results can be found in [7].

Investigation with ground-based lidars, 2013 and 2016 campaigns

From these two tests, several comparisons can be made. The first one consisting in comparing the speed-up factors measured by the two lidars in 2016 with the original site calibration. Prior analysing the results, the following differences with the original site calibration test should be noted:

- Here the comparison is Lidar vs. Lidar while the original site calibration was a cup anemometer vs. cup anemometer;
- Only the *WindCube V2* lidar close to T13 is corrected for terrain effect (using *Leosphere*'s FCR algorithm);
- The T13 Lidar is not at the same locations of the T13 Mast (but along the ridge);
- The turbine was present and operating.

The 10-minute speed ratios are shown in Figure A. 37 as a function of wind direction including bin.

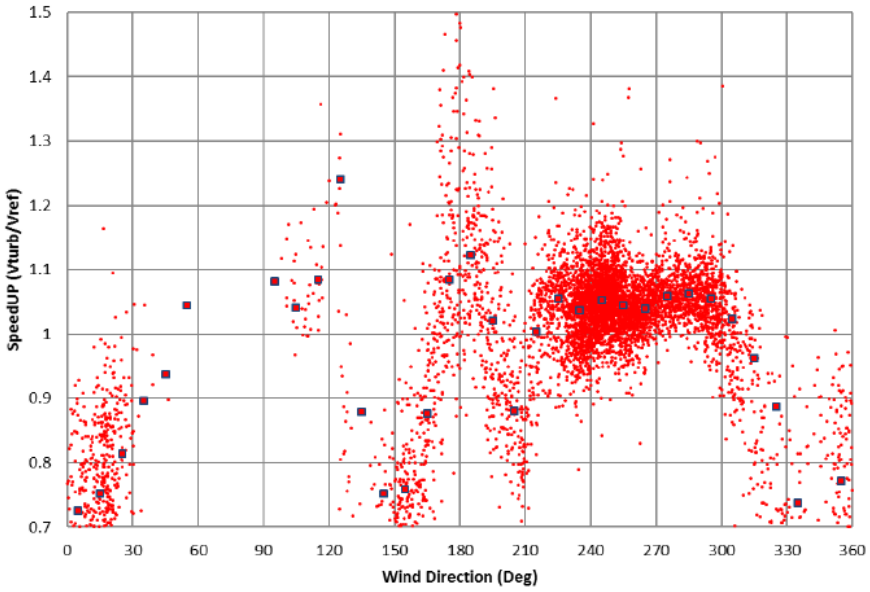

Figure A. 37. 10-minute wind speed ratios as a function of wind direction including bin averages from the third experiment in 2016.

The same bin-averaged values are displayed in Figure A. 38 and overlapped with the results from the original site calibration.

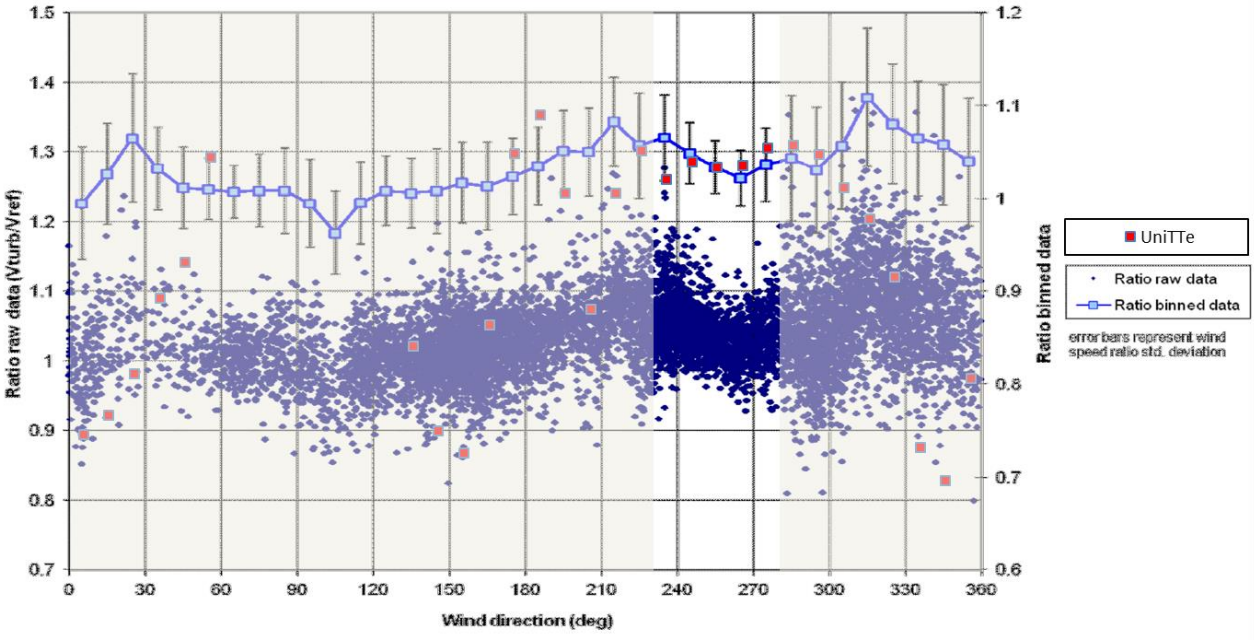

Figure A. 38. Results from 2016 overlapped with original site calibration results.

In order to analyse how significant the impact of the presence of the operating turbine is on the speed ratio when the turbine is aligned with the reference lidar (ZP300), the speed ratios are plotted as a function of wind speed (Figure A. 39). A slight increase at low wind speed (high thrust coefficient) can be observed resulting from significant wind speed deficit at the reference lidar position. The comparison with the original site calibration gets slightly better when using wind speeds above 8 ms^{-1}.

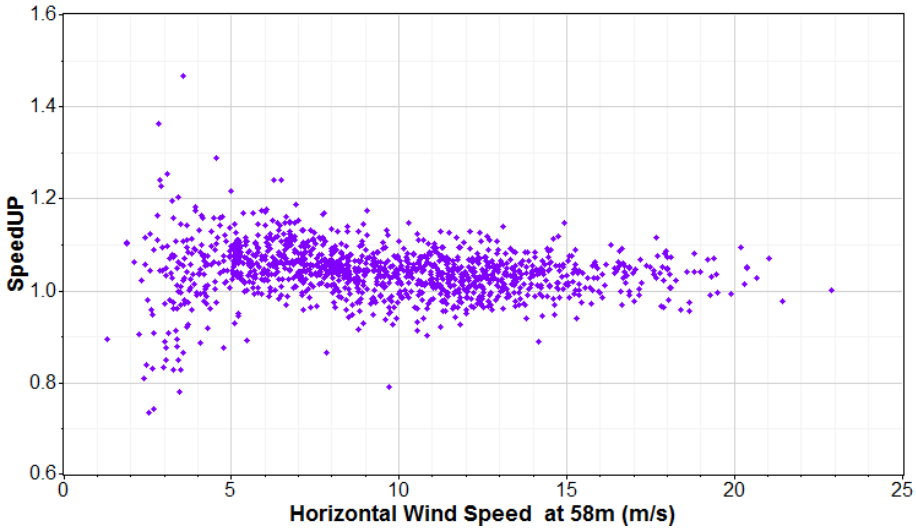

Figure A. 39. 10-minute speed ratio as a function of wind speed, showing the impact of the presence of the operating turbine.

The comparison between the newly found speed-up factors and the original ones shows, as expected, some differences but not very significant ones. Given that the comparison between the original site calibration campaign and the campaign of 2016 is indicative only, the differences in the measured speedups are not large enough to cast into doubt the validity of the original site calibration measurement at the time of the 2016 campaign.

The campaign in 2013 included concurrent measurements in the same locations despite coming from different wind sensors..

The following two figures show the comparison between the results of the 2013 and 2016 campaigns in terms of 10-minutes wind speed ratios. Figure A. 40 shows the scatter plot of the measured speed ratios, while the wind sector bin means and standard deviations are shown in Figure A. 41.

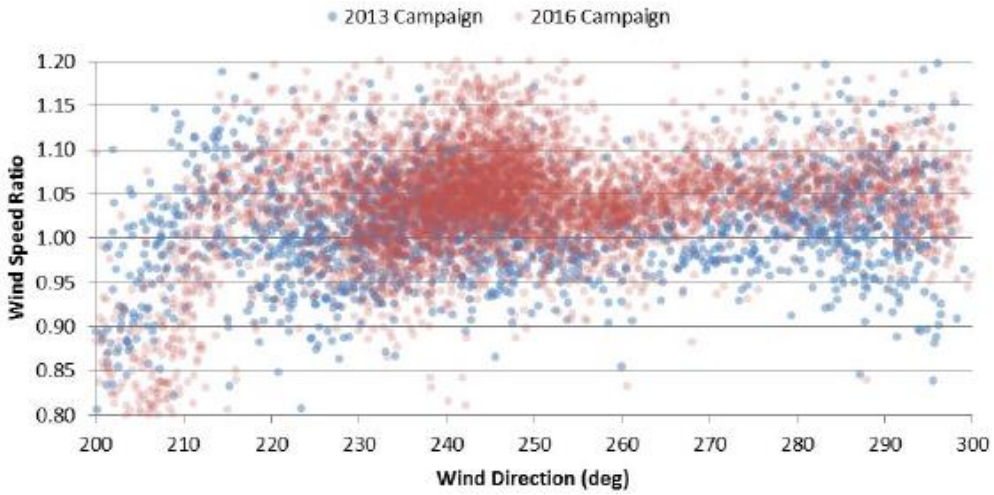

Figure A. 40. Comparison of site calibration results from the second (2013) and third experiment (2016): scatter plot of 10-minute wind speed ratios as a function of wind direction.

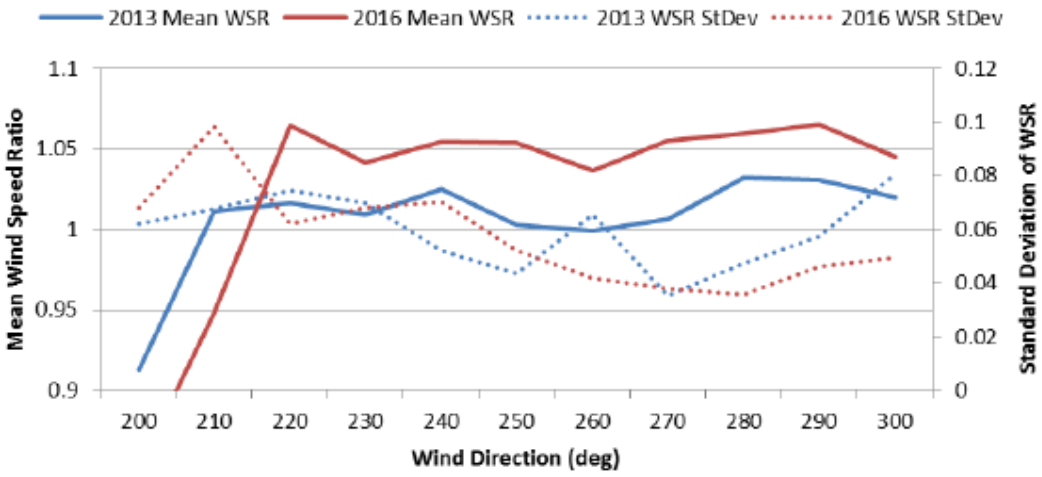

Figure A. 41. Comparison of site calibration results from the second (2013) and third experiment (2016): bin mean and standard deviation values for each direction sector.

In order to evaluate the causes of such differences between the 2011 vs. 2016 campaigns on one hand, and between the 2013 vs. 2016 campaigns on the other hand, the following must be taken into account:

- Measurements made close to the turbine location are both lidar-based;
- The ZephIR 300 lidar used in the 2013 and 2016 campaigns had no flow model correction;
- The *Leosphere WindCube V2* lidar used in 2016 employs a flow model correction (FCR).

The following three effects have been identified to possibly contribute to the observed differences:

1) There was some tree felling in the South-West of the site (near T2) in 2013;
2) Potential for growth of trees near T13 to effect the wind speed ratios;
3) (ground-based) Lidar errors inherent to their use in complex terrain.

Both forestry effects (points 1 and 2 above) were modelled using a flow model conservatively assuming 4m/year tree growth. Modelling suggests negligible impact on wind speed ratios.

In order to quantify the accuracy of the ground-based lidars at the site (point 3 above) in estimating the horizontal wind speed, the error caused by inhomogeneity of the flow within the lidar probe volume was modelled using WAsP Engineering, both at the reference mast and turbine location. The same terrain data used for the terrain correction in the wind field reconstruction (see Chapter 6) was used to predict the 3D flow over the site by means of the LINCOM flow model. Grid independence of the result was achieved with a 10m resolution. The results for both location and for both ground-based lidars (ZP300 and WindCube V2) scanning geometry are shown in Figure A. 42.

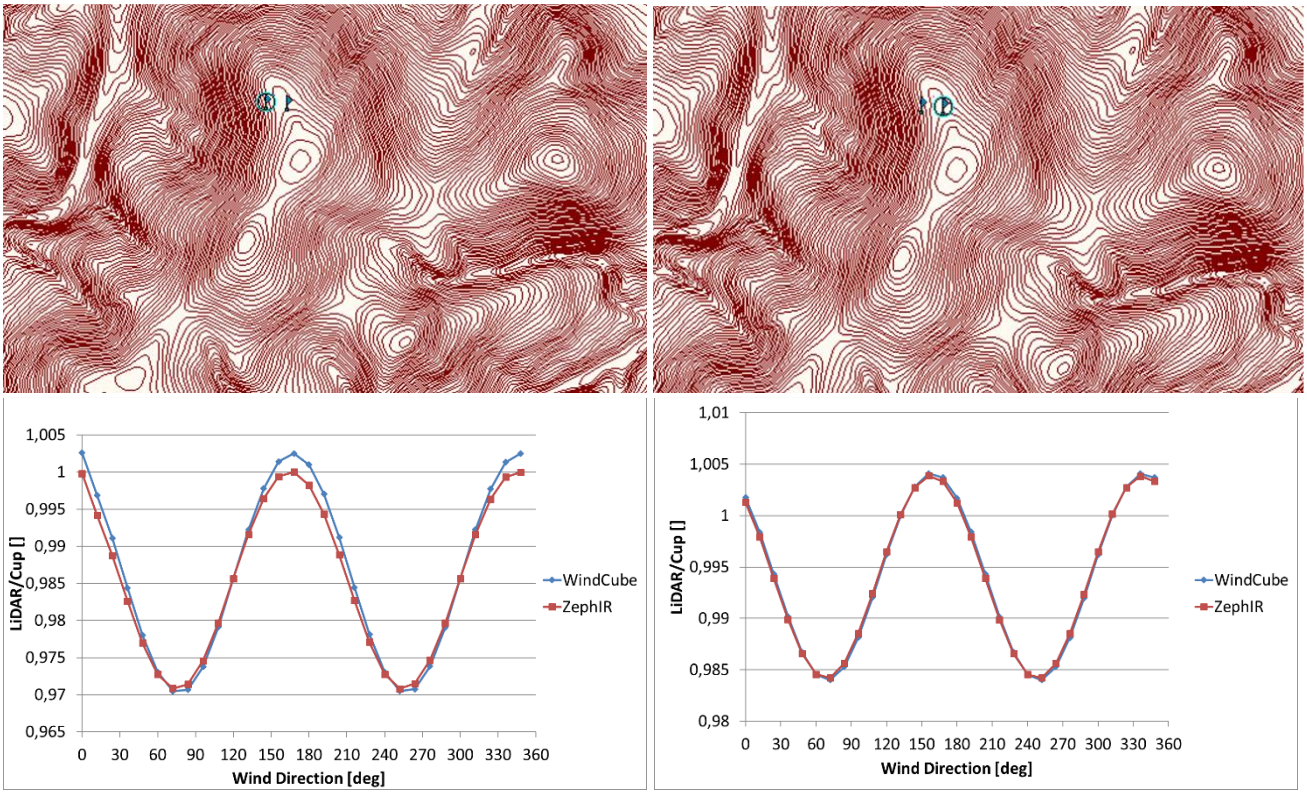

Figure A. 42. Ground-based lidar locations (top – ref. mast on the left and turbine lidar on the right) and corresponding modelled bias as a function of wind direction (bottom).

The variation of inflow angle within the probed volume is the main driver for such bias according to the modelling performed. Figure A. 43 shows such variation in the main wind direction. While the top of the ridge is usually the place to avoid, the location with a higher variation in inflow angles in the probe volume is actually found at the ref. mast position.

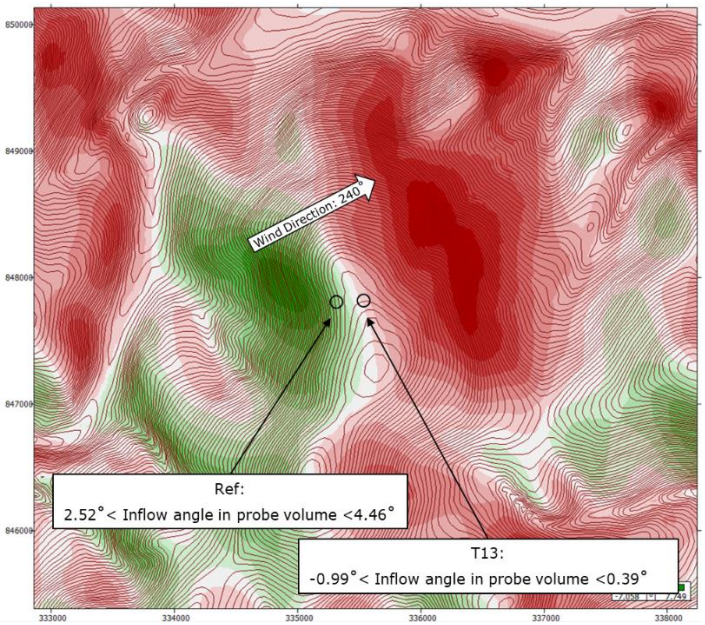

Figure A. 43. Modelled Inflow angle over the Hill of Towie site in the 240° wind direction. The black circles indicates the ground based lidar position and the size of the probe volume at hub height.

The bias obtained from the modelling can be used to attempt to make the situation in 2016 similar to 2013. This means correcting the ref. lidar (ZephIR 300) to the mast value first, and then work on the turbine lidar (*WindCube V2*). As measurements of the V2 LiDAR near T13 (2016 campaign) are flow-corrected, we can reverse the correction using the modelled correction factors. Figure A. 44 shows that the deviations are significantly reduced after applying such corrections, giving us confidence that the differences are due to measurement bias and the speed up factors seems to be very stable with time. Once again, although direct validation of the original site calibration is not possible during site operation, the agreement of the 2013 and 2016 datasets is sufficient and does not give any reason to question the validity of the original site calibration.

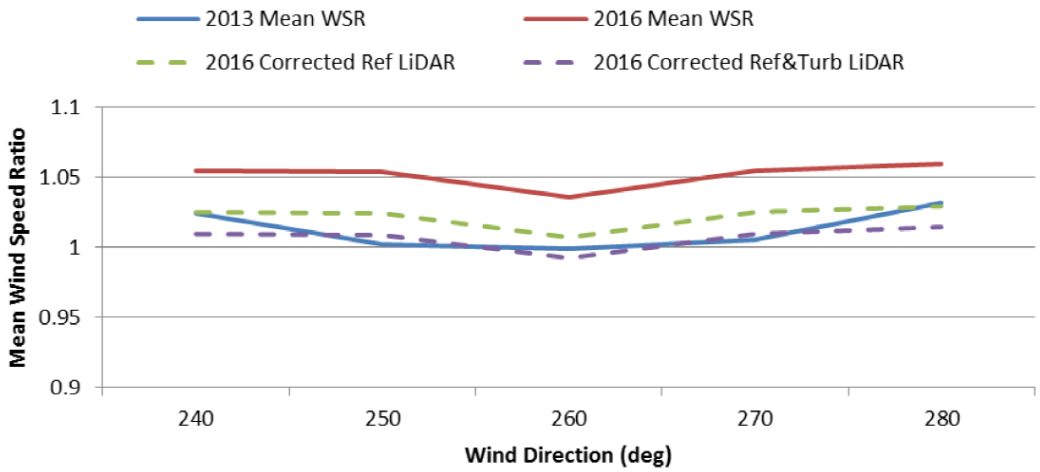

Figure A. 44. Difference between original site calibration and model-corrected the speed-up factors measured during the 2013 and 2016 campaigns.

Site calibration with nacelle lidar

A site calibration requires speed-up factors in function of wind direction. One way for the nacelle lidars to estimate the wind direction is to add the yaw misalignment estimated by the lidars to the nacelle yaw position. In this campaign, the turbine yaw position was fixed to 251°. In Figure A. 45, such wind direction from the ZDM is compared on a 10-minute basis to the wind direction estimated by the ground-based lidar (ZP300). The comparison shows a good agreement between the two giving confidence in the use of the combination of yaw misalignment and yaw position as a proxy for wind direction.

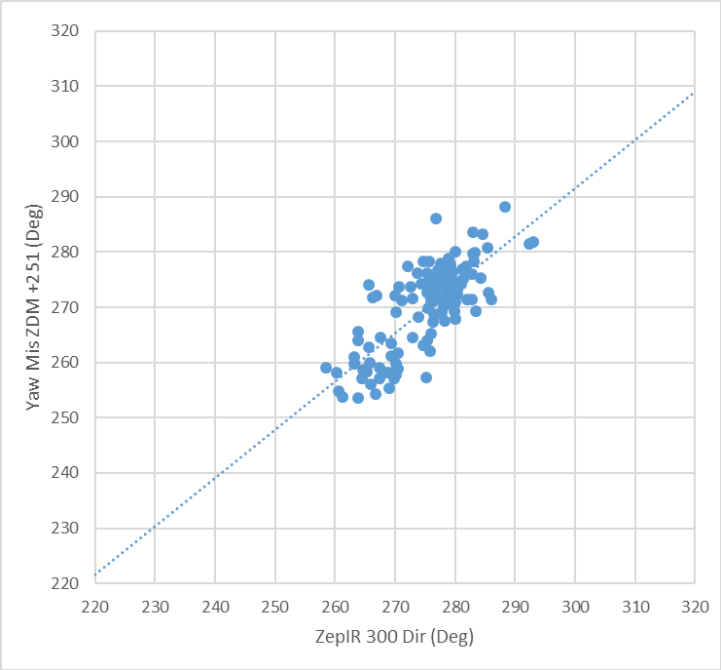

Figure A. 45. Scatter plot of the 10-minute wind direction estimated from the nacelle-mounted ZDM and ground-based ZP300 lidars during the 2017 site calibration test.

Obtaining speed up factors from nacelle lidars is on principle straightforward. The 10-minute means of the horizontal wind speed estimated at a distance close to the turbine is divided by the wind speed measured at a distance of 2.5 rotor diameters. Since the two lidar units are profiling nacelle lidars and can estimate the wind speed at different heights with the help of the built-in inclinometers, tilting the units was not necessary to account for the terrain difference of 16m between the turbine and ZP300 positions.

In the case of the ZDM, the speed-up factors can be obtained as the ratio of wind speed estimated at hub height (58.5m agl.) close to the turbine and the wind speed estimated at 42.1m (in reference to the turbine height asl) at a distance of 2.5D in front of the turbine. It is interesting also to see the difference in results using the two different algorithms in available the ZDM lidar software and providing the wind speed estimates: the first algorithm (Pair-derived) uses two opposite LOS at different heights over the circle, while all the LOS around the circle are used in the fit-derived algorithm.

Figure A. 46 shows 10-minute averages of such quantities in function of time for the length of the test followed by the convergence of the speed up factors for different directions for both reconstruction algorithms. Two observations can be made: the first is that the speed-up factors are well below unity; the second is that the two algorithms produce significantly different results.

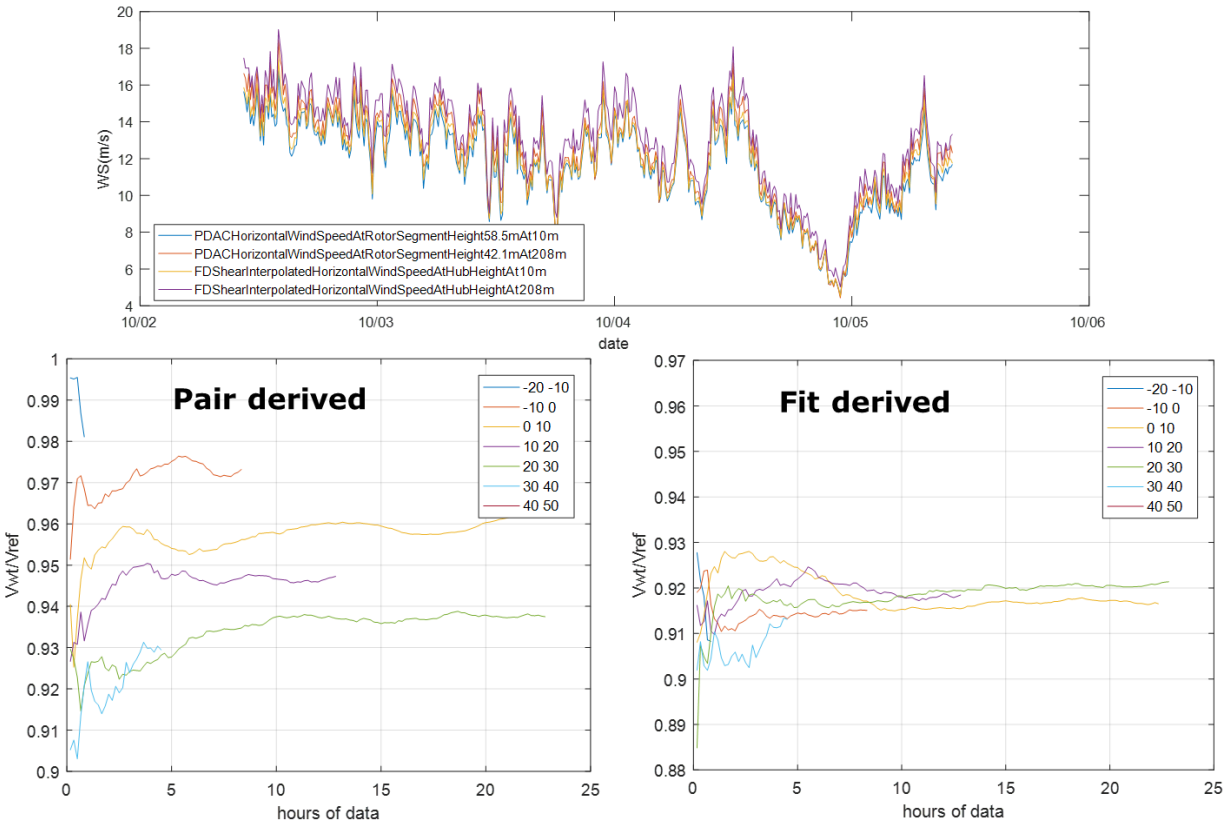

Figure A. 46. Wind speeds estimated by the ZDM over the test (above) and convergence of the speed-up factors during the 2017 site calibration test.

Figure A. 46 shows that the ZDM measurement as 10m is suffering from the turbine blockage effect and is not suitable for use in a site calibration measurement. As such, it is of interest to inspect the speedup measured using the other nacelle lidar system installed on the same turbine of type 4-beam Wind Iris. It should be noted that the closest measurement to the turbine rotor that could be acquired using the Wind Iris was 48 meters which is likely sufficiently far from the turbine location to necessitate additional flow modelling to complement the measurements for use in site calibration

The Wind Iris LOS wind speed component along the four different beams highlight some problems in LOS1 and LOS3 (beams on the right of the lidar trajectory), while the other two LOS seem to provide valid measurements (Figure A. 47). By comparing the rotor position to the lidar geometry, it is clear that LOS 1 and 3 were blocked by one of the blades.

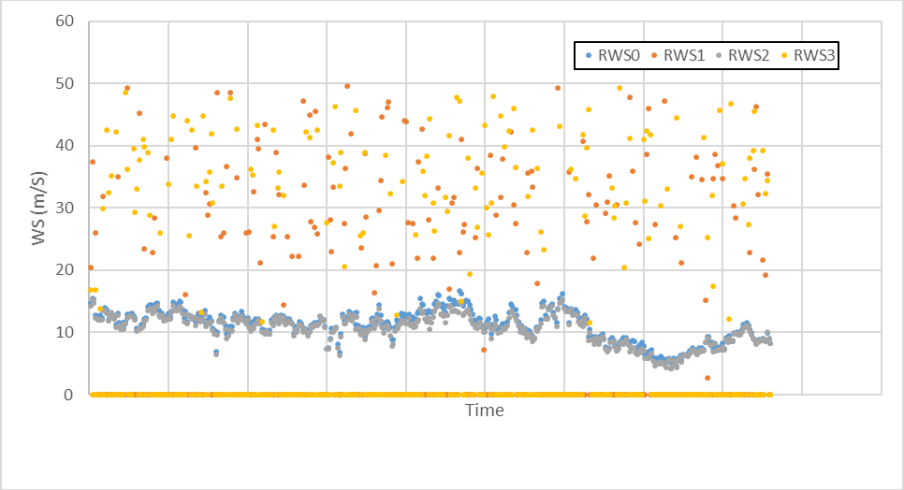

Figure A. 47. Time series of LOS wind speeds measured by the Avent 4-beam Wind Iris during the 2017 site calibration test.

The lack of data on both "right" LOS (see trajectory in Figure 4) makes the wind field reconstruction impossible. However, the wind speed measured along LOS2 can still be used to provide a rough estimate of the measured speed-up factors from the 4BWI nacelle lidar. This is possible thanks to the fact that acceleration or deceleration of the flow can be detected also from the ratio of a component of the wind vector. Luckily a 16m difference in terrain height over 208m corresponds to a angle close to the 5° vertical separation of LOS2 to a horizontal plane. Thus, the LOS2 speed-ratio ratio calculated as

$$\frac{V_{turb}}{V_{ref}} = \frac{V_{LOS2}@48m}{V_{LOS2}\ @208m}$$

can be compared to the ratios derived from the original site calibration (Figure A. 48).

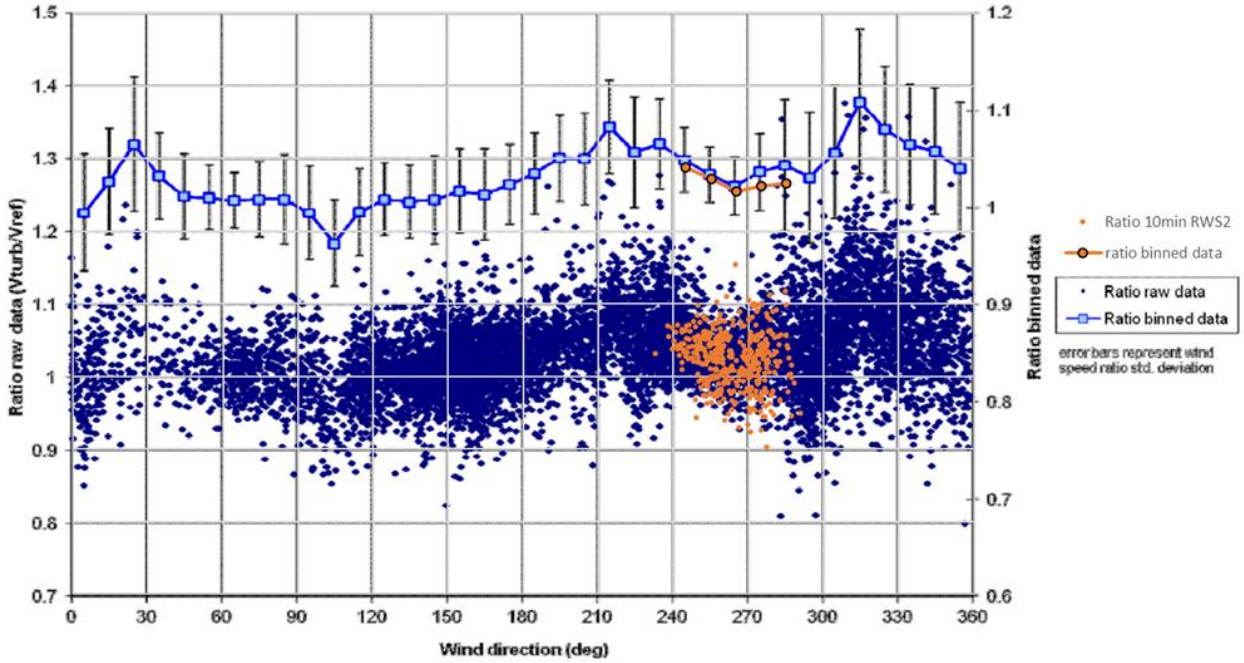

Figure A. 48. Results of site calibration test for the 4-beam Wind Iris nacelle lidar during the 2017 campaign. The 4BWI speed ratio is obtained from the LOS speeds measured along LOS2.

Table 10. Results of the site calibration test using wind speeds estimated combining LOS velocity from beam 2 of the 4BWI and the wind direction from the ZDM.

Yaw mis bin	center bin	ratio binned data	ref site cal	difference	Wind dir	beam angle-wind dir
-10-0	-5	1.0405	1.048	0.0075	245	0
0-10	5	1.0285	1.033	0.0045	255	10
10-20	15	1.0159	1.022	0.0061	265	20
20-30	25	1.0215	1.036	0.0145	275	30
30-40	35	1.0241				

E.4. Takeaways

This chapter reports on verification of the original site calibration and new methodologies related to experimental site calibration for the purposes of wind turbine power performance testing in complex terrain. As such, it was at first not clear what kind of results could be expected from such investigations.

The test with the ground-based lidars (2016) confirms that the effects of complex terrain on the wind flow are more significant than the bias introduced by the presence of the turbine and the displaced location of the lidar on the ridge. However, the flow complexity leads to too uncertain site calibration factors. Despite this, supplementing the measurements with computational modelling, it has been possible to verify qualitatively that the results of the original site calibration hold over time.

The main takeaways are related to the planning and execution of the three-day test with the nacelle lidars (2017 campaign). First, the ZDM measurements have shown that the close-to-rotor measurements suffered significant blockage effect meaning this concept does not yield a valid site calibration result. The measurements showed that the wind at such a short distance is slowed down by the presence of the nacelle (blockage effect), and thus unusable for site calibration. Maybe, using measurements from a distance of approximately 20-25m would lead to more usable results, with the awareness that the 20-25 meters of terrain effect would be missed. It is in any case recommended to conduct a preliminary CFD study of the flow around the nacelle in order to select the nacelle lidar measurement ranges appropriately.

The stopped turbine rotor lead to full blockage of two of the four beams of the 4BWI. An idling rotor would mitigate this issue at the expense of some ZDM data availability. However, 40m is already too far to be used as a measurement for site calibration. This corresponds in this campaign to a site calibration between 0.5D and 2.5D. Some modelling would be required to determine the correction to be applied to get from 0.5D to 0D. This approach would feature quite a high uncertainty. For Hill of Towie, the slope close to the turbine T13 is small and so the terrain effect in the last 0.5D is likely to be small. As a result, in this case, the 0.5D – 2.5D SC from the 4BWI agrees quite well with the original SC. This however may not generalise well.

The takeaways from the somewhat limited investigations on using nacelle for site calibration is that this approach is not comparable to a classic site calibration due to the inability of measuring the undisturbed wind at the turbine position, however the procedure seems reasonable in order to measure speed up (or –down) factors between 2.5D distance and 0.5D . More investigations and tests are required to confirm or reject this idea.

This chapter reports on a test representing a rare investment of money and resources with the purpose of providing information on the potential of using lidars instead of cup anemometers for site calibration.

References

[1] Wagner R., Pedersen T.F., Courtney M., Antoniou I., Davoust S., Rivera R.L.: "Power curve measurement with a nacelle mounted lidar", [2014], Wind Energy, Vol: 17, issue: 9, pages 1441–1453 (http://dx.doi.org/10.1002/we.1643).

[2] Borraccino A.: "*Remotely measuring the wind using turbine-mounted lidars: Application to power performance testing*", [2017], Ph.D. thesis, DTU Wind Energy, Roskilde, Denmark. (http://dx.doi.org/10.11581/DTU:00000021).

[3] IEC 61400-12-1 (edition 2), [2017], "*Power performance measurements of electricity producing wind turbines*", International Electrotechnical Commission.

[4] Borraccino A. et al.: "*Wind field reconstruction from nacelle-mounted lidar short-range measurements*", [2017], Wind Energy Science, vol: 2, issue: 1, pages 269–283 (http://dx.doi.org/10.5194/wes-2-269-2017).

[5] IEC 61400-12-1 (edition 1), [2005], "*Power performance measurements of electricity producing wind turbines"*, International Electrotechnical Commission.

[6] Renewable Energy Systems Ltd, Feeney S.: "*Hill of Towie power performance – Valid direction sector*", [2011], Report, ref: 01184-010531.

[7] Renewable Energy Systems Ltd, Feeney S.: "*Hill of Towie wind farm – Site calibration result*", [2011], Report, ref: 01184-011098.

[8] Renewable Energy Systems Ltd, Cogle I., Gleave D.: "*ZephIR 300 LiDAR – Installation and commissioning Proforma – Hill of Towie*", [2017], Report, ref: TC01-039161.

[9] Renewable Energy Systems Ltd, Gleave D.: "*UniTTe – Hill of Towie – Nacelle lidars installation report*", [2017], Report, ref: TC01-039518.

[10] Wagner R., Borraccino A., Forsting A.R.M.: "*Power performance verification in complex terrain using nacelle lidars: the Ogorje campaign*", [2017], Technical Report, DTU Wind Energy, Roskilde, Denmark (DTU Wind Energy E; No. 0157).

[11] Bingöl F., Mann J., and Foussekis D.: "*Conically scanning lidar error in complex terrain*", [2009]. Meteorologische Zeitschrift (Stuttgart, Germany) 18, number 2 (): 189–195. doi:10.1127/0941-2948/2009/0368.

[12] Pitter M., Abiven C., Vogstad K., Brady O.: "*Lidar and computational fluid dynamics for resource assessment in complex terrain*", [2012], In Proceedings, EWEA 2012, Copenhagen, Denmark (https://www.researchgate.net/publication/273868335_Lidar_and_computational_fluid_dynamics_for_resource_assessment_in_complex_terrain).

[13] Leopshere: "*WindCube FCR measurements – Principles, performance and recommendations for use of the Flow complexity Recognition algorithm for the WindCube ground-based Lidar*", [2017] (https://www.ieawindtask32.org/wp-content/uploads/2017/11/GM2017-Leosphere-Windcube-FCR-measurements.pdf).

[14] Wagner R., Bejdic J.: "*WindCube + FCR test at Hrgud, Bosnia and Herzegoivan*", [2014], Technical Report, DTU Wind Energy, Roskilde, Denmark (DTU Wind Energy E; No. 0039), (http://orbit.dtu.dk/en/publications/windcube--fcr-test-at-hrgud-bosnia-and-herzegovina(de4febab-3ce2-435c-9aba-0583d677981c).html).

[15] Meyer Forsting A.R.: "*Modelling wind turbine inflow: The Induction Zone*", [2017], Ph.D. thesis, DTU Wind Energy, Roskilde, Denmark. (http://dx.doi.org/10.11581/DTU:00000022).